XXI Seminar on Software for Nuclear, Subnuclear and Applied Physics

Perspectives about in-plasma investigation of nuclear beta decays of astrophysical interest

David Mascali,

on behalf of INFN-LNS Plasma Team and the PANDORA collaboration

Istituto Nazionale di Fisica Nucleare
Laboratori Nazionali del Sud

Plasmas for Astrophysics Nuclear Decay Observation and Radiation for Archaeometry

samothrace
Sicilian Micro and Nano Technology Research and Innovation Center

Università di Catania

NQSTI
National Quantum Science and Technology Institute

➢ **Laboratory magnetoplasmas in compact traps are historically used for ion beams production**

High-Resolution X-ray Spectroscopy and Imaging (Space and Time-Resolved)

RF probes

Advanced Sensors R&D

Ion Beams Production for Accelerators

Fundamental plasma investigation

Ultra Compact Proton Source & negative noble-gas ions injector

Fundamental nuclear astrophysics research

Optical Emission Spectroscopy

RF Interferometry

RF Polarimetry

Plasmas for Astrophysics Nuclear Decay Observation and Radiation for Archaeometry

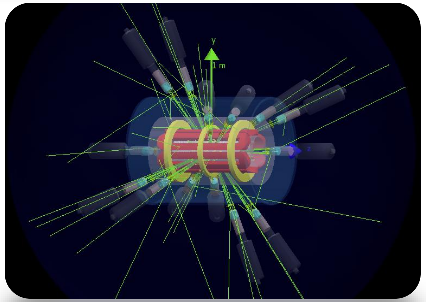

D. Mascali et al., Universe, 2022, 8(2), 80
D. Mascali et al., EPJ-A, 53, 2017, 7

➢ **Laboratory magnetoplasmas are also suitable and interesting for fundamental physics researches!**

Efforts at INFN since 10-15 years to make an innovation of research goals, methods, instruments → **use of plasmas for fundamental science and applications**

From a laboratory ECR "Plasma star" to…

New heating and diagnostics technology for Fusion

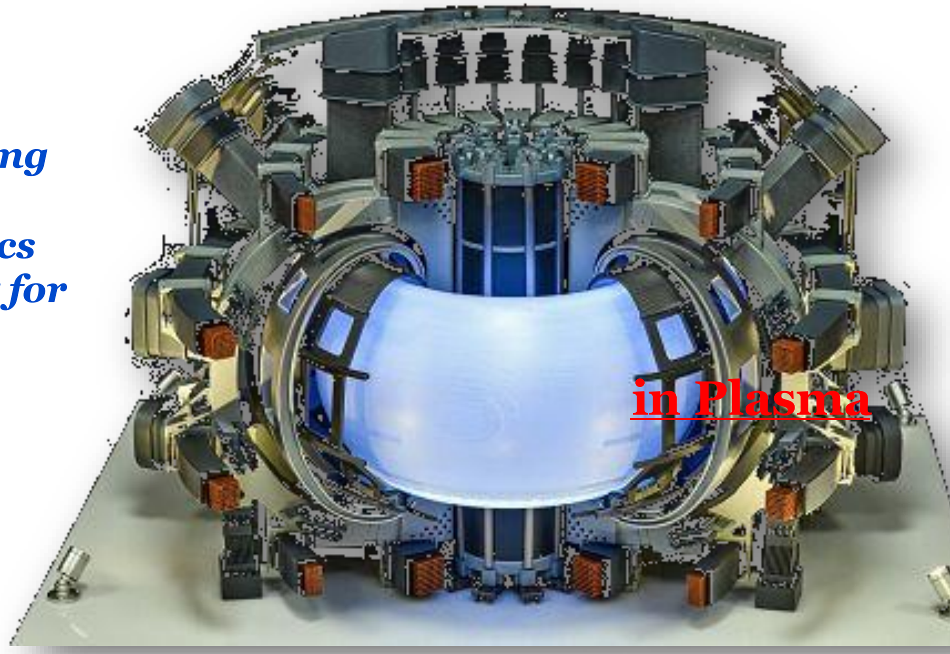

in Plasma

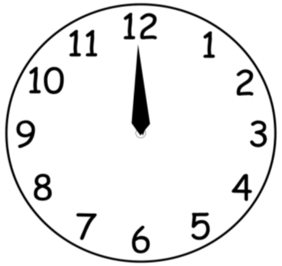

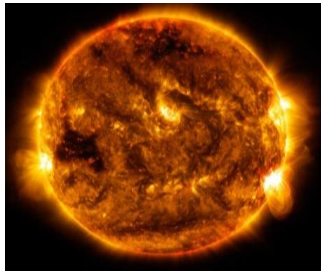

β-decay accelerates in hot plasmas!!

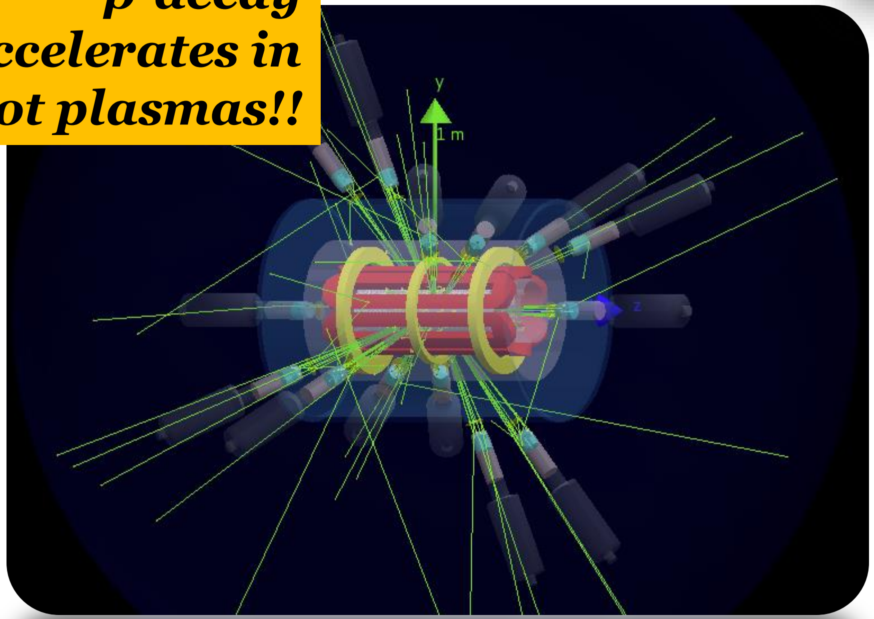

Divertor Tokamak Test:
LNS is partner of the Consortium

INFN LNS
Istituto Nazionale di Fisica Nucleare
Laboratori Nazionali del Sud

Plasmas for Astrophysics Nuclear Decay Observation and Radiation for Archaeometry

PANDORA project is founded by INFN (National Institute of Nuclear Physics)
The collaboration includes 34 departments/laboratories in Italy and Europe

SAMOTHRACE (SiciliAn MicronanOTecH Research And innovation CEnter) **Ecosystem funded by the EU Next Gen Program**

NQSTI
National Quantum Science and Technology Institute

Production of new isotopes (from metals) for Quantum Technology manufacturing and optimization

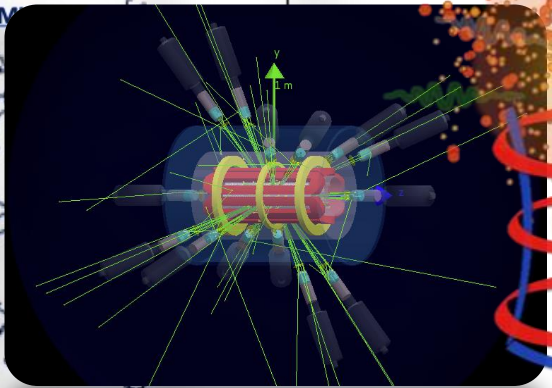

IRIS 2.0

Innovative R&D for Plasma Diagnostics: Detectors and technologies for Fusion Power **(Energy)**

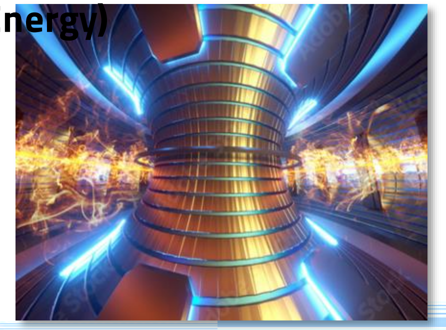

Elements of Nuclear Astrophysics

Nuclear astrophysics deals with the quantitative and qualitative explanation of the elemental abundance.

REVIEWS OF
MODERN PHYSICS
VOLUME 29, NUMBER 4 OCTOBER, 1957

Synthesis of the Elements in Stars*

E. MARGARET BURBIDGE, G. R. BURBIDGE, WILLIAM A. FOWLER, AND F. HOYLE

Kellogg Radiation Laboratory, California Institute of Technology, and Mount Wilson and Palomar Observatories, Carnegie Institution of Washington, California Institute of Technology, Pasadena, California

"It is the stars, The stars above us, govern our conditions";
(*King Lear*, Act IV, Scene 3)

but perhaps

"The fault, dear Brutus, is not in our stars, But in ourselves,"
(*Julius Caesar*, Act I, Scene 2)

TABLE OF CONTENTS

NUCLEAR ASTROPHYSICS[1]

BY A. G. W. CAMERON

Atomic Energy of Canada Ltd., Chalk River, Ontario, Canada

INTRODUCTION

Like many interdisciplinary subjects, that of nuclear astrophysics has had a very slow beginning, followed by a rapid spurt of activity during the last five years, when simultaneous progress in each of its parent fields reached the stage where experiments and calculations in nuclear physics could throw meaningful light on astrophysical observations. At the turn of the century Kelvin and Helmholtz had shown that release of gravitational potential energy would suffice to maintain the luminosity of the sun for some tens of millions of years, but it was soon realized that this was an insufficient source of solar energy, since the geologists found that many of the earth's rocks had ages nearly two orders of magnitude greater than the above figure. It was then proposed that the sun derived its energy from the disintegration of heavy elements such as uranium and thorium, but this theory also became inadequate when it was found that the sun was composed mostly of hydrogen and contained only very small traces of the heaviest elements. Eddington and Jeans thought that the source of solar energy must lie in the conversion of mass into energy, either in some total conversion process or through the transformation of hydrogen into heavier elements. Nuclear physics was then too young a science to allow these hypotheses to be investigated.

A vital step forward was taken when Atkinson & Houtermans (1) showed that charged particles had a small but finite probability of penetrating Coulomb potential barriers, and that there could thus be a slow but significant rate for the amalgamation of charged particles in stellar interiors at the temperature of several million degrees which had been calculated to exist there. It became apparent that solar-energy generation must result from

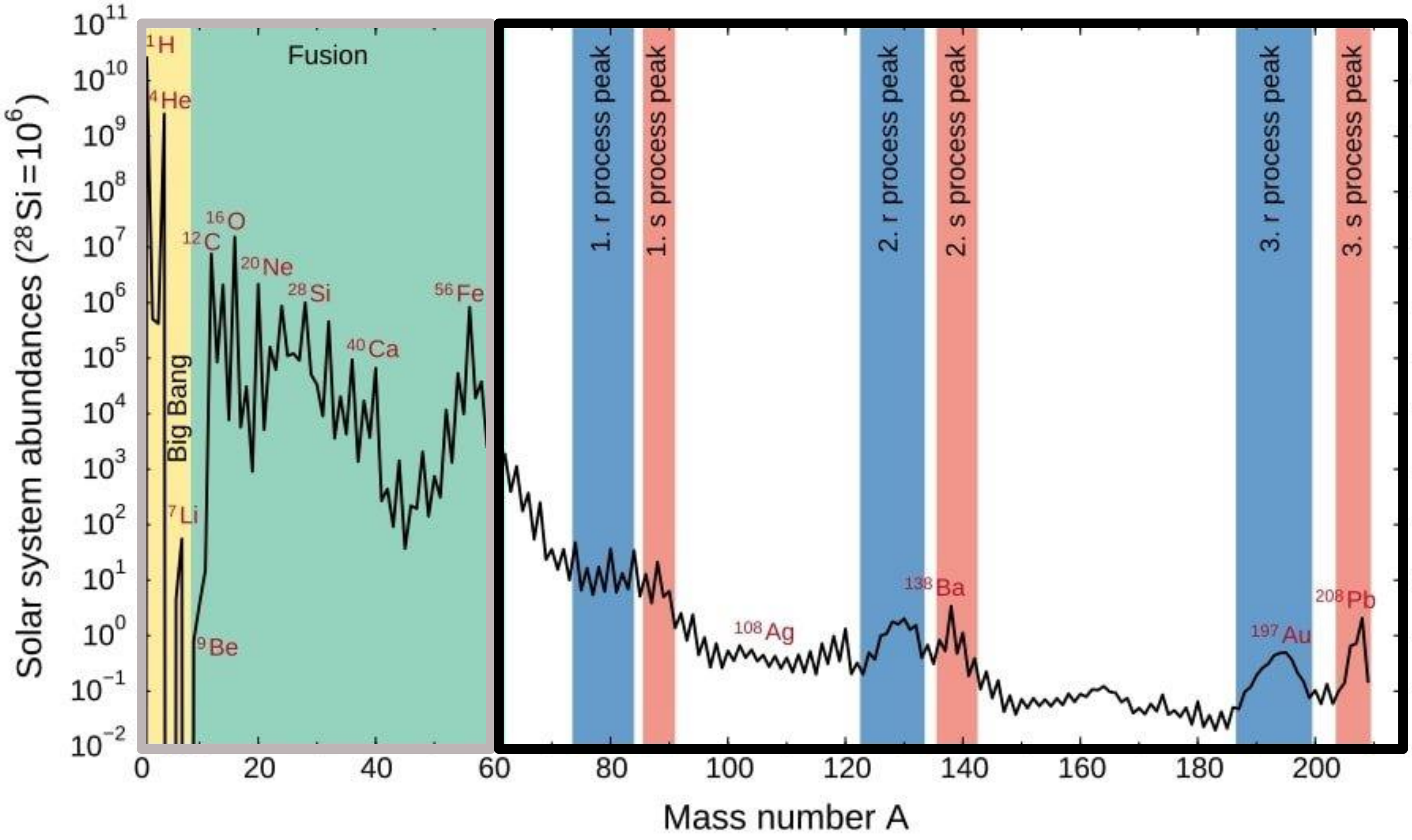

Elements till ^{56}Fe (iron peak) are synthesised through successive **thermonuclear fusion** reactions

99% of elements beyond the iron peak are produced through **neutron capture reactions**

Neutron Capture Processes

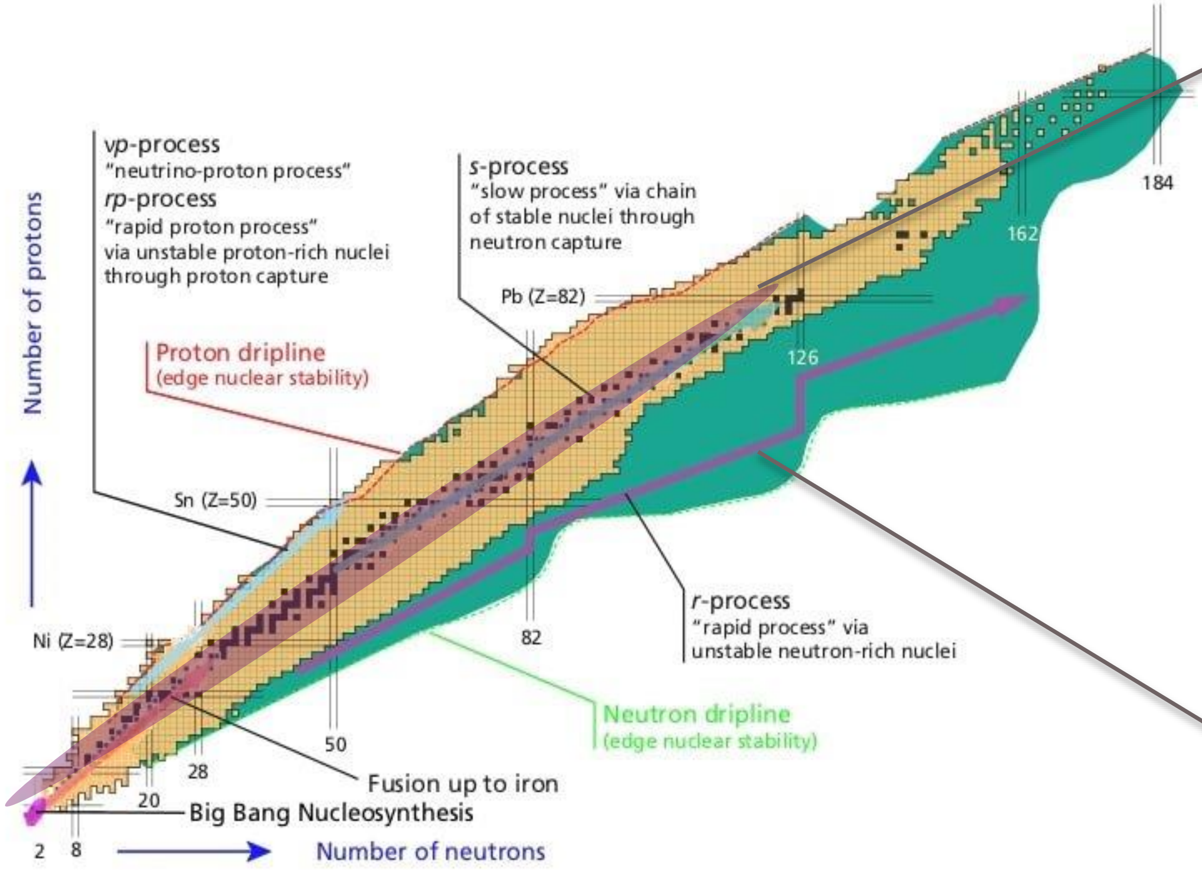

Chart of nuclei and nucleosynthesis pathways. R-process takes place far from the valley of stability and proceeds through waiting point nuclei.

T.R. Rodriguez, J. Phys. Conf. Ser. ***503*** *(2014)*

Slow Neutron Capture (s-process)

- Takes place inside **AGB stars** (main branch) and **massive stars** (weak branch)
- Neutron density around $10^{5\text{-}6}$ cm^{-3} from either $^{13}C(\alpha,n)^{16}O$ or $^{22}Ne(\alpha,n)^{25}Mg$ reactions
- τ_n ~ [d to yrs] competes with τ_β [d to yrs] to synthesise 60<A<208 elements in equilibrium

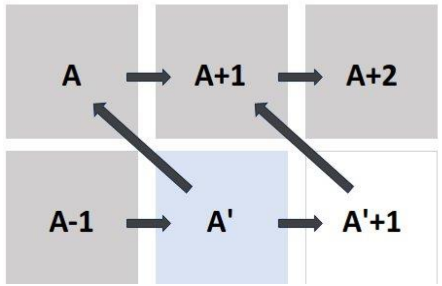

Rapid Neutron Capture (r-process)

- Takes place in **core collapse supernovae** (CCSNe) and **neutron star mergers** (NSM)
- Neutron density $>10^{20}$ cm^{-3}
- τ_n ~ [s] synthesises the heaviest element along each isotopic chain till freeze-out, followed by decay to stability

The Problem

Slow Neutron Capture (s-process)

Abundance of isotopes, particularly at branching points, depends on

- Maxwell Averaged Cross Sections (MACS) of neutron capture and
- **β-decay rates**

$$B = \frac{N_s(A,\tau)\langle\sigma\rangle_A}{N_s(A+1,\tau)\langle\sigma\rangle_{A+1}} = \frac{\lambda_\beta(A')}{\lambda_\beta(A') + \lambda_{n\gamma}(A')}$$

S. Palmerini et al, ApJ ***921****, 7 (2021)*

Rapid Neutron Capture (r-process)

Kilonova light curve analysis can furnish details on r-process nucleosynthesis, but modelling light curves requires knowledge of **elemental opacity**

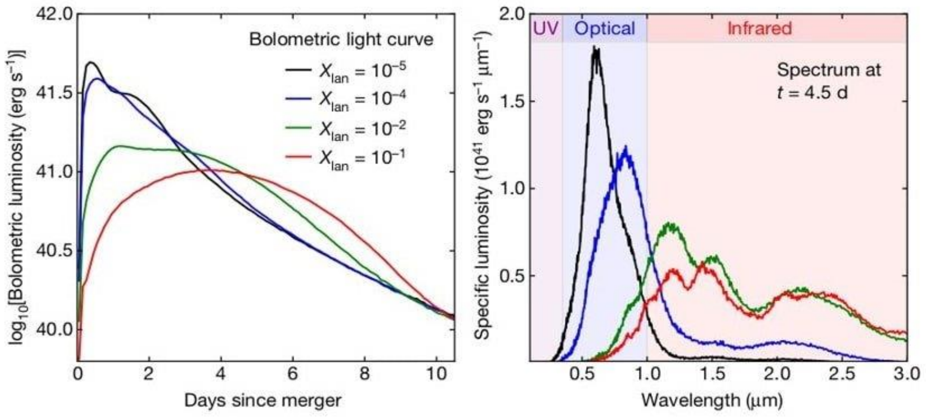

B.D. Metzger, Kilonovae. Living Rev Relativ ***23*** *(2020)*
D. Watson et al. Nature ***574497-500*** *(2019)*

Stars and neutron star merger ejecta as plasmas:
How sure are we about these quantities in a plasma environment?

PANDORA main goal: *Investigating β-radioactivity in a «stellar» environment*

Make β-decay measurements in plasmas of astrophysical interest: ***many isotopes can change their lifetime of several order of magnitude when ionized!!***

The effect is mainly driven by the opening of a new decay channel: the bound state beta decay

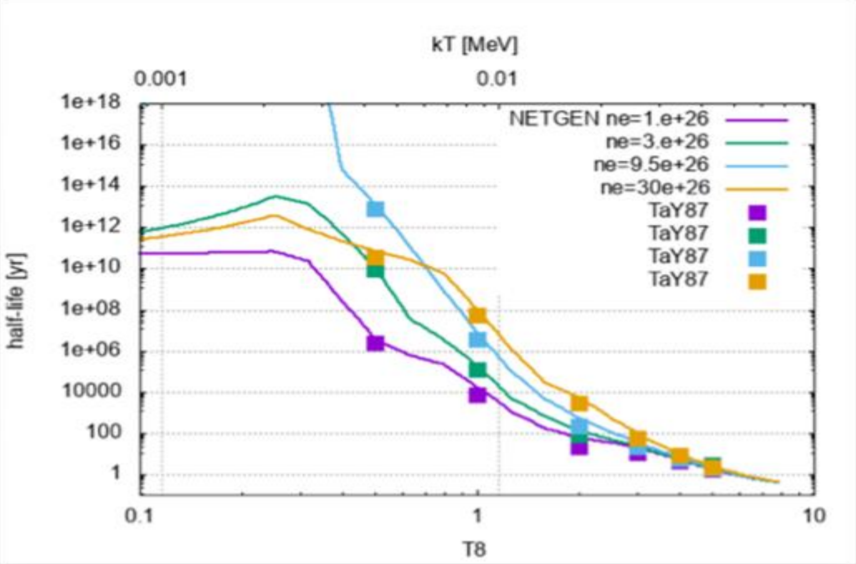

Takahashi et al. 1987, Phys Rev C 36, 1522.

Direct implication on branching points in s-process nucleosynthesys chain competition of neutron capture vs β-decay

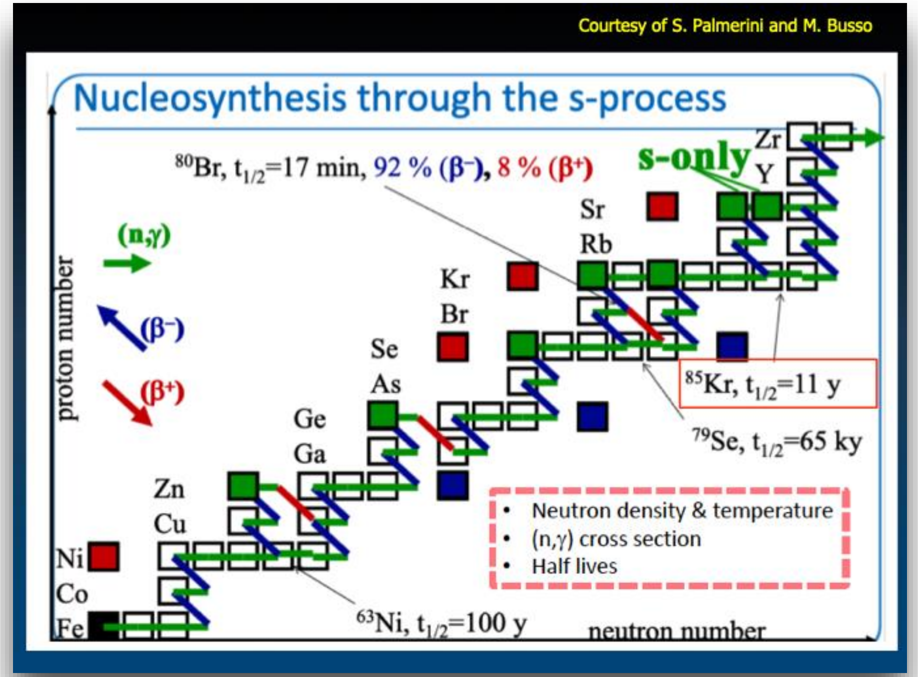

Isotope	$T_{1/2}$ (yr)	Eg (keV)
^{176}Lu	3.78×10^{10}	88-400
^{134}Cs	2.06	>600
^{94}Nb	2.03×10^{4}	>700

COSMO-CHRONOMETER

reproduction of ^{134}Ba, ^{136}Ba s-only isotope yields

Solving the puzzle about the contribution of s-processing to ^{94}Mo: β-decay or binary stars

Other Astrophysical implications of β-decays in plasmas

NUCLEOSINTHESIS

→ <u>β-decay occur with hugely different lifetimes in a plasma:</u> this has a huge impact in stellar nucleosynthesis chains

→ **COSMOCHRONOMETERS: ^{187}Renium, ^{176}Luthetium, etc**

^{14}C: for dating of fossils
$T_{1/2}$ = 8267 years

^{187}Re: dating astrophysical or cosmological objects
$T_{1/2}$ = 42 billios of years!

The cases of ^{187}Re or **^{176}Lu are quite impressive**:
→ Neutral atoms have lifetime of **<u>>30 billions of years</u>**,
In can be **<u>reduced to 30-40 years only</u>** if in plasma-highly ionized state!

<u>A BILLION OF TIMES SHORTER!!!</u>

<u>sulla Terra</u>

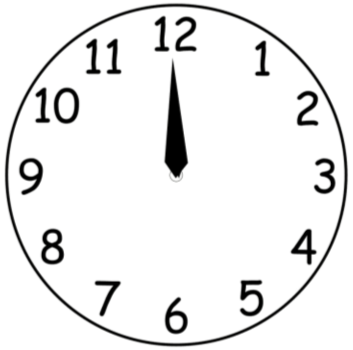

<u>in Plasma</u>

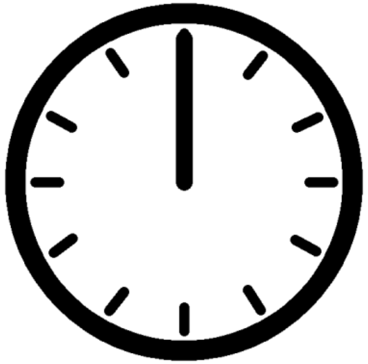

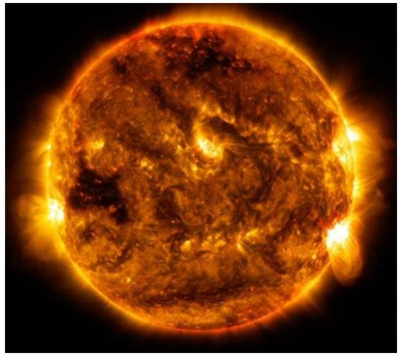

https://www.nasa.gov/multimedia/imagegallery/iotd.html

PANDORA: A New ECRIT – ECR Ion Trap for β-decay measurements in plasmas

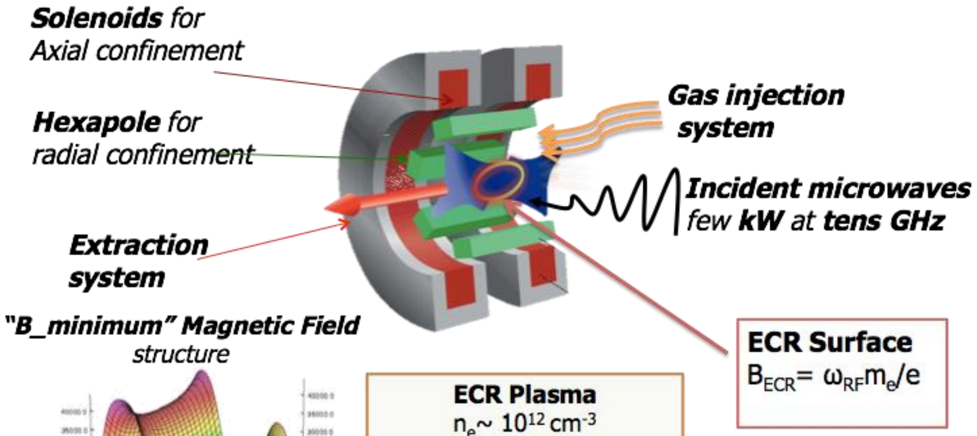

***"B_minimum" Magnetic Field** structure*

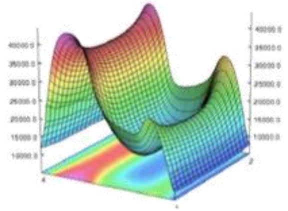

ECR Plasma
$n_e \sim 10^{12}$ cm^{-3}
$T_e \sim$ tens keV
$T_{ion} \sim$ ms

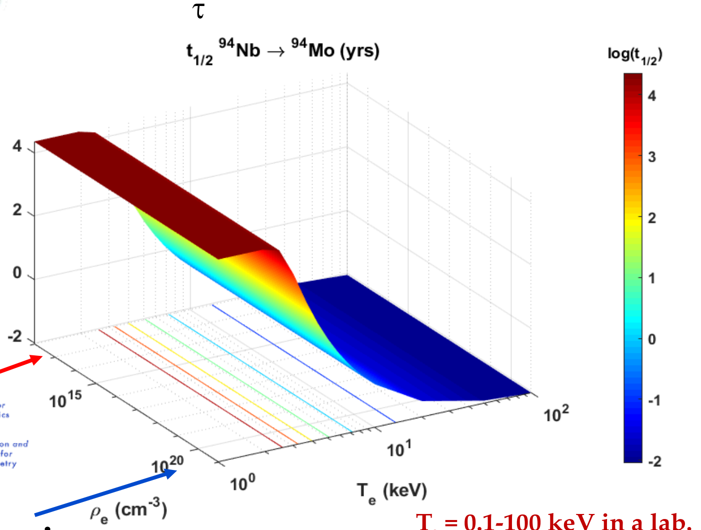

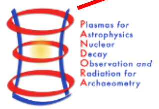

Nucleosynthesis in stars

T_e = 0.1-100 keV in a lab. Magnetoplasma

Variation with T_e stronger than with ρ so "stellar effect" can be modelled in ECR plasmas

Magnetic traps for hot plasmas excited by e.m. waves

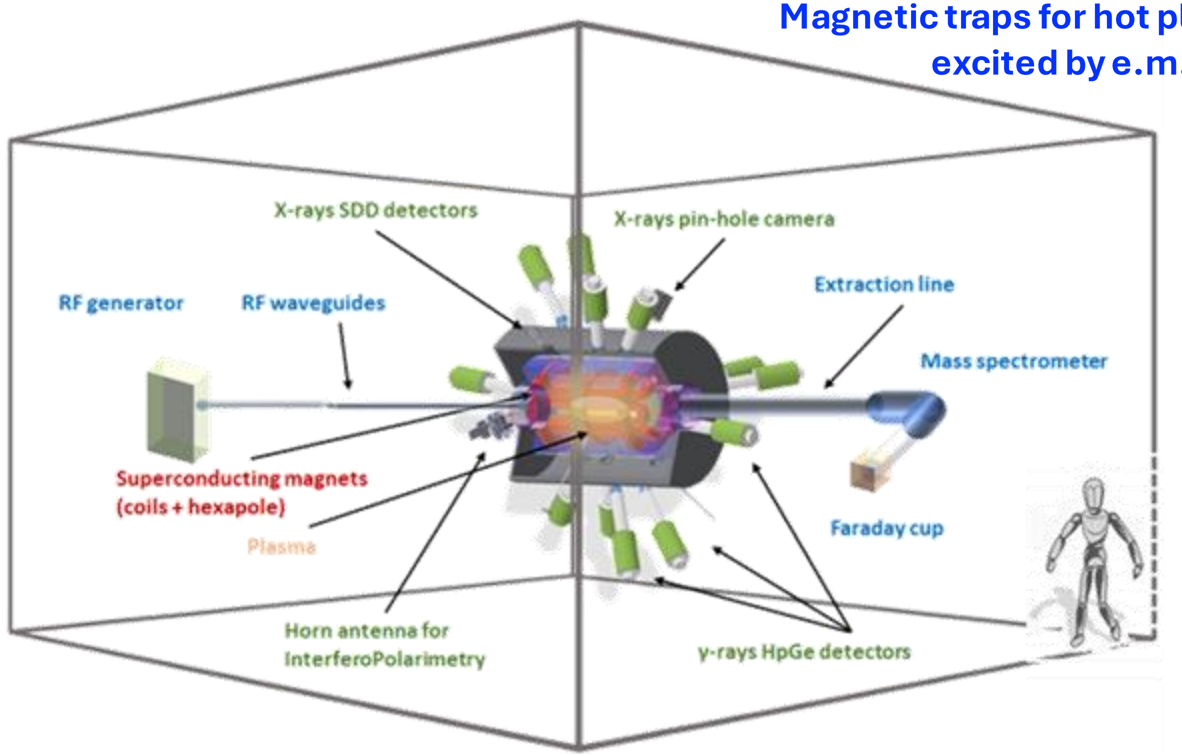

Additional Goal

- Measuring plasma opacity relevant for compact binary ejecta (Kilonovae)

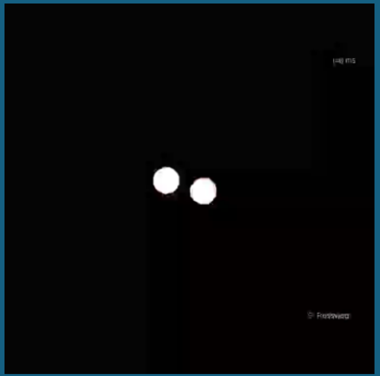

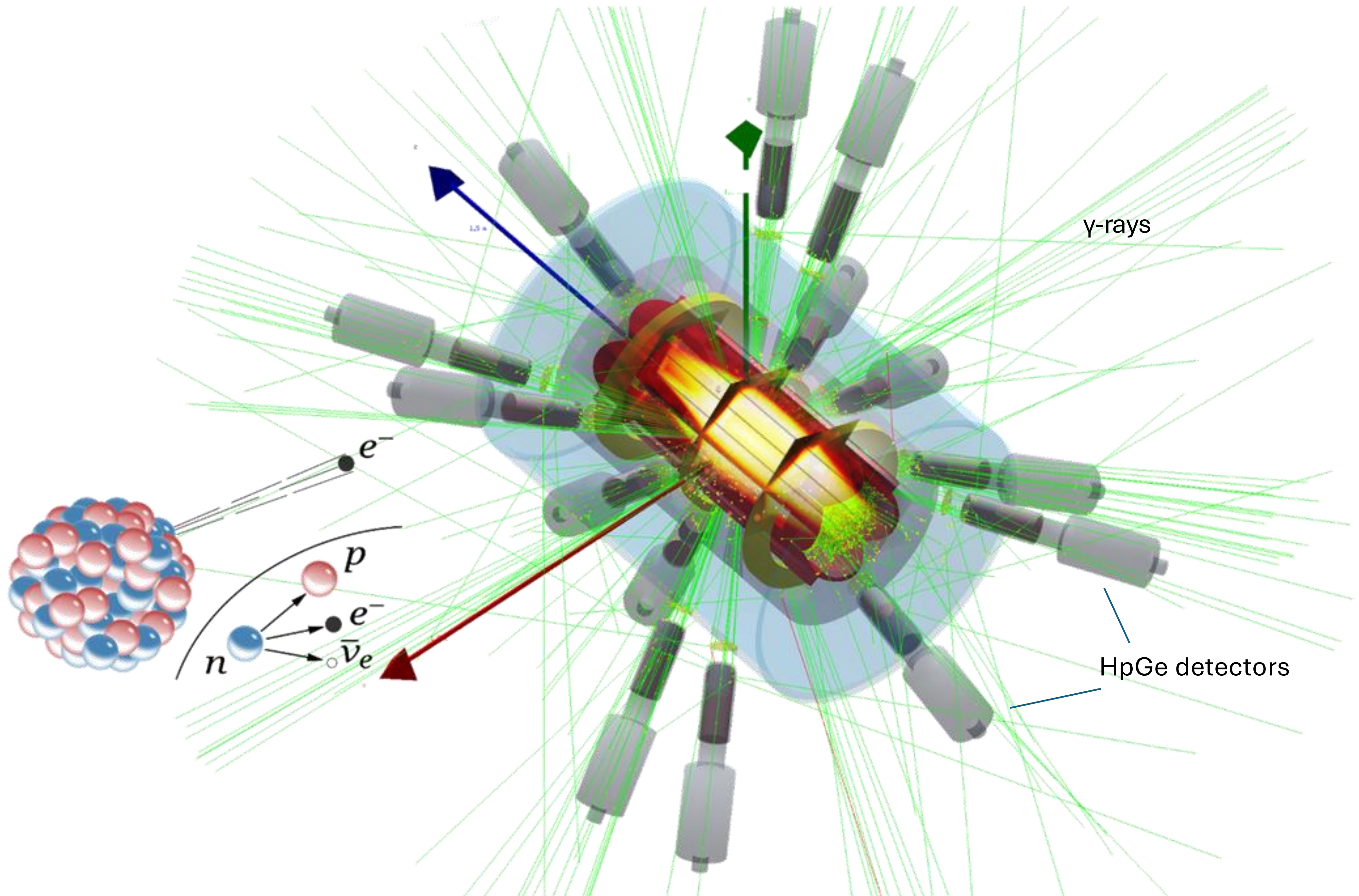
γ-rays
HpGe detectors
e^-
p
e^-
n
$\bar{\nu}_e$

A challenge similar to the “fusion dream”…

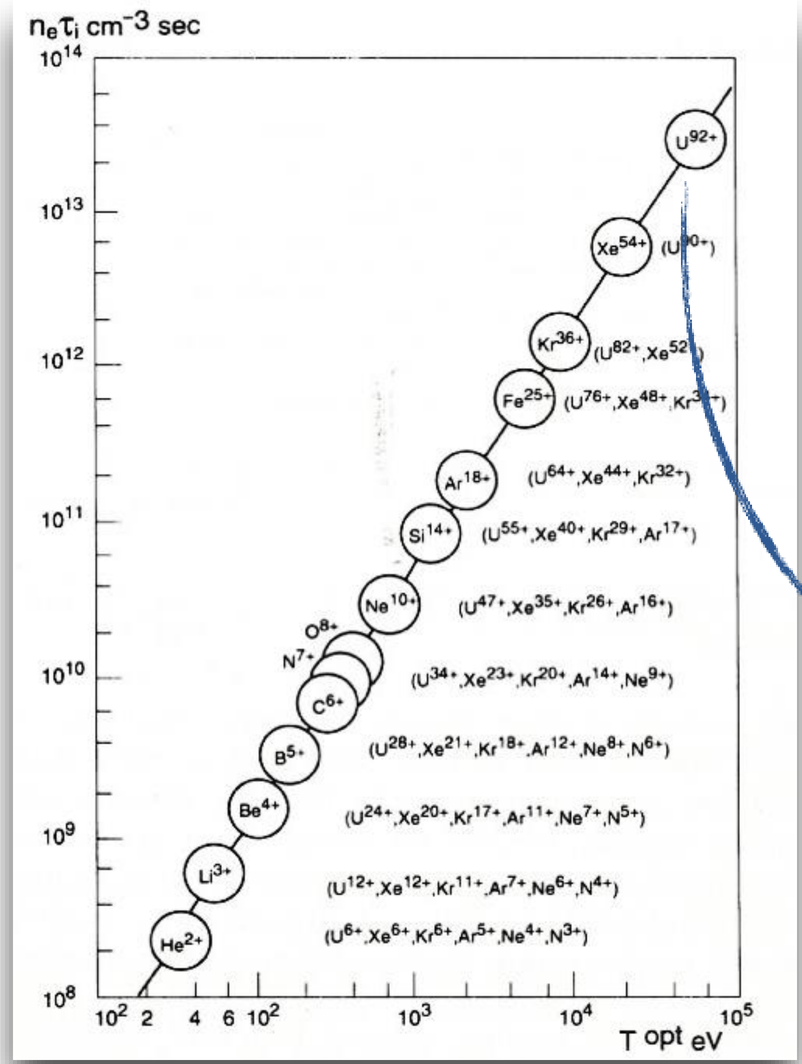

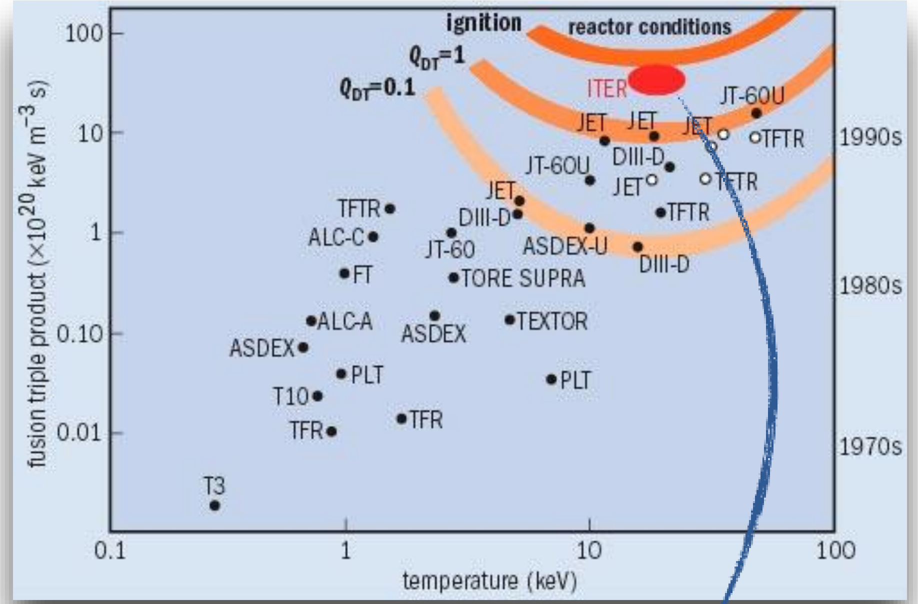

The triple product of density, magnetic field and temperature for obtaining fully-stripped heavy ions is the same of “Ignition”

BROAD RANGE OF TEMPERATURES AND DENSITIES

- Plasma temperatures and densities range from relatively cool and tenuous (like aurora) to very hot and dense (like the central core of a star)
- The word "PLASMA" was first applied to ionized gas by Irving Langmuir, an american chemist and physicist, in 1929.

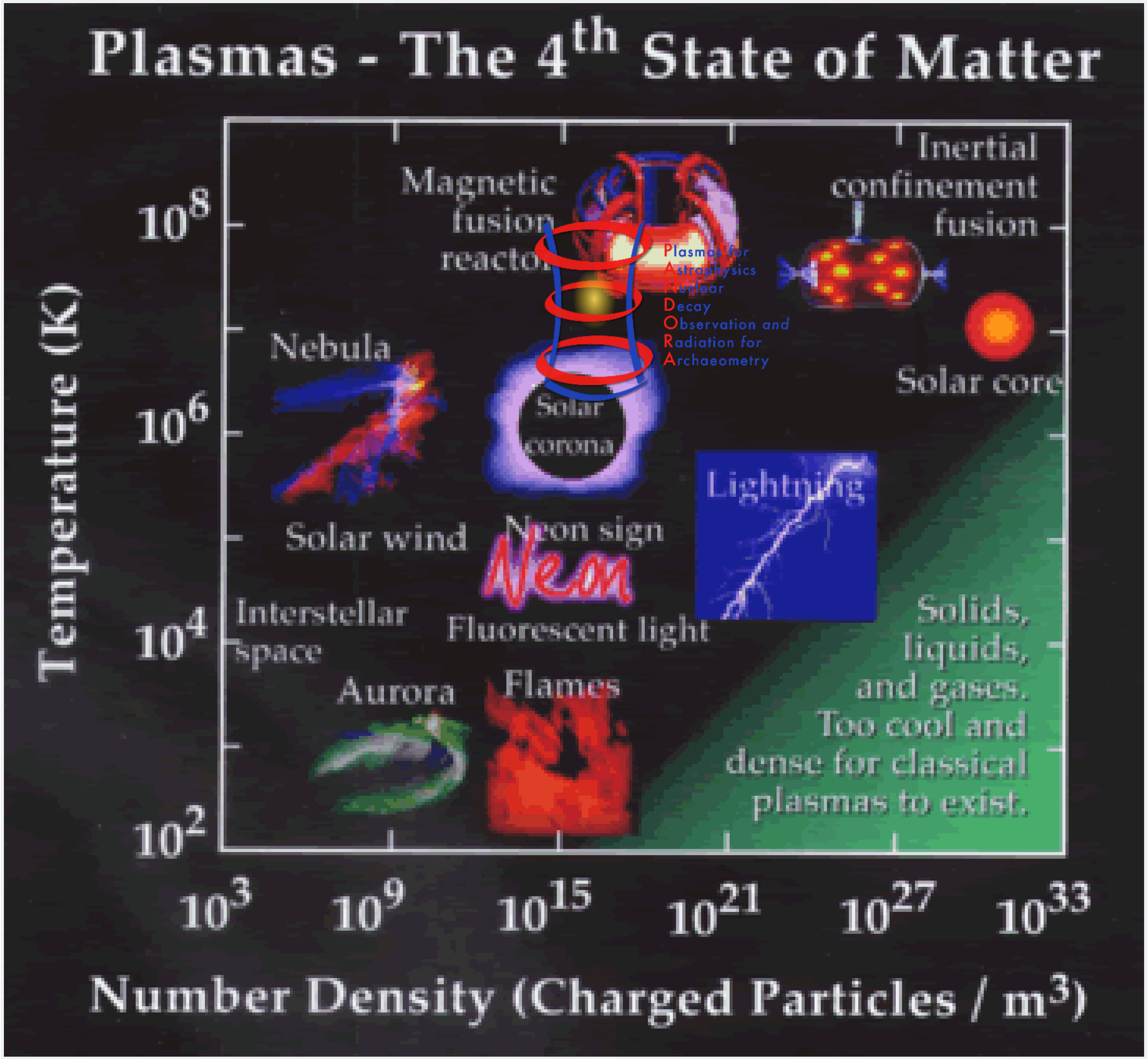

Magnetic Confined plasmas

Magnetic fields intrinsically force charged particles to reduce freedom degrees: electrons spiralyze around the field lines and can be trapped for several ms in mirror machines or toroidal structures.

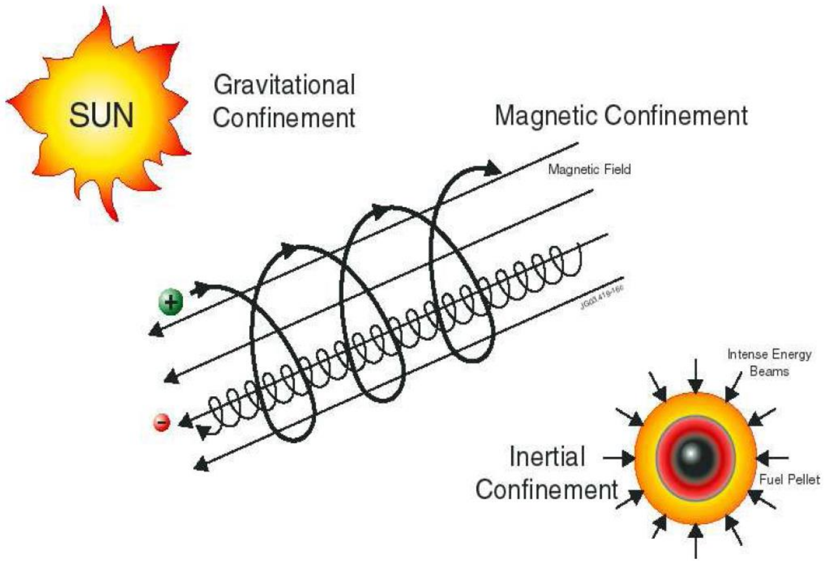

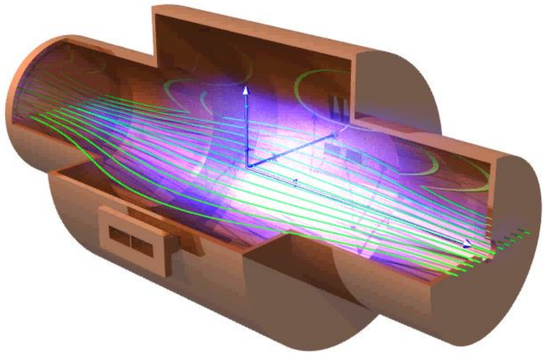

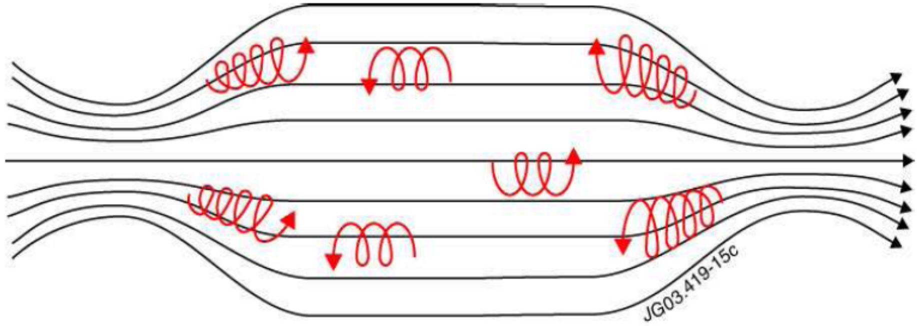

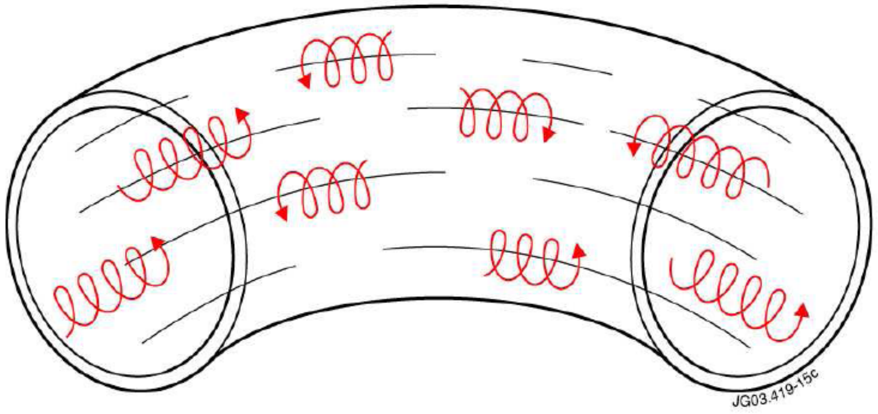

MIRROR STRUCTURES
have axial symmetry and can be produced by sequences of room temperature or SC coils. They are commonly used in ion sources field

TOROIDAL CONFINEMENT
is typical of Fusion Machines like TOKAMAKS or STELLARATORS

How do plasmas can be confined?

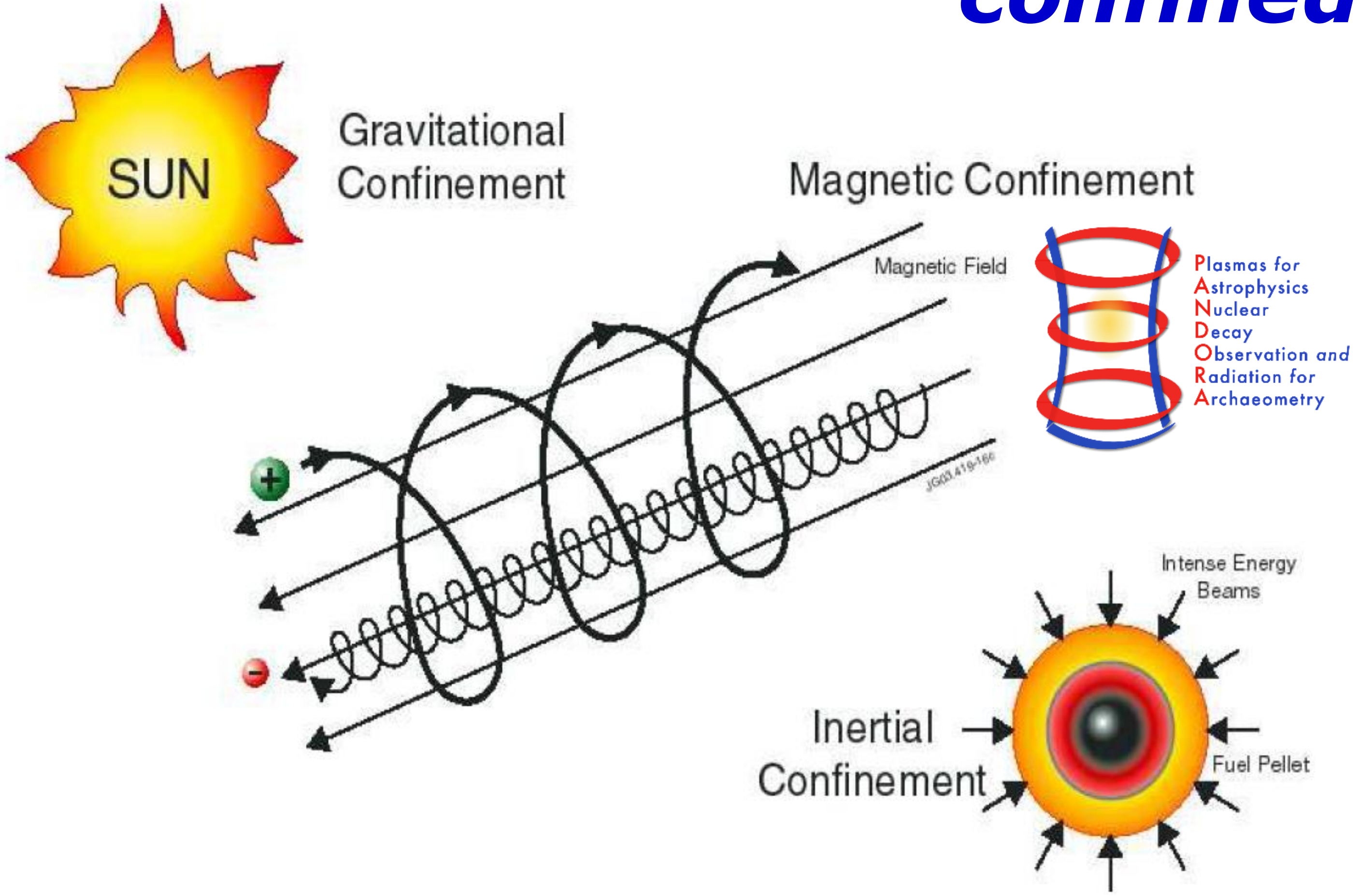

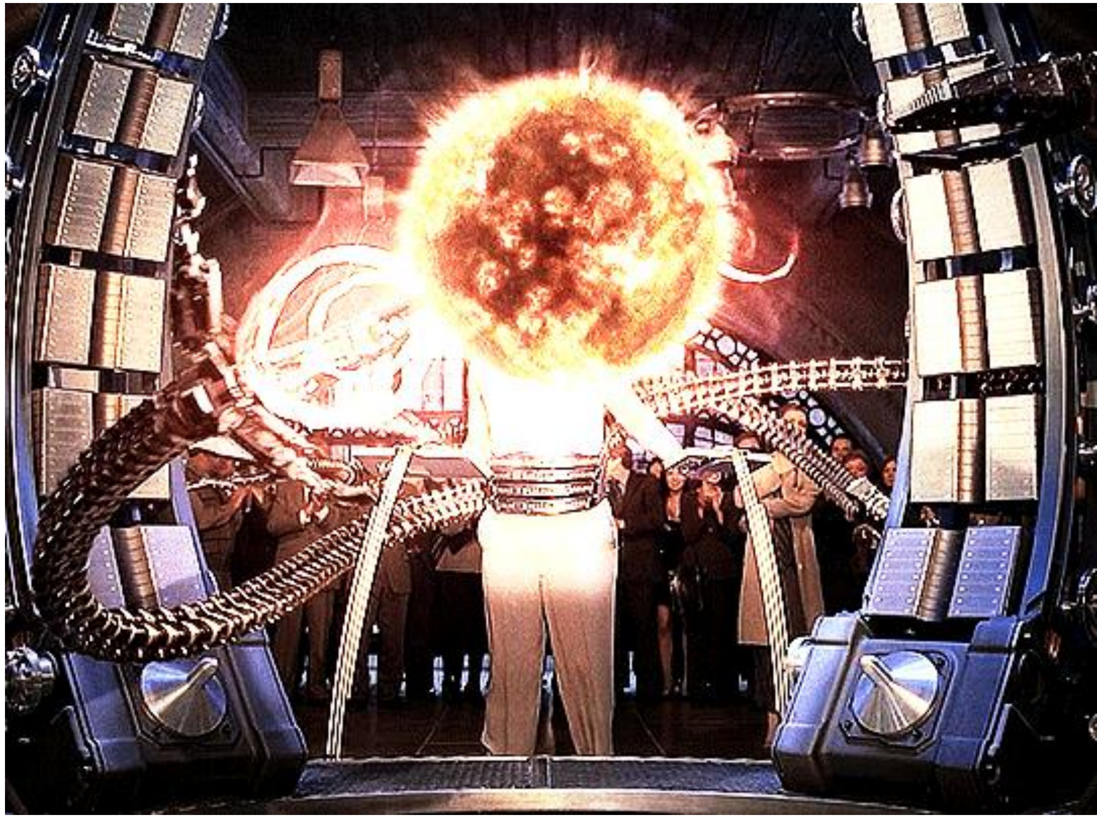

Thermonuclear reactors and Ion sources are typically based on magnetic confinement

PRINCIPLES OF QUASI-AXYSYMMETRIC ECR TRAPS

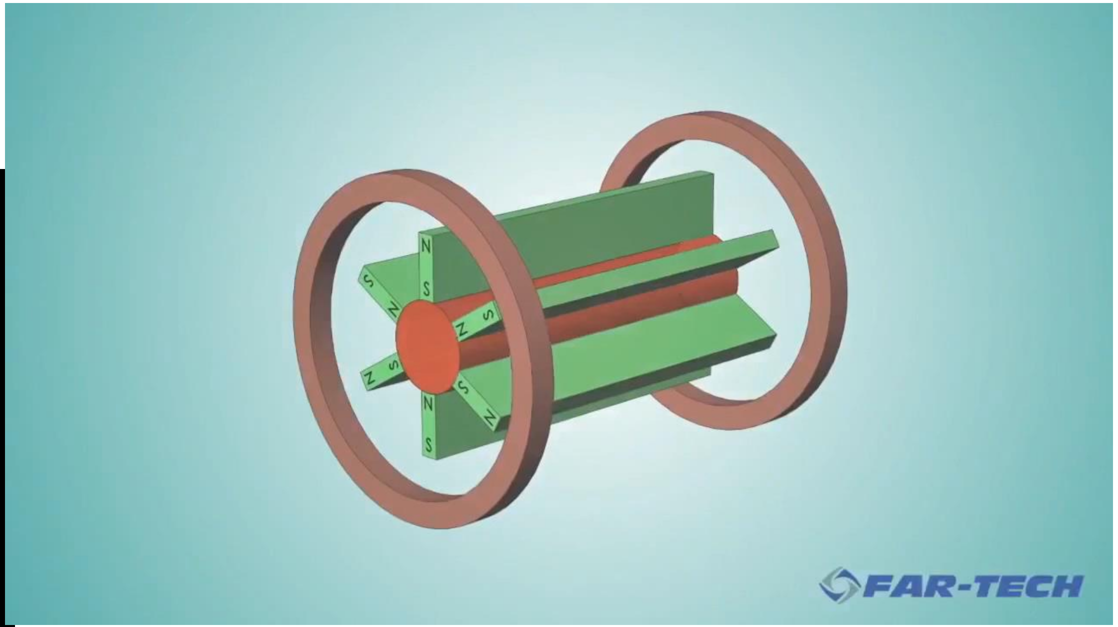

The ELECTRON CYCLOTRON FREQUENCY ω_C :

$$\omega_C = eB/m$$

<u>Electron Cyclotron Resonance</u>:

$$\omega_{RF} = \omega_C = eB/m$$

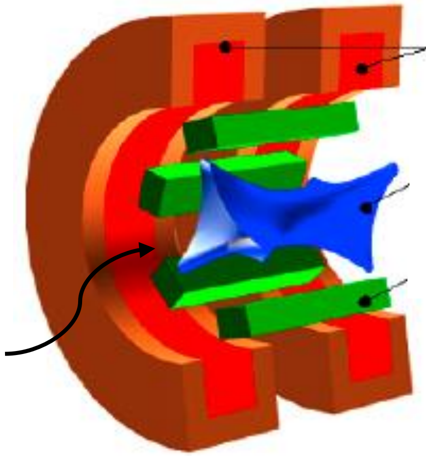

Fundamentals of Beta decay theory

The comprehension of beta decay theory is central to understand the effect of stellar conditions on β-decay lifetimes

Stellar environment

$({}^A_Z X_N)^{i,j} \rightarrow ({}^{A}_{Z+1} Y_{N-1})^{i+1,j'} + e_f^- + \bar{\nu}_e$ (continuum state β^- decay)

$({}^A_Z X_N)^{i,j} \rightarrow ({}^{A}_{Z-1} Y_{N+1})^{i-1,j'} + e_f^+ + \bar{\nu}_e$ (continuum state β^+ decay)

$({}^A_Z X_N)^{i,j} \rightarrow ({}^{A}_{Z+1} Y_{N-1})^{i,j'} + e_b^- + \bar{\nu}_e$ (bound state β decay)

$({}^A_Z X_N)^{i,j} + e_b^- \rightarrow ({}^{A}_{Z-1} Y_{N+1})^{i-1,j'} + \nu_e$ (electron capture)

$({}^A_Z X_N)^{i,j} + e_f^- \rightarrow ({}^{A}_{Z-1} Y_{N+1})^{i,j'} + \nu_e$ (free electron capture)

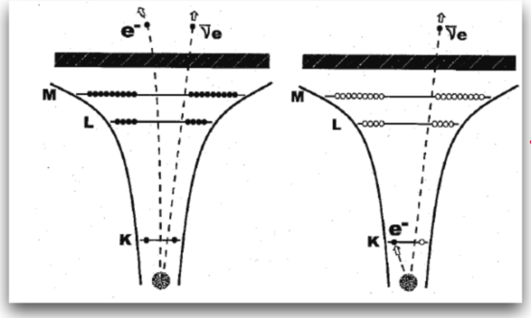

A more general form the Q value for:

- continuum state β^- decay
- bound state β^- decay
- orbital EC

$$Q = [m({}^A_Z X_N) - m({}_{Z+1}^{\ A} Y_{N-1})]c^2 + \boxed{[E^*_X - E^*_Y]} + [B_X - B_Y] - \boxed{[B^*_{X_x} - B^*_{Y_{x+1}}]} + \boxed{[e^*_{X_{x,k}} - e^*_{Y_{x+1,k'}}]}$$

E^*_X : excited nuclear state energy
B^*_X : ionisation energies to obtain a charge state
e^*_X : level excitation energies of state *j* of a nucleus with charge state i

For continuum state β^+ decay: $Q - 2m_ec^2$

For free EC: $+K_e$

Decay rate in stellar environment

$$\lambda_{tot} = \left[\frac{\ln 2}{f_{IF(m)} t_{1/2}}\right] \sum f^*_{IF(m)}$$

CSD and level population of ions

EEDF of electrons

The ***ft*** of the decay is given, from the theory, by the relation:

$$f_L(Z', Q) t_{1/2} = \frac{(\ln 2) 2\pi^3 \hbar^7}{g^2 m_e^5 c^4 |M^L_{if}|^2}$$

Terrestrial and stellar decays can have widely different f_L and therefore different $T_{1/2}$

Fundamentals of β-Decay

$$\boxed{f_L(Z', Q_0)}\boxed{T_{1/2}} = \frac{(\ln 2)2\pi^3\hbar^7}{g^2 m_e^5 c^4 \boxed{|\mathcal{M}_{if}^L|^2}}$$

Lepton phase volume

- *Describes the volume of the phase space (position + momentum) that can be occupied by the electron-neutrino pair*
- *Depends on electronic configuration of atomic shells*

Decay half-life

Nuclear Matrix Element (NME)

- *Indicates the transition strength*
- *Depends on the levels of the parent and daughter nucleus, and selection rule*
- *Purely nuclear in nature, no dependence on electronic configuratiion*

- $f_L(Z',Q_0)T_{1/2}$ is connected to the NME and is independent of atomic configuration
- If $f_L(Z',Q_0)$ changes, $T_{1/2}$ changes as well keeping the product constant
- NME is expressed and recorded in literature as log *ft* value

General Model of In-Plasma β-Decay

β-Decay Rates of Individual Ions + Ion Charge State Distribution in Plasma → In-plasma rates

Calculated with appropriate plasma model

- Uniform plasma with fixed n_e and k_BT_e → Decay rate In uniform plasma (ex. stellar interior)

- Non-uniform plasma with space-resolved n_e and k_BT_e → Decay rate in laboratory plasma (ex. PANDORA)

By validating the model with PANDORA, the parameters can be modified to reflect the stellar plasma and calculate in-plasma β-decay rate in s-process nucleosynthesis sites.

Orbital Electron Capture Decay in ^{7}Be for *ij* configuration

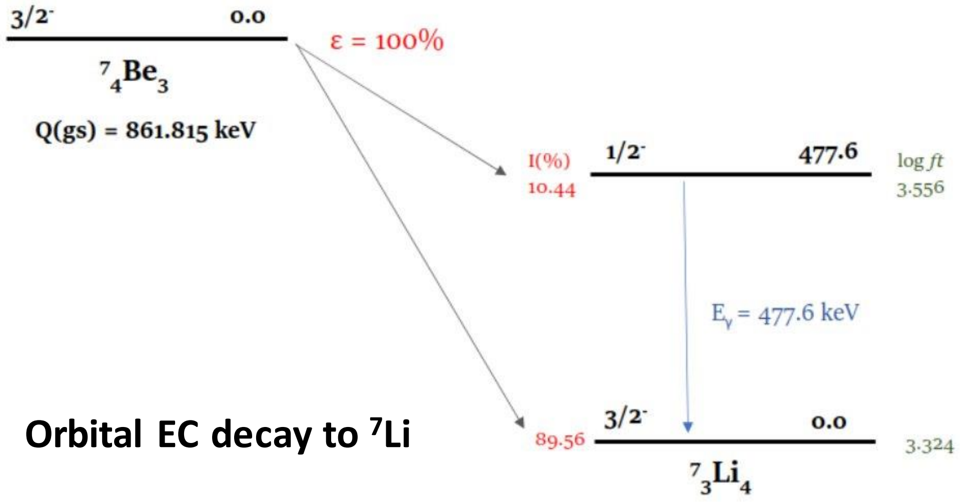

Orbital EC decay to ^{7}Li

NB: 7Be is considered for PANDORA phase 2, but it was taken as first isotope for decay estimate due to small number of electrons and its relevance in cosmology and solar physics

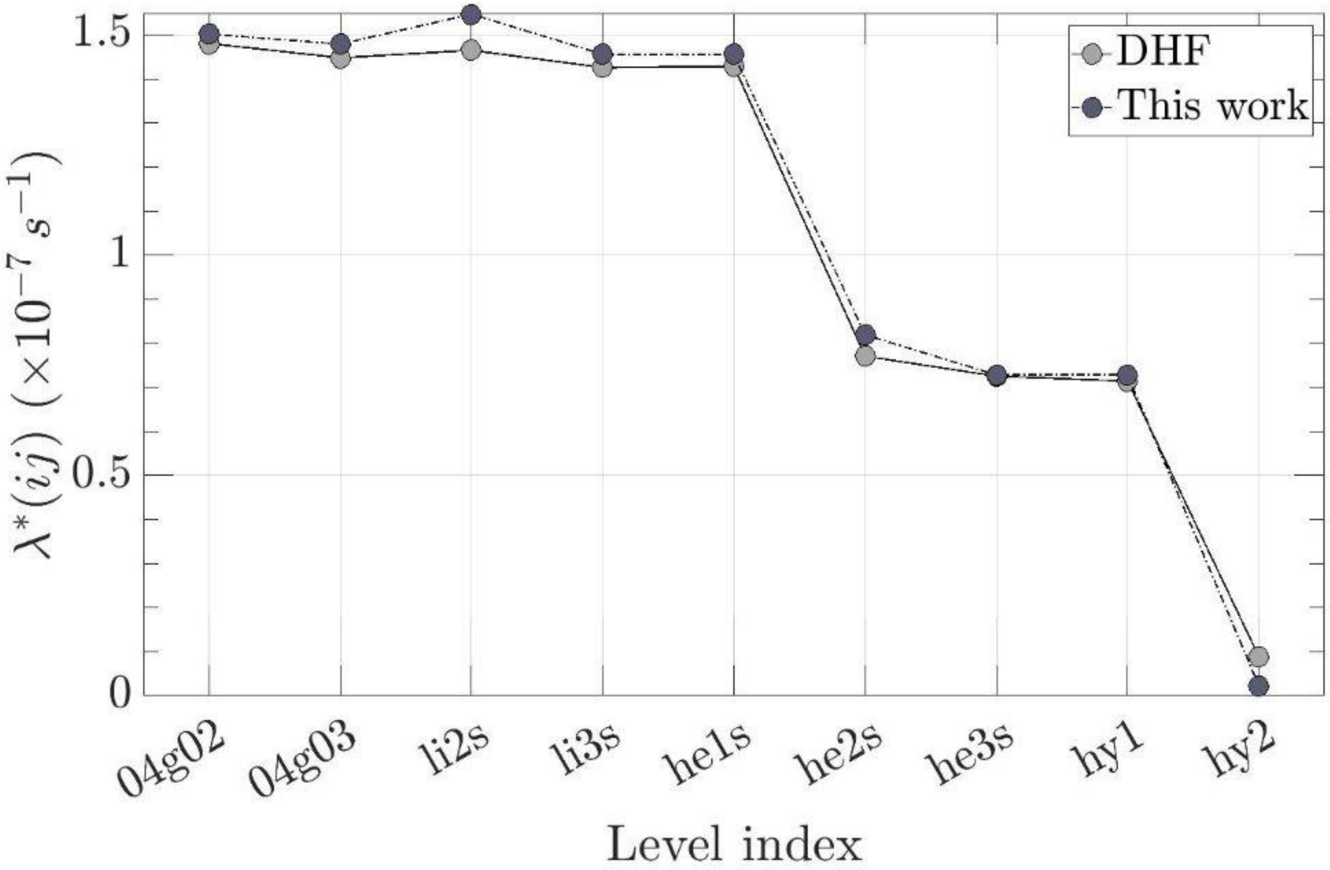

Lepton phase volume for charge state *i* and level *j*

$$f^*_{m,EC/\beta_b}(ij) = \sum_{x(ij)} \sigma_x(\pi/2)[g_x \text{ or } f_x]^2(Q/m_e c^2)^2 S_{(m)x(ij)}$$

Configuration-Dependent Decay Rate

$$\lambda^*(ij) = \ln 2\left(\frac{f^*_{gs}(ij)}{f_{0,gs}t} + \frac{f^*_{es}(ij)}{f_{0,es}t}\right)$$

Orbital Electron Capture Decay in ^{7}Be in uniform plasma

Configuration-Dependent Decay Rate

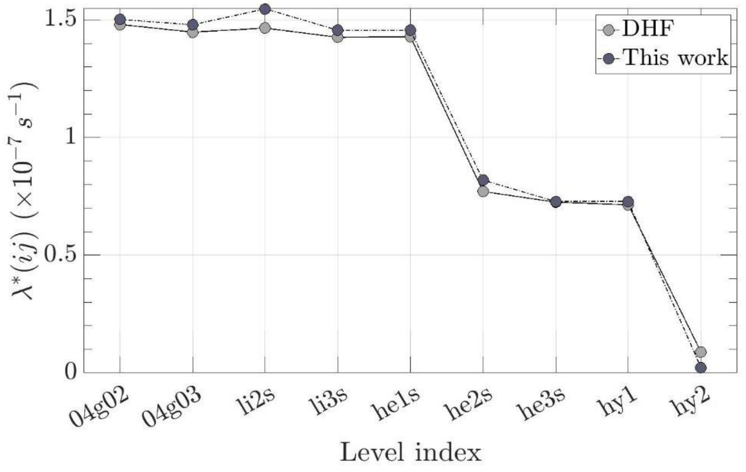

Ion CSD in uniform plasma with n_e=10^{12} cm^{-3} and varying k_BT_e

Calculated with FLYCHK under LTE and NLTE conditions

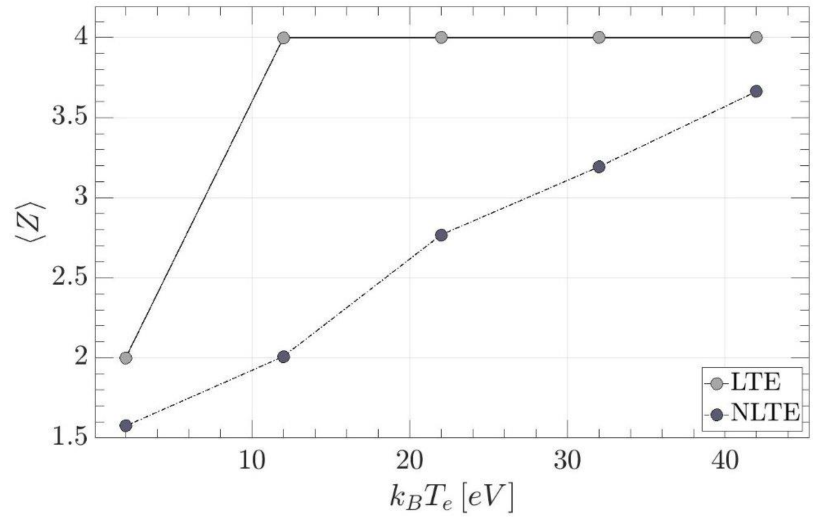

In-plasma orbital EC rate

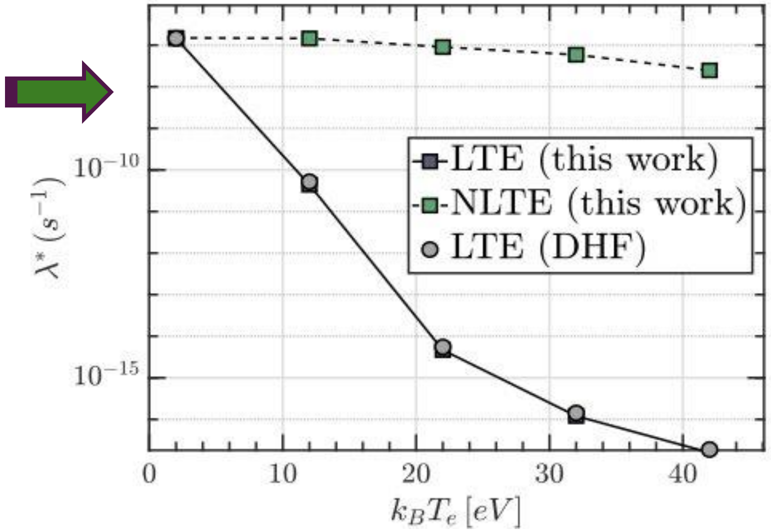

Results highlight that in-plasma decay models designed for LTE plasmas (ex. DHF) will predict wrong values in NLTE plasmas like PANDORA. The new model is universal and can be applied to both systems.

Bound State Beta Decay in heavier nuclei

Calculations are now almost ready for 134Cs, that is in the PANDORA shortlist !!

BSBD in Fully-Ionised System: $^{163}Dy^{66+} \rightarrow ^{163}Ho^{66+}$

Calculating decay rate: (3) Rate λ and $T_{1/2}$

$$\lambda^* = \ln 2 \sum_m \sum_{ij} p_{ij} \frac{f^*_m(ij)}{f_{m0} T_{1/2}} \xrightarrow{\text{Simplified formalism}} \lambda^*(ij) = \ln 2 \left(\frac{f^*_m(ij)}{f_{m0} T_{1/2}} \right)$$

Only one charge state considered hence no CSD and LPD (no p(ij)). Also, only a single transition (m) considered

$\log(f_{m0} T_{1/2}) = 4.99$

$^{163}Dy^{66+}$ BSBD $T_{1/2}$ 47^{+5}_{-4} d measured by Jung et al
[M. Jung, F. Bosch et al, First Observation of Bound State β- Decay, Phys. Rev. Lett 69, 2164 (1992)]

Parent→daughter	Transition [E(keV), J^π]	Decay mode	Q_b (keV)	Estimated $\log ft$	Neutral T	Bare $T_{\beta_b^-}$
$^{163}_{66}$Dy → $^{163}_{67}$Ho	$[0.0, \frac{5}{2}^-] \rightarrow [0.0, \frac{7}{2}^-]$	*a*	49.837	4.99	Stable	49.52 d

$^{163}Dy^{66+}$ BSBD $T_{1/2}$ calculated by Liu et al

$^{163}Dy^{66+}$ BSBD $T_{1/2}$ calculated by this model = ln 2/λ*(ij) = 49.77 d

Build a plasma trap where ion species are confined in a magnetic field and a plasma is created with:

- Electron Density: $10^{12} - 10^{14}$ cm^{-3}
- Electron Temperature: 0.01 – 100 keV
- Ion Density: 10^{11} cm^{-3} (this density values relies on the radiactive isotope concentration in plasma)
- Ion Temperature: ~ 1 eV

Gamma-rays emitted by the daughter nuclei after the beta decay will be detected by an array of HPGE

$$\boxed{\frac{dN}{dt} = \lambda n_i V} \Rightarrow \int_0^{t_{meas.}} dN = \int_0^{t_{meas.}} \lambda n_i V dt \Rightarrow \boxed{N(T_{meas.}) = \lambda n_i V_{plasma} T_{meas.}}$$

$\lambda n_i V$ is constant

Isotope decay constant

Density of the isotope in the plasma (const.)

Plasma volume (const.)

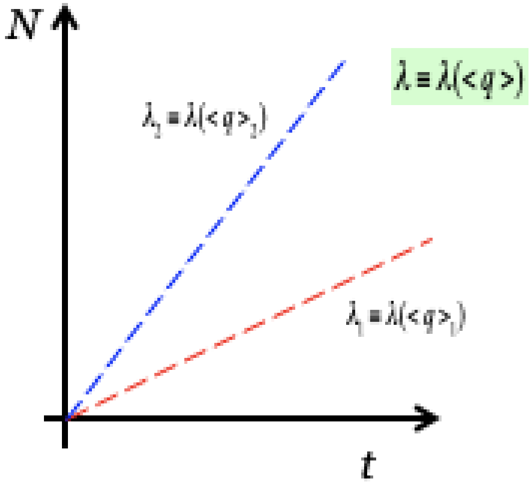

Charge State Distribution f (ρ_{plasma}, T_{plasma})

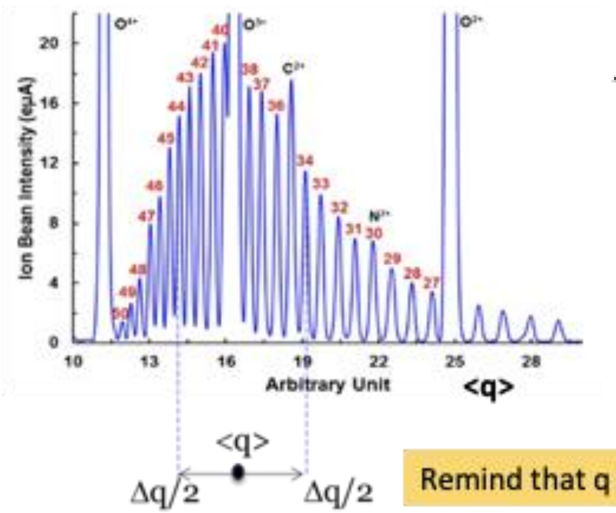

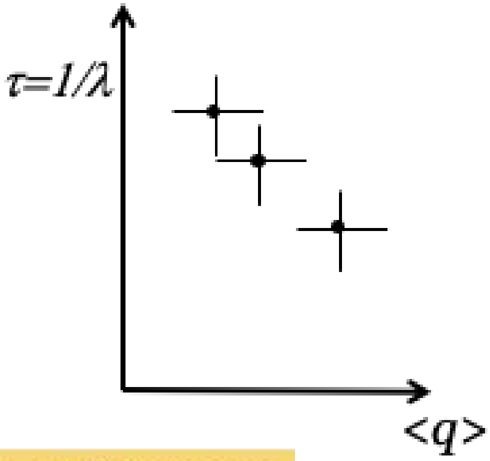

Remind that q = q(r) in the plasma

Plasma parameters to be measured using multiple diagnostic tools

MAIN SUBSYSTEMS UPDATES: Trap procurement
(LNS ACTIVITY)

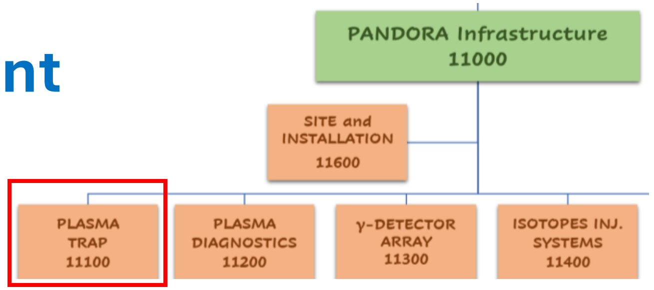

The magnetic system, fully superconductive, consists of:

1. #3 axial coils that generates the axial magnetic field;
2. #6 hexapole coils that generates the radial magnetic field.

It will enclose a plasma chamber with:

- inner radius $\mathbf{R_{CH\_IN} = 140}$ **mm**
- length **L = 700 mm**.

MAGNETIC FIELD REQUIREMENTS	
B_{inj} max @ z = - 350 mm	3 T
B_{inj} operative range	1.7 T – 3 T
B_{ext} max @ z = 350 mm	3 T
B_{ext} operative range	1.7 T – 3 T
B_{min} @ z = 0 mm	0.4 T
B_{hex} @ R_{CH_IN} = 140 mm	1.6 T
Lhe	Free
Warm Bore radius	150.5 mm
Distance between mirrors	700 mm
Stray field (as above specified)	Less than 0.2 T

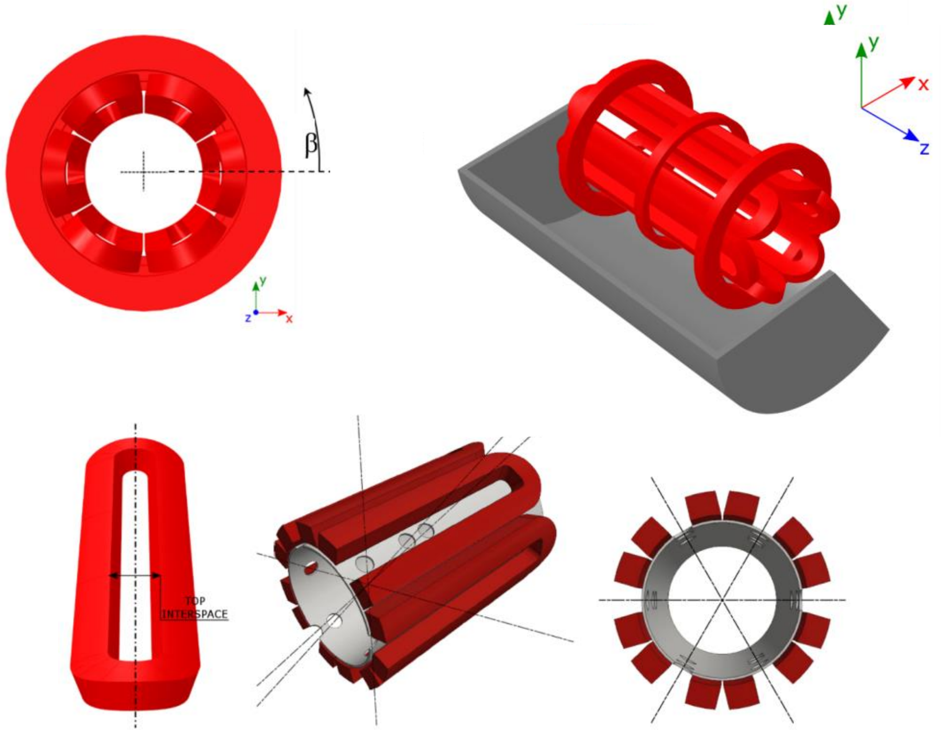

The PANDORA's trap has been designed to operate at 18 + 21 GHz.

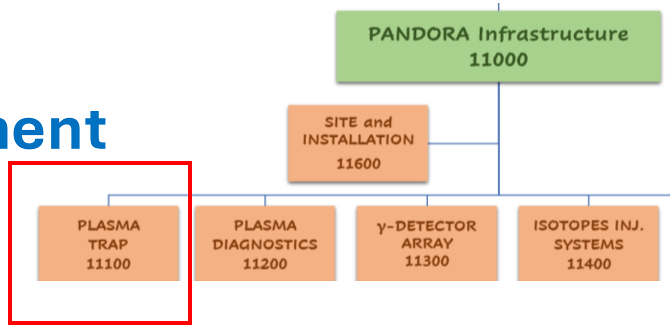

MAIN SUBSYSTEMS UPDATES: Trap procurement

Competitor #1-Executive Design

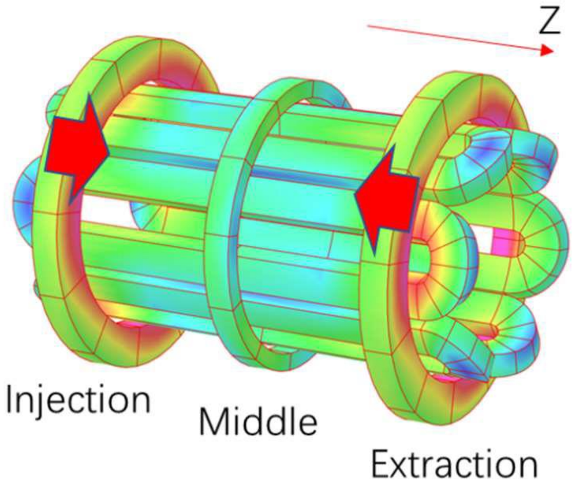

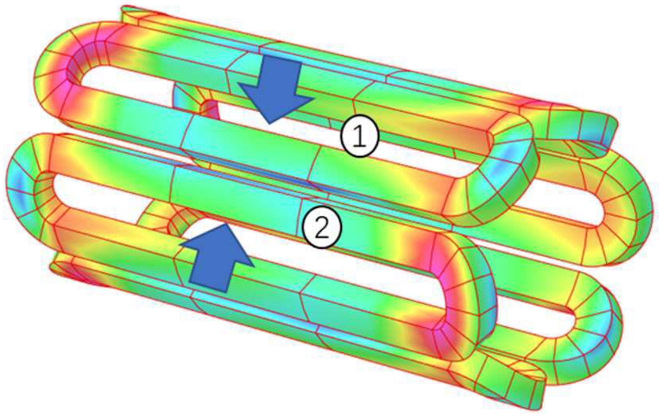

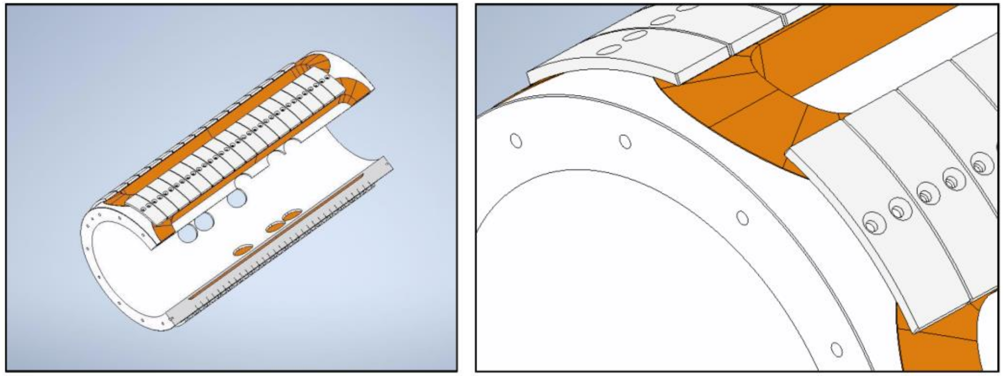

Detail of radial containment brackets

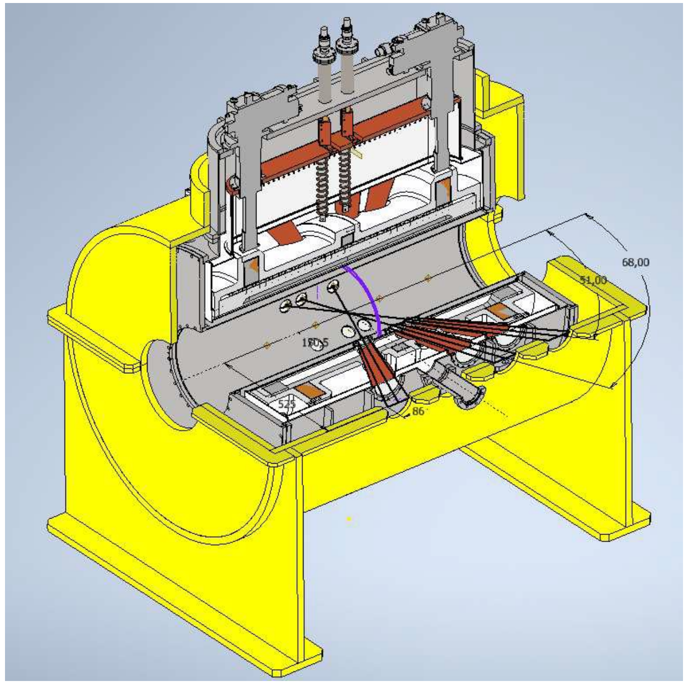

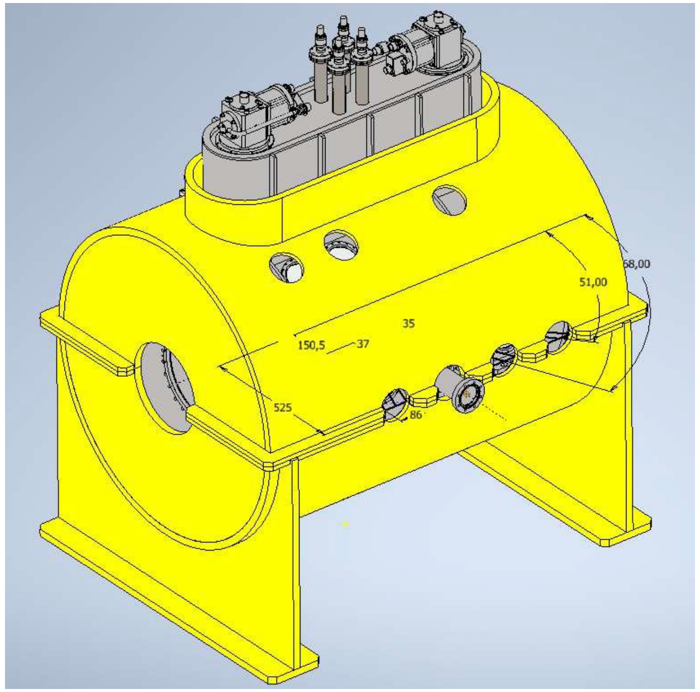

Both the competitors are able to provide the total number of requested holes

Different solutions in SC wire alloys, clamping, etc

MAIN SUBSYSTEMS UPDATES: RF system

(LNS ACTIVITY)

GREEN: already purchased
YELLOW: planned to be procured in 2024

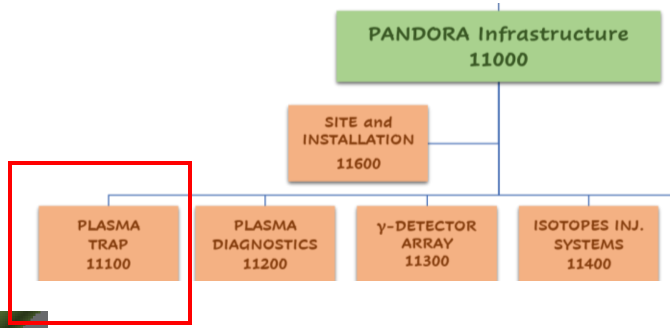

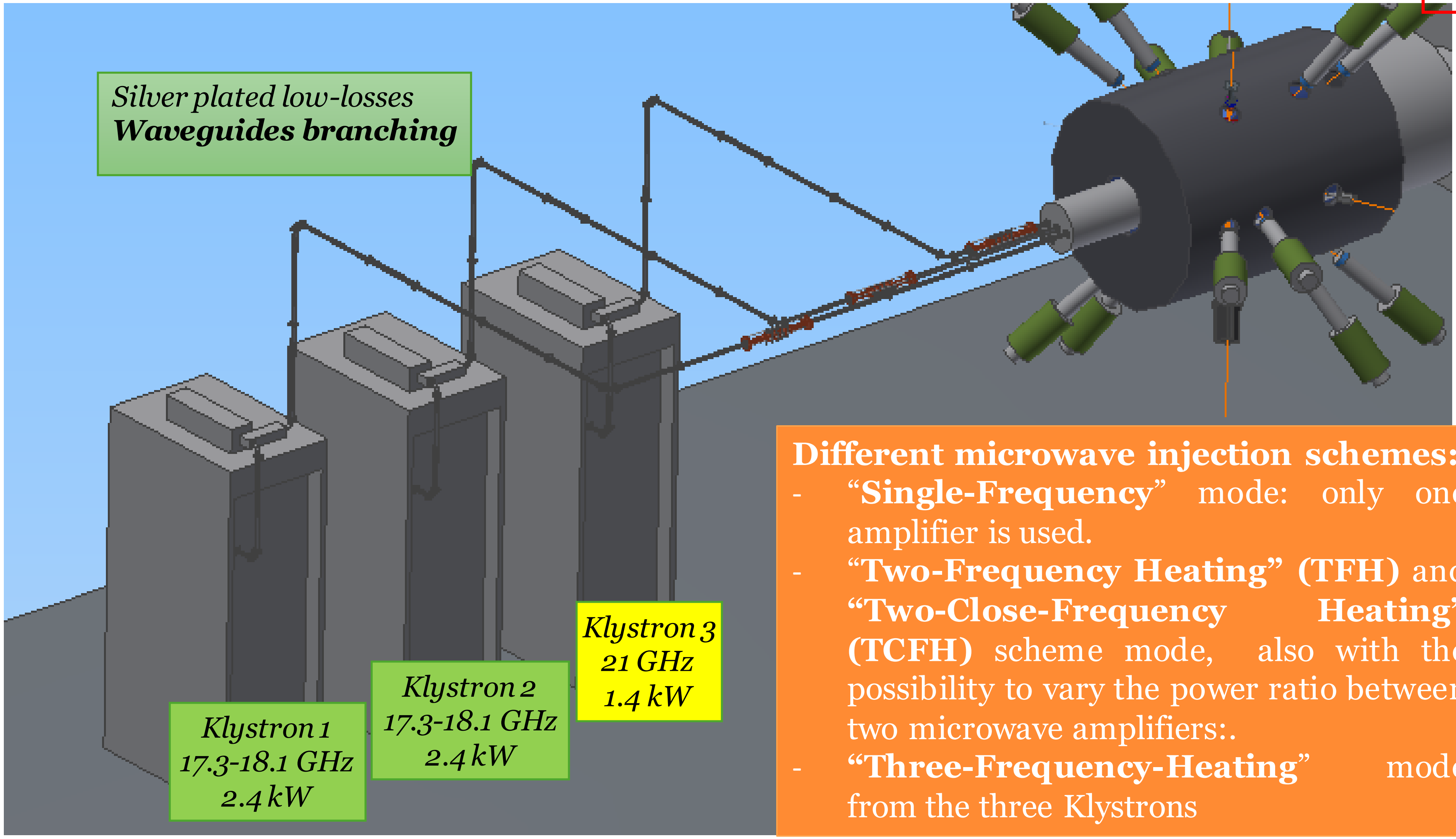

Different microwave injection schemes:

- **"Single-Frequency"** mode: only one amplifier is used.
- **"Two-Frequency Heating" (TFH)** and **"Two-Close-Frequency Heating" (TCFH)** scheme mode, also with the possibility to vary the power ratio between two microwave amplifiers:.
- **"Three-Frequency-Heating"** mode from the three Klystrons

Target power density of 1.38 kW/l

PANDORA ECR plasmoid volume ~ 3 l

required total microwave power $\mathbf{P_{MW} \approx 4}$ **kW**

"compliant" with the planned total amount of power delivered by the three klystrons 6 kW to reach high charge states

Method: ECR plasmas emit radiation from microwave to hard X-rays and this radiation can be used to investigate plasma parameters in different regimes;

Plasma Emitted Radiation

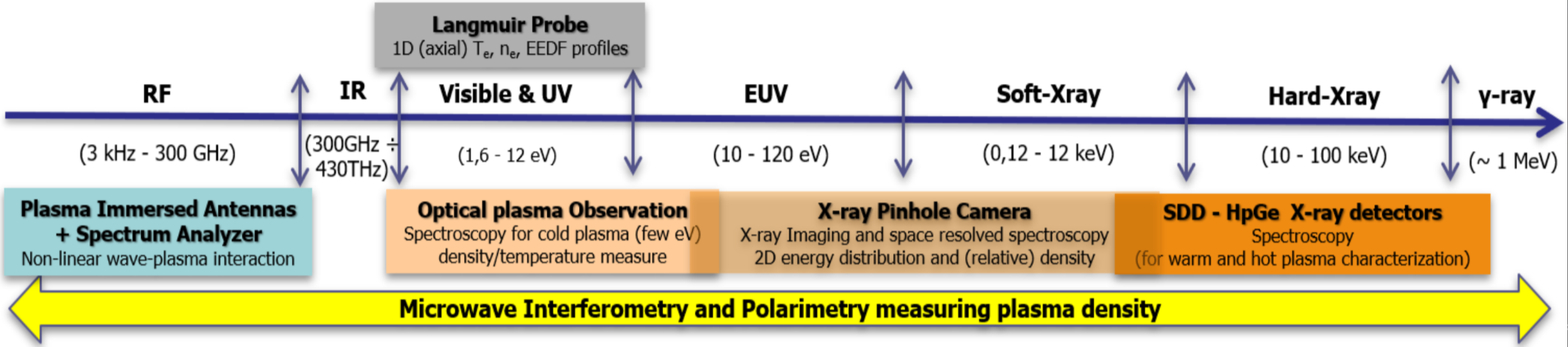

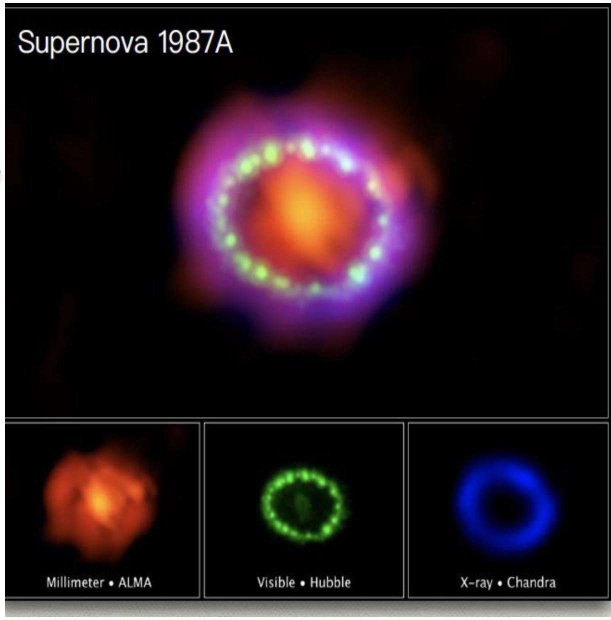

Multimessenger Astronomy Era:
→ Exploring the Universo across the EM spectrum

Typical diagnostic in ECRIS

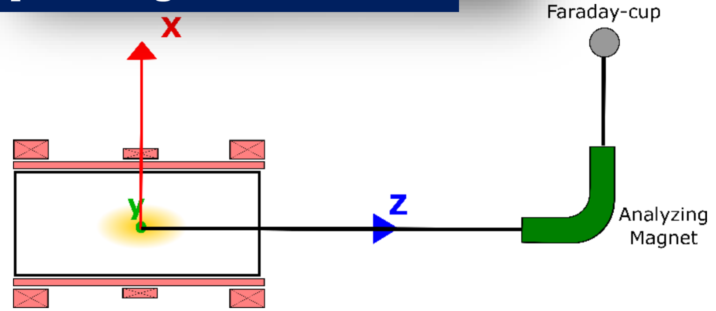

PANDORA plasma multidiagnostics systems

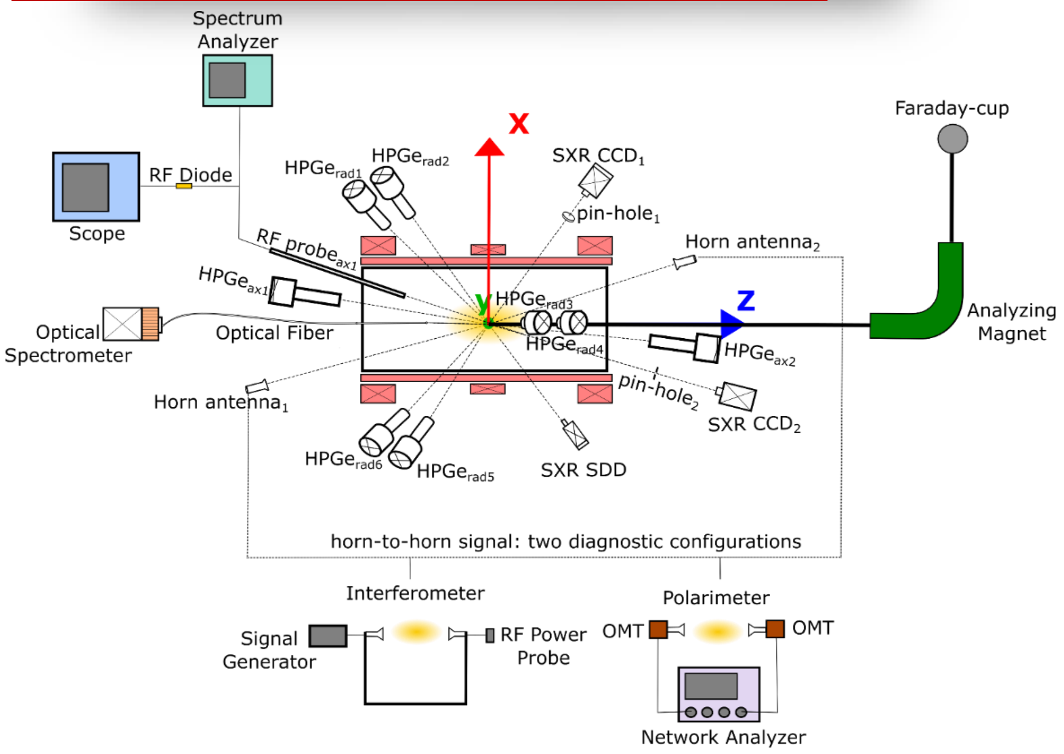

In the frame of the **PANDORA** project an **innovative multi-diagnostic approach** to correlate plasma parameters to nuclear activity has been proposed. This is based on several detectors and non-invasive techniques (*Optical Emission Spectroscopy, RF systems, InterferoPolarimetry, time- and space-resolved X-ray spectroscopy*), allowing **detailed investigations of magnetoplasma properties**.

Diagnostic tool	Sensitive Range	Measurement	Resolution - Measure Error
SDD	1 ÷ 30 keV	Volumetric soft X-ray Spectroscopy: warm electrons temperature and density	Resolution ~ 120 eV ε_{ne} ~ 7%, ε_{Te} ~ 5%
HPGe detector	30 ÷ 2000 keV	Volumetric hard X-ray Spectroscopy: hot electrons temperature and density	FWHM @ 1332.5 keV < 2.4 keV ε_{ne} ~ 7%, ε_{Te} ~ 5%
Visible Light Camera	1 ÷ 12 eV	Optical Emission Spectroscopy: cold electrons temperature and density	$\Delta\lambda$ = 0.035 nm R = 13900
X-ray pin-hole camera	2 ÷ 15 keV	2D Space-resolved spectroscopy: soft X-ray Imaging and plasma structure	Energy Resolution ~ 0.3 keV Spatial Resolution ~ 0.5 mm
W-band super-heterodyne polarimeter	W-band 90 ÷ 100 GHz	Plasma-induced Faraday rotation: line-integrated electron density	ε_{ne} ~ 25%
Microwave Imaging Profilometry (MIP)	60 ÷ 100 GHz	Electron density profile	ε_{ne} ~ 1% ÷ 13%
Multi-pins RF probe	10 ÷ 26.5 GHz	Local EM field intensity	ε ~ 0.073 ÷ 0.138 dB
Multi-pins RF probe + Spectrum Analyzer (SA)	10 ÷ 26.5 GHz *(probe range)*	Frequency-domain RF wave	SA Resolution bandwidth: RBW = 3 MHz
Multi-pins RF probe + Scope + HPGe detector	10 ÷ 26.5 GHz *(probe range)*	Time-resolved radiofrequency burst and X-ray time-resolved Spectroscopy	80 Gs/s *(scope)* time scales below ns
Thomson Scattering	0.5 ÷ 500 eV	EEDF, absolute electron density global electron drift velocity	Condition-dependent (a function of spectral width, dependent on temperature, and area, dependent on density)

E. Naselli et al., Journal of Instrumentation 14 (2019) C10008

Plasmas for Astrophysics Nuclear Decay Observation and Radiation for Archaeometry

Typical Electron-Cyclotron-Resonance (ECR) ion source

Ext. Beam diagnostic

Analyzing Magnet + Faraday cup

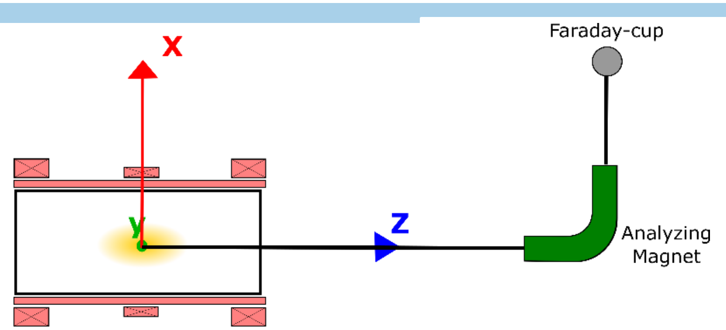

PANDORA trap as facility for Nuclear Astrophysics studies

Online plasma multidiagnostic

Diagnostic tool	Sensitive Range	Measurement	Resolution - Measure Error
SDD	1 ÷ 30 keV	Volumetric soft X-ray Spectroscopy: warm electrons temperature and density	Resolution ~ 120 eV ε_{ne} ~ 7%, ε_{Te} ~ 5%
HPGe detector	30 ÷ 2000 keV	Volumetric hard X-ray Spectroscopy: hot electrons temperature and density	FWHM @ 1332.5 keV < 2.4 keV ε_{ne} ~ 7%, ε_{Te} ~ 5%
Visible Light Camera	1 ÷ 12 eV	Optical Emission Spectroscopy: cold electrons temperature and density	$\Delta\lambda$ = 0.035 nm R = 13900
X-ray pin-hole camera	2 ÷ 15 keV	2D Space-resolved spectroscopy: soft X-ray Imaging and plasma structure	Energy Resolution ~ 0.3 keV Spatial Resolution ~ 0.5 mm
W-band super-heterodyne polarimeter	W-band 90 ÷ 100 GHz	Plasma-induced Faraday rotation: line-integrated electron density	ε_{ne} ~ 25%
Microwave Imaging Profilometry (MIP)	60 ÷ 100 GHz	Electron density profile	ε_{ne} ~ 1% ÷ 13%
Multi-pins RF probe	10 ÷ 26.5 GHz	Local EM field intensity	ε ~ 0.073 ÷ 0.138 dB
Multi-pins RF probe + Spectrum Analyzer (SA)	10 ÷ 26.5 GHz *(probe range)*	Frequency-domain RF wave	SA Resolution bandwidth: RBW = 3 MHz
Multi-pins RF probe + Scope + HPGe detector	10 ÷ 26.5 GHz *(probe range)*	Time-resolved radiofrequency burst and X-ray time-resolved Spectroscopy	80 Gs/s *(scope)* time scales below ns
Thomson Scattering	0.5 ÷ 500 eV	EEDF, absolute electron density global electron drift velocity	Condition-dependent (a function of spectral width, dependent on temperature, and area, dependent on density)

E. Naselli et al., Journal of Instrumentation (JINST) 14, 2019, C1008

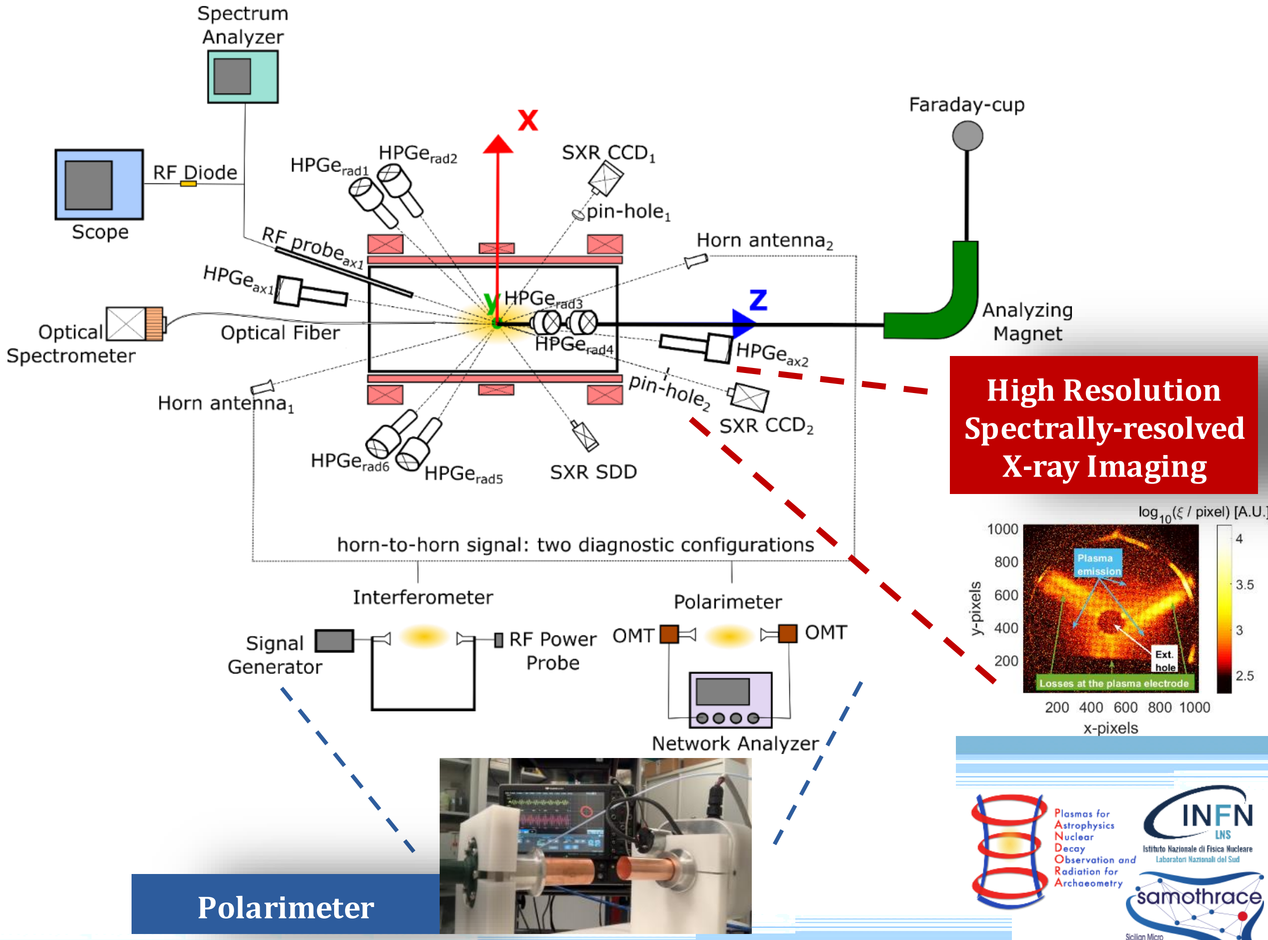

New Particle ID Techniques

Advanced design of the plasma chamber walls

Fluorescence lines can be used to get info about where the electrons collide on the chamber walls

in order to have well separated component of the emitted X-ray:
→ Special design of plasma chamber for studying confinement dynamics
(plasma vs losses X-radiation emission)

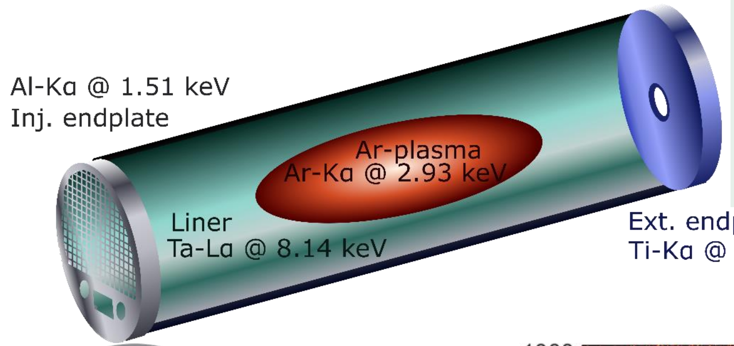

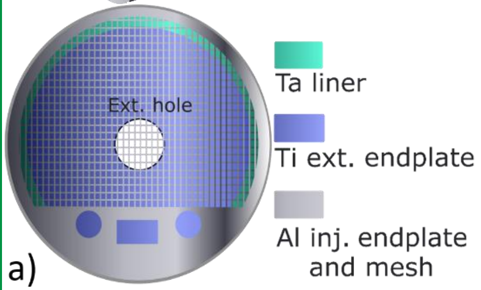

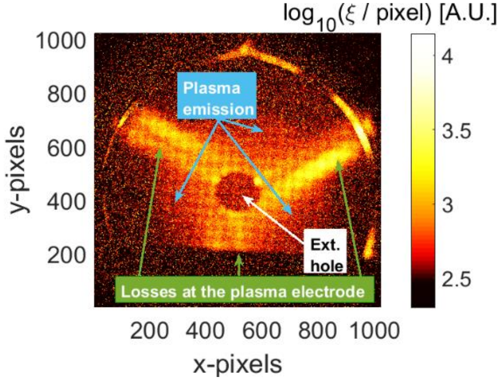

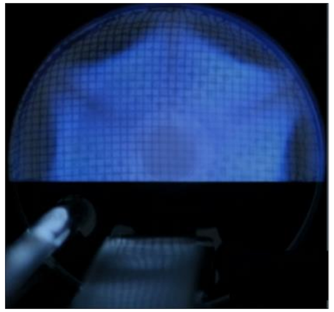

Perspective front-view in the FULL-FIELD X-ray pin-hole camera setup

Integrated Soft X-ray image (50 sec of exposure time)

Optical image by Optical Emission spectroscopy

- X-rays coming from **Plasma** are mostly due to ionized **Kα Argon lines**
- X-rays coming from **Magnetic Branches** consist of mostly **fluorescence from Ti**
- X-rays coming from **Poles** are mostly due to radial losses impinging on the **Ta liner**

Lead multi-disks collimator

Lead multi-disks collimator properly designed to perform high resolution X-ray imaging at high energy (up to 200 W). It allows:

- ❑ **Reduce the noise**
- ❑ **Improve the signal/noise ratio**
- ❑ **Increase the resolution**

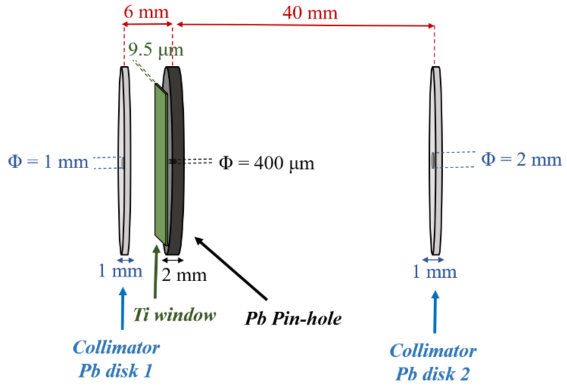

Without the Collimator

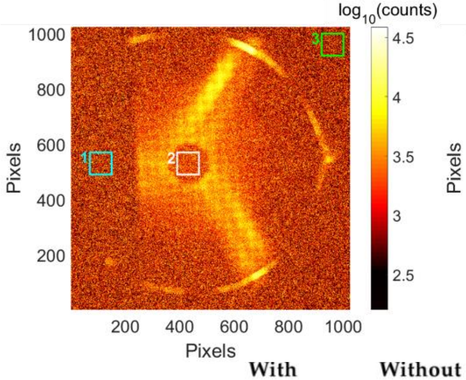

With the Collimator

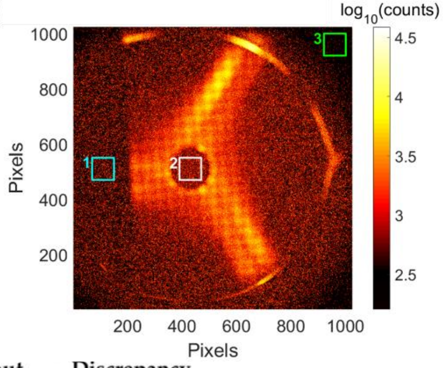

	With Collimator	Without Collimator	Discrepancy Percentage
$\frac{N_{hole}}{N_{bkg_{out}}}$	8.70 ± 0.50	2.65 ± 0.08	+ 70 %
$\frac{N_{hole}}{N_{bkg_{in}}}$	3.41 ± 0.13	2.08 ± 0.05	+ 39 %

INFN LNS

Plasmas for Astrophysics Nuclear Decay Observation and Radiation for Archaeometry

S. Biri et al., Journal of Instrumentation 16 (2021) 02006

Spatially-resolved X-ray Spectroscopy

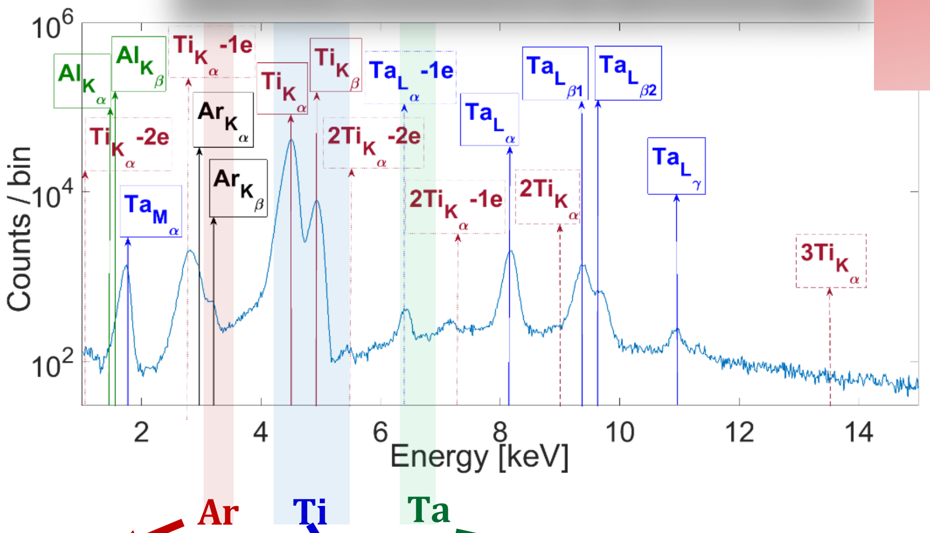

Plasma structure inspection

Axial losses inspection

Radial losses inspection

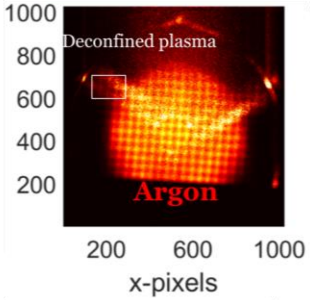

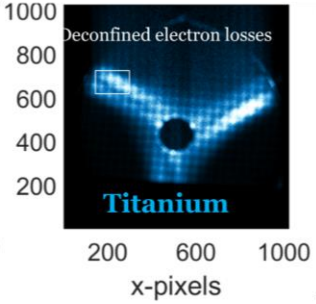

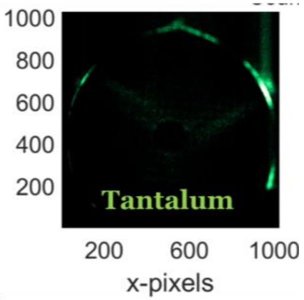

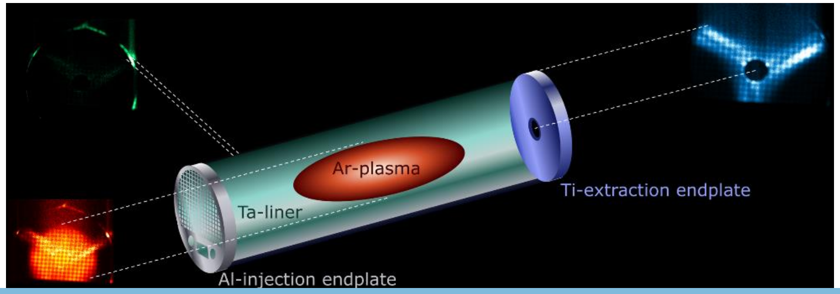

By an Advanced Algorithm for Single Photon Counted (SPhC) → X-ray space-resolved spectroscopy

The data on the spectrum contains the spatial information on the emitting positions: the definition of a ROI allows the imaging of the elemental distribution.

High space and energy resolutions:

- Energy Resolution ~ 260 eV @ 8 keV
- Spatial Resolution ~ 450 μm

2 complementary analysis:

1) It is possible pixel-by-pixel to investigate the balance between plasma emissions vs. losses emissions

Plasma radius evaluation (uncertainty of 5%)

Spectrally-resolved X-ray Imaging

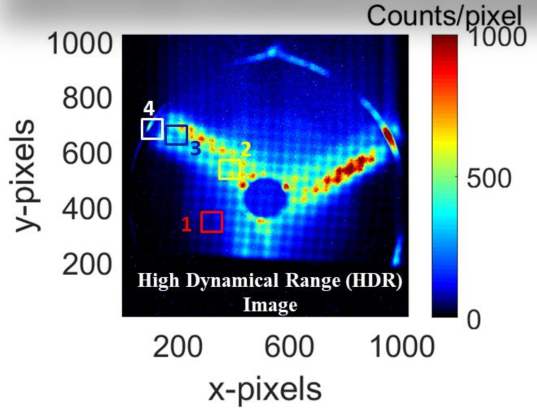

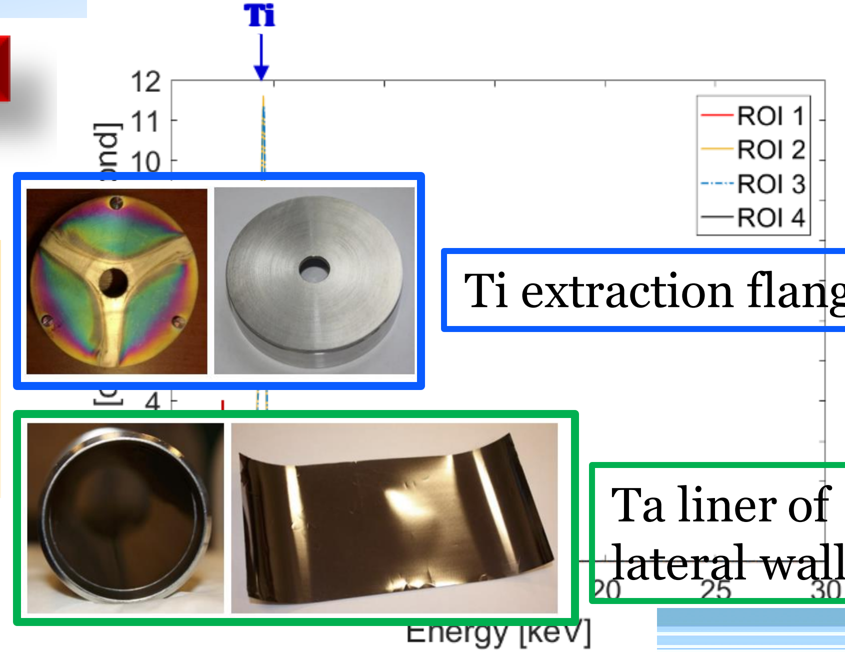

Ti extraction flange

Ta liner of lateral walls

2) Analyzing each ROI-spectrum elemental analysis and plasma parameters measurements can be performed

E. Naselli et al., Condensed Matter 7(1), 5, 2022
E. Naselli et al., JINST (2022) **17** C01009
S. Biri et al., JINST 16, 2021, P03003
B. Mishra et al., Physics of Plasmas 28, 102509 (2021)

Energy-resolved imaging

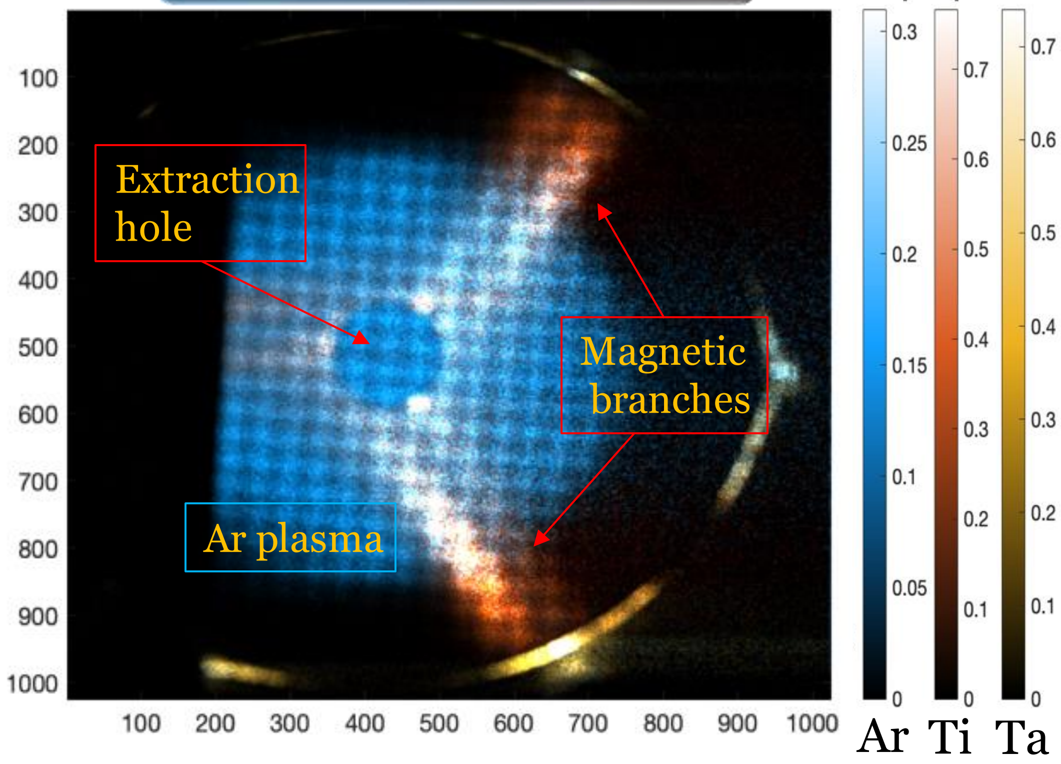

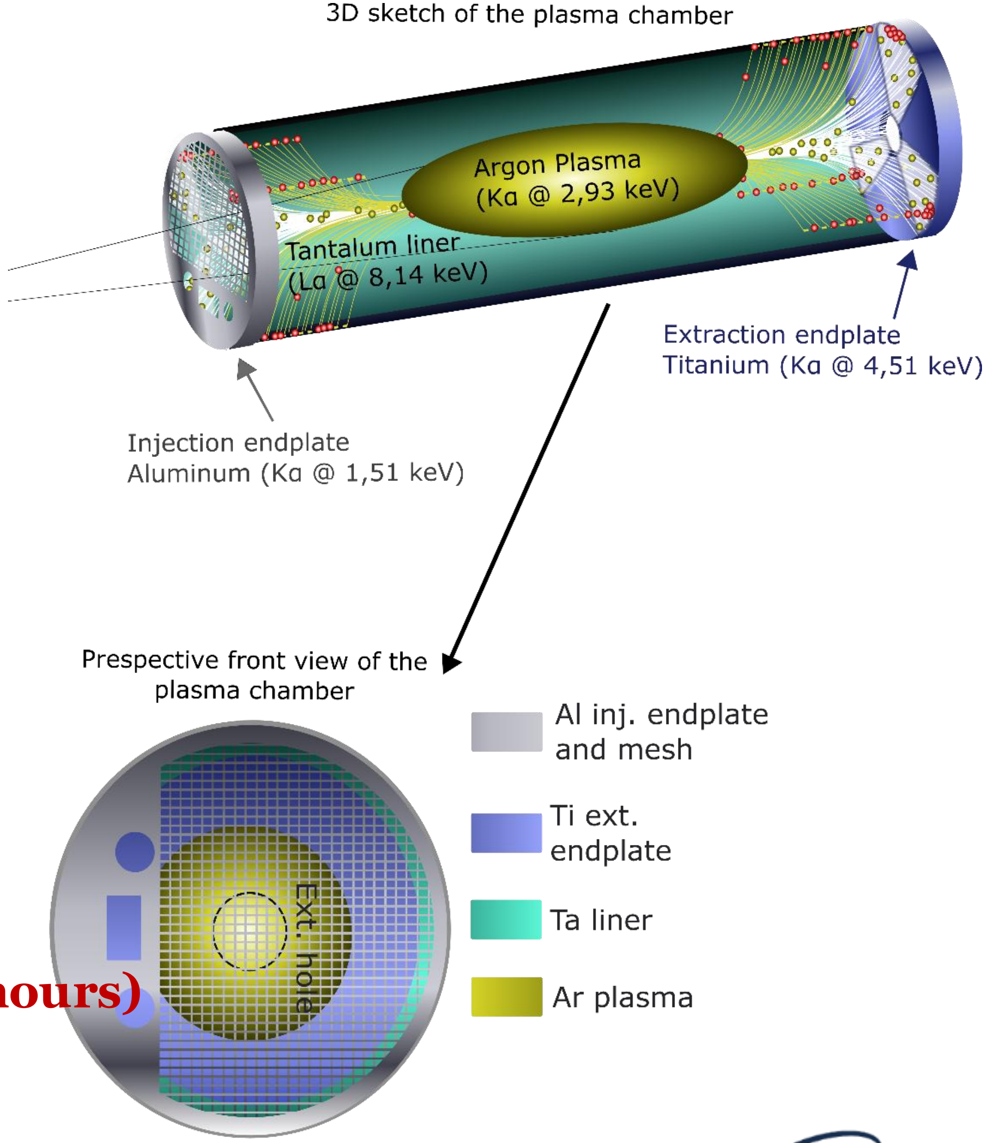

- **Slow response – advanced analysis**
- **Thousands of low exposed frames (meas.time 4hours)**
- **Deeper investigation**

D Mascali et al., Plasma Physics and Controlled Fusion 64(3):035020
Jan. 2022, DOI: 10.1088/1361-6587/ac4349

Towards VESPRI 2.0 Prototype

Design and development of the **VESPRI 2.0** (**VE**ry **S**ensitive evaluation of **P**lasma density by mic**R**owave polar**I**metry) **mm-wave polarimeter prototype**:

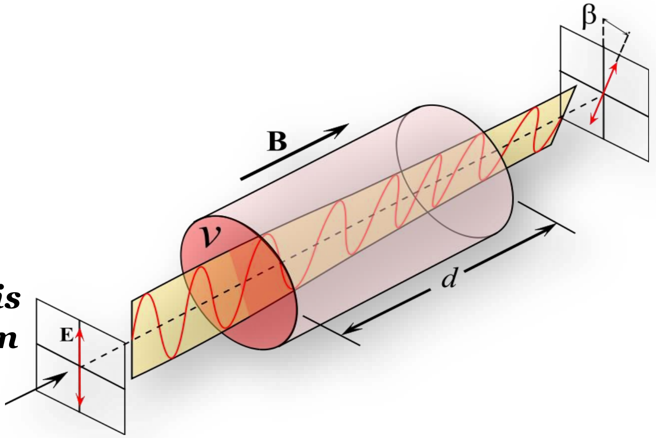

1) The **polarimetry** method is based on the evaluation of the **Faraday rotation angle** of the polarization plane of an e.m. wave that passes through the **plasma**.

$$\boxed{b = \frac{q_e^3}{8\pi^2 c^3 m_e^2 \varepsilon_0} B d n_e \lambda^2}$$

Faraday rotation angle is proportional to the plasma electron density and the magnetic field

2) The scheme based on the **Detection of Lissajous figure** consists of direct RF signals detection through a scope, allowing the real-time reconstruction of the State of Polarization curve described by the electric field vector;

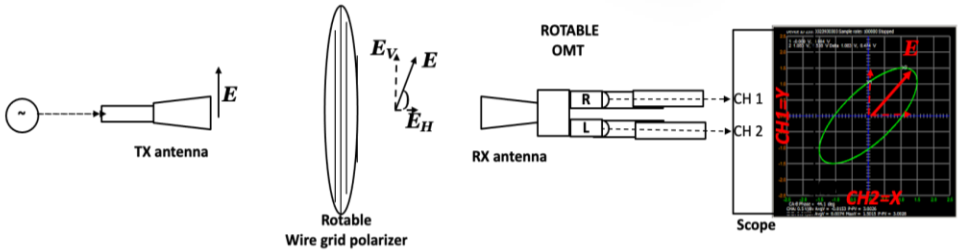

3) The **Super-Heterodyne scheme** allows to down-shifted the detected frequency (1 GHz) compared to the probing one (20 or 100 GHz) in order to be detected in a scope;

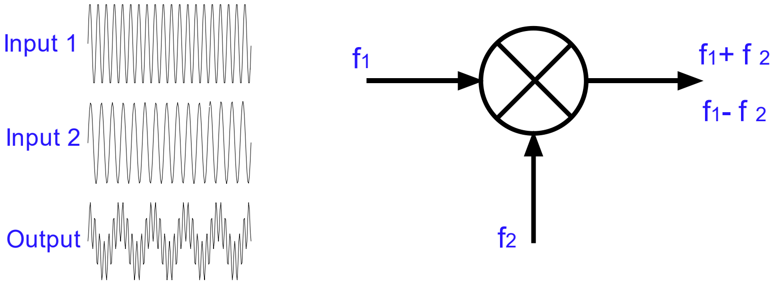

Plasma system scenarios

The system was designed to be tested on the PANDORA plasma trap (C) which represents an "*intermediate*" case between the ultra-compact plasma ion sources (FPT (B) and **Test-bench (A)**) and the large-size thermonuclear **Fusion devices (D)**.

(A)

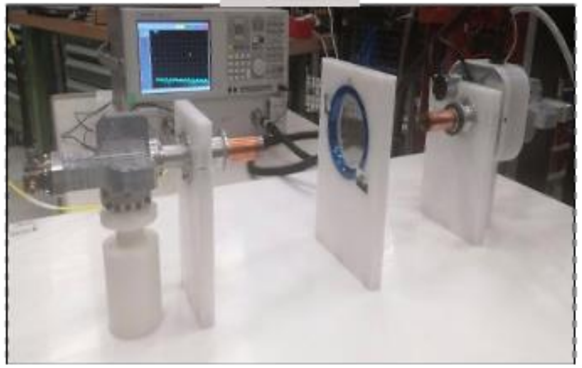

Test-Bench (without plasma)

(B)

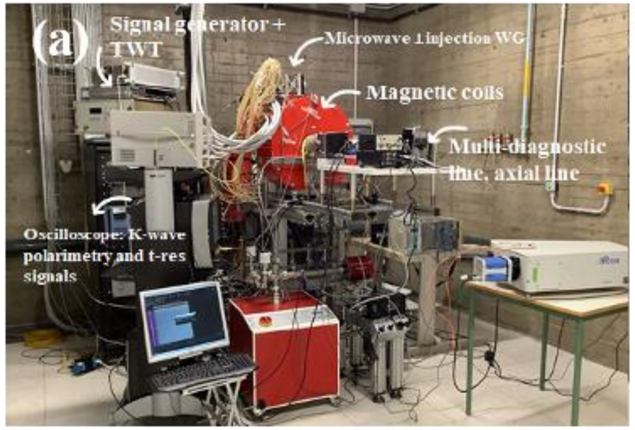

Flexible Plasma Trap

(C)

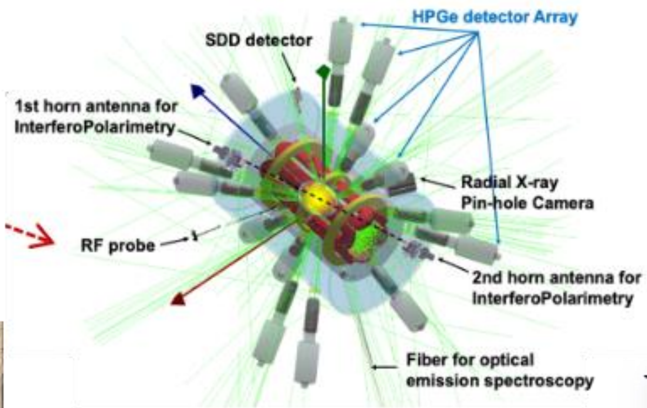

PANDORA Trap

(D)

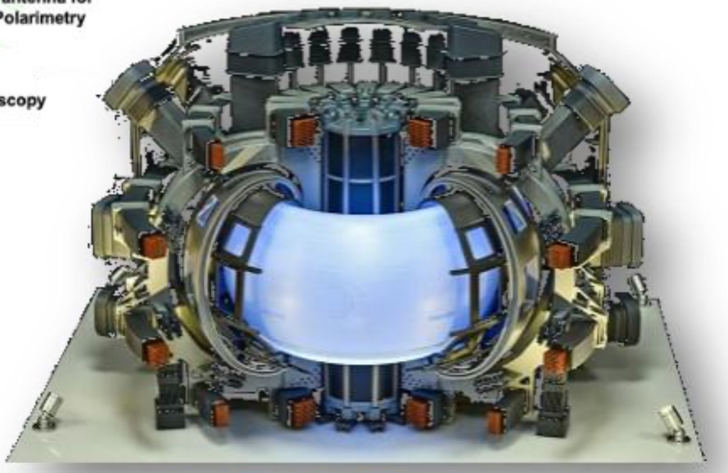

Fusion Device

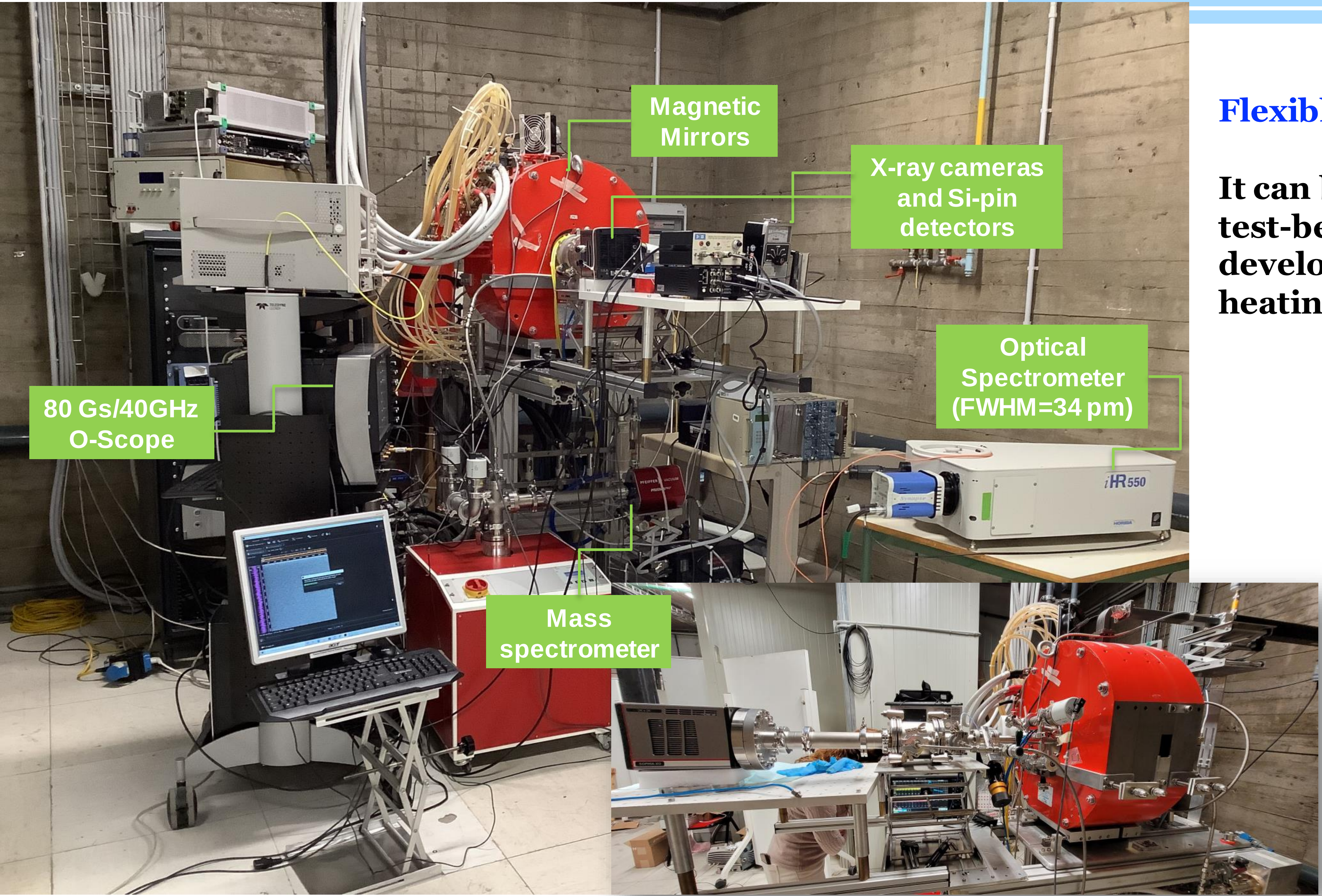

Flexible Plasma Trap @ LNS

It can be considered as a test-bench for the development of diagnostics, heating systems, etc.

ECRIS @ Atomki Laboratory (Debrecen, Hungary)


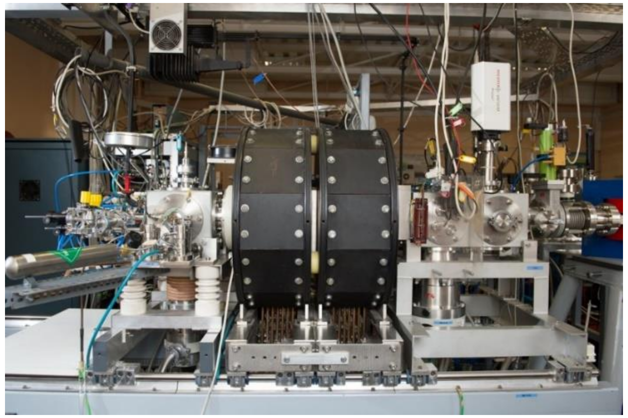

- 14.25 GHz ECRIS
- Permanent magnet hexapole and room temperate coils
- No post acceleration
- Used for atomic physics, material science, ECR plasma physics

B-min magnetic field

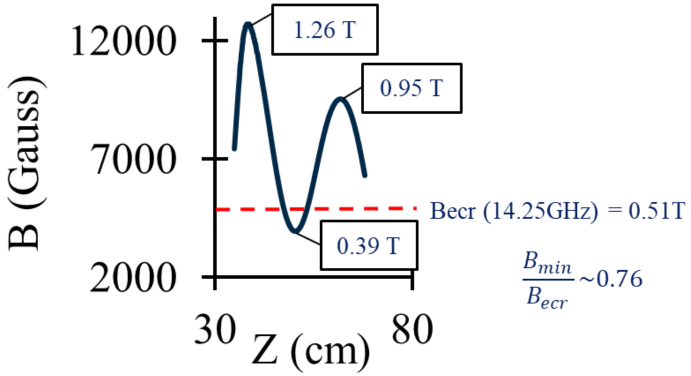

Flexible Plasma Trap @ LNS

It can be considered as a test-bench for the development of diagnostics, heating systems, etc.

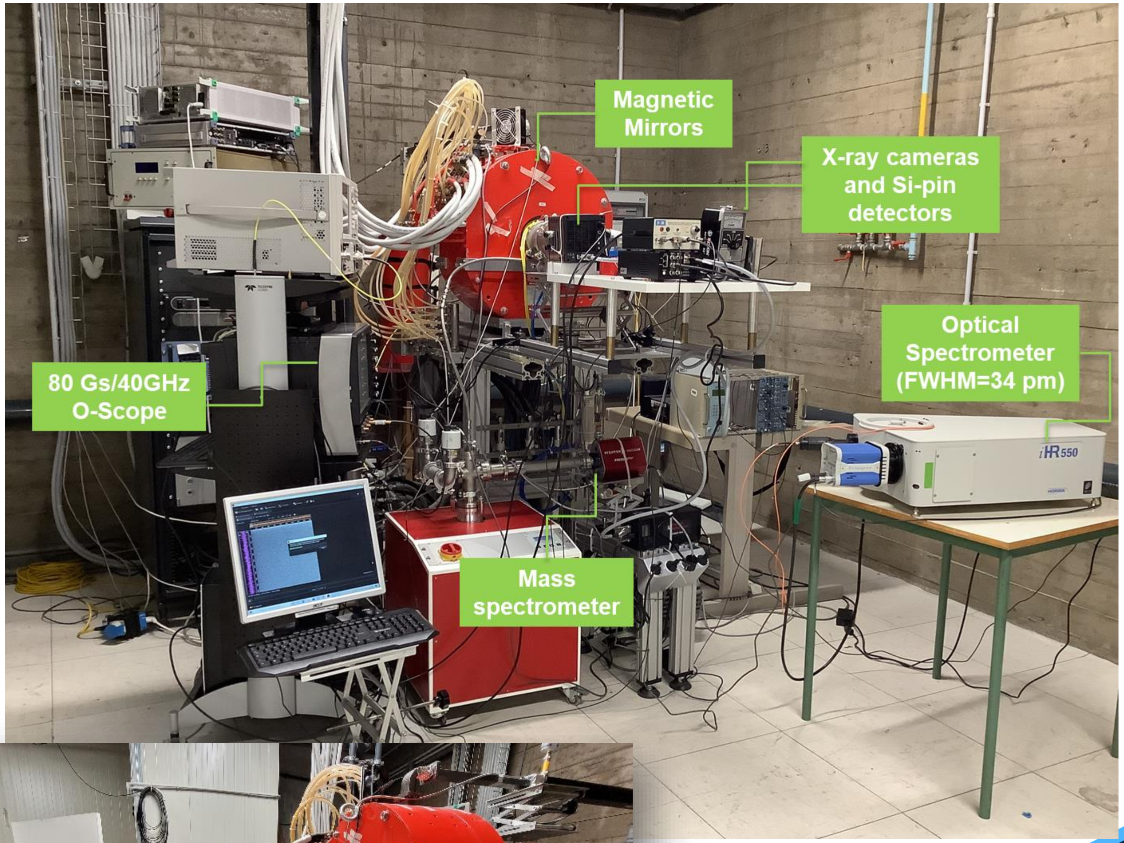

Towards the PYN-HO prototype

The **PYN-HO** (**P**robing x-ra**Y**s by imagi**N**g and pin-**H**ole spectr**O**scopy) prototype has been designed as diagnostic testbench for X-rays and optical emission spectroscopy:

→ conceived to operate in **four different configurations**;

A. Configuration 1.0 – *Test-bench for X-ray calibration and characterization*

test-bench; high counting rate SDD (from 400 eV); X-ray tube; samples to be irradiated with an X-ray tube; pin-hole CCD camera system.

B. Configuration 2.0 – *Test-bench for X-ray imaging, spectroscopy and tomography in magnetized plasma*

Pin-hole system; CCD cameras (two CCDs for tomography); Flexible Plasma Trap; high counting rate SDDs (one from 400 eV and another from 2 keV).

C. Configuration 3.0 – *Test-bench for diffractometric measurements on test-bench and in plasma*

X-ray diffraction system based on grating and nanometric movers; Flexible Plasma Trap; high counting rate SDDs; CCD camera.

D. Configuration 4.0 – *Test-bench for optical emission spectroscopy on test-bench and in-plasma*

High resolution optical spectrometer based on grating with integrated CCD; test-bench; plasma trap; calibrated light source; integrating sphere; lenses, fibers, collimators.

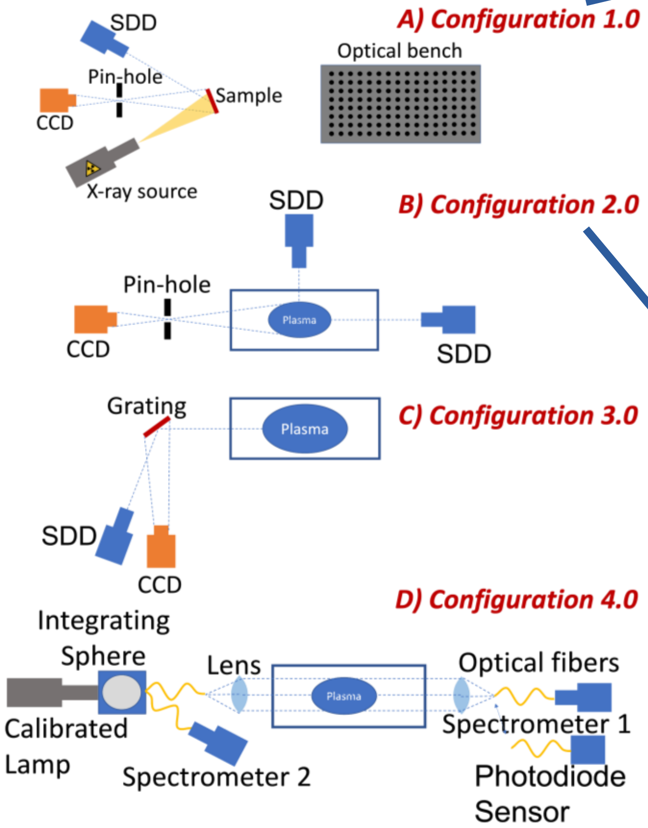

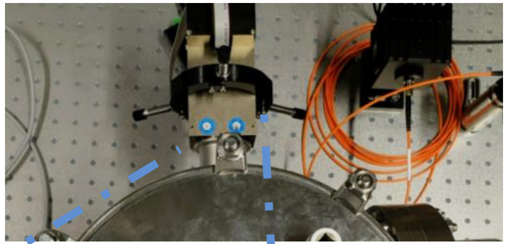

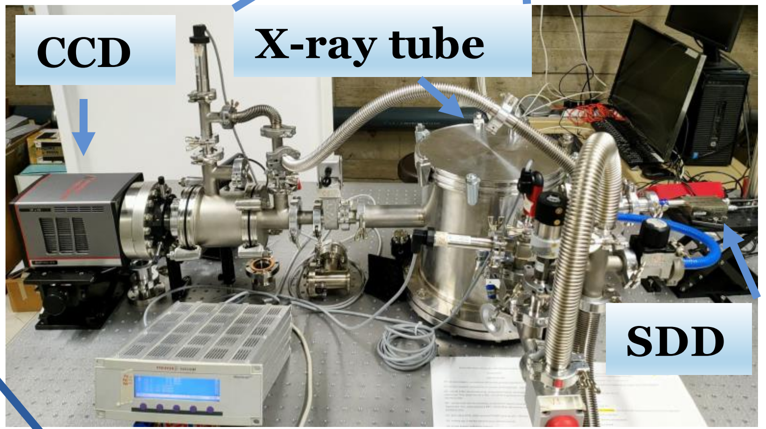

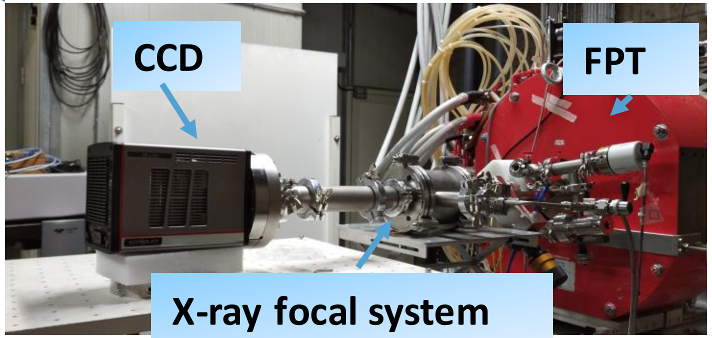

All systems and configurations must be compatible to be installed and used in the plasma testbench - named FPT (Flexible Plasma Trap) - installed at INFN-LNS for R&D on diagnostics and detectors.

Multimaterial target inside the vacuum chamber

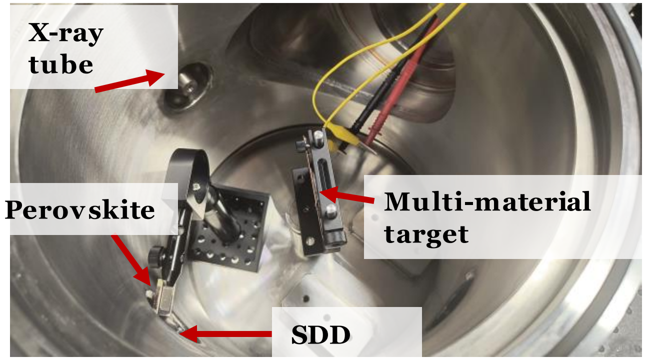

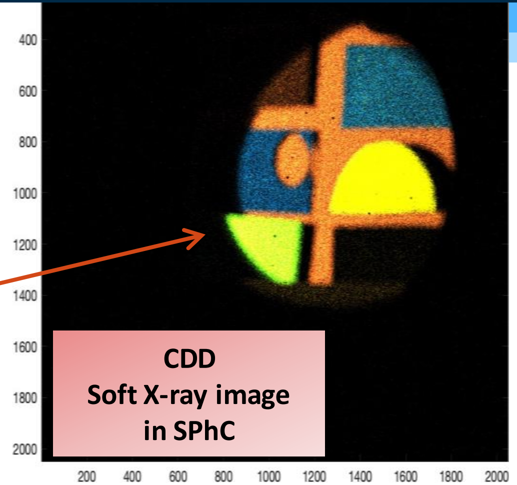

350 X-ray frames (100 seconds of exposure time) acquired in SPhC mode by **CCD pyn-hole system** and **X-ray spectra by SDD**

Testbech setup

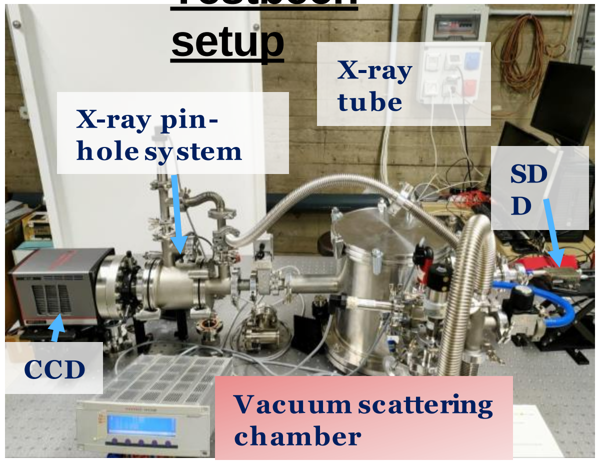

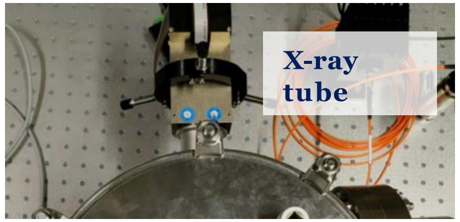

Interdisciplinary R&D (with CNR-IMM) about new detectors and techniques for X-ray measurements in plasma

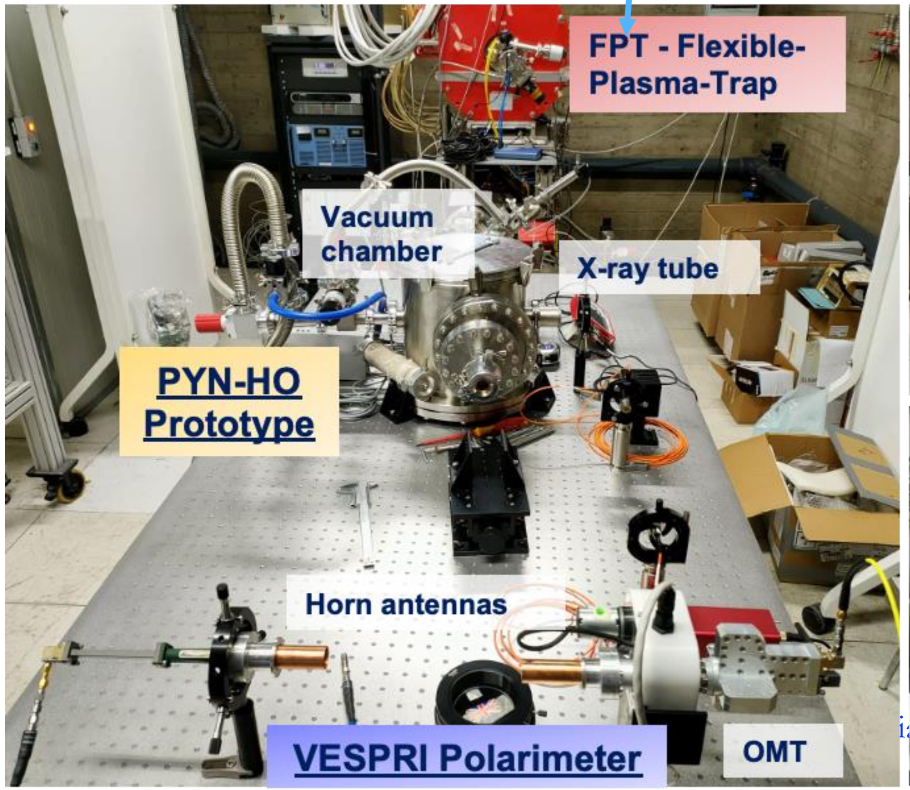

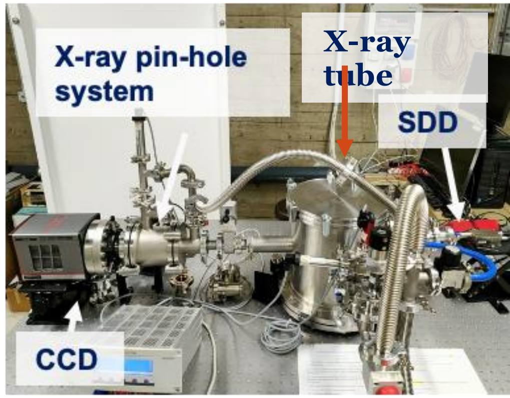

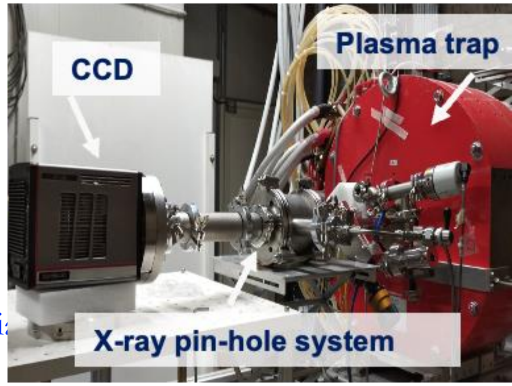

Plasma multidiagnostics has to work sinergically with γ detection to tag β-decays

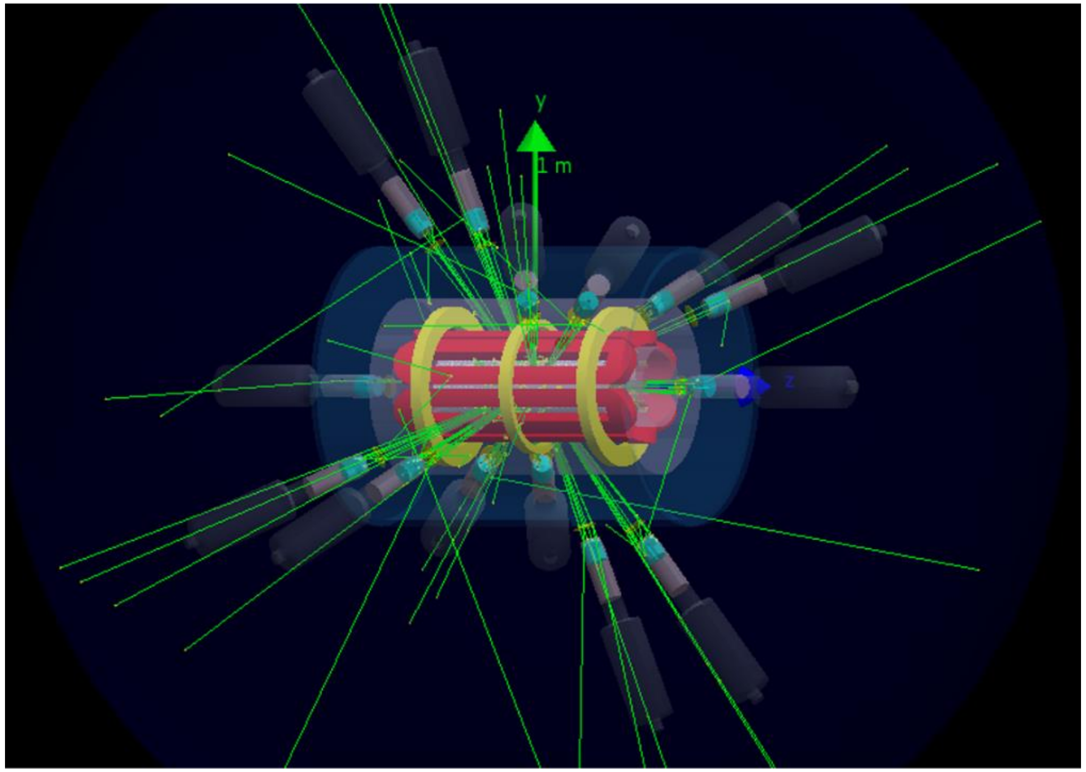

PANDORA: numerical simulation by GEANT4 to perform a «Virtual Experimental Run»

Physics Cases

Isotope	$T_{1/2}$ [yr]	E_{γ} [keV]
^{176}Lu	$3.78 \cdot 10^{10}$	202.88 & 306.78
^{134}Cs	2.06	795.86
^{94}Nb	$2.03 \cdot 10^{4}$	871.09

- The **decay-products can be tagged by γ-rays coming out from the "radio-product"** with typical energies between 200 keV and 1800 keV
- **Numerical simulation by GEANT4** according to a certain plasma model to design the array of detector and **to estimate the total efficiency** of the system

Plasmas for Astrophysics Nuclear Decay Observation and Radiation for Archaeometry

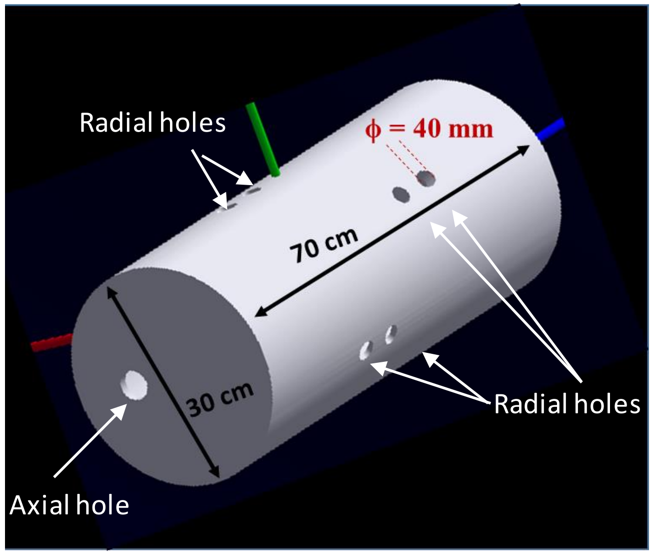

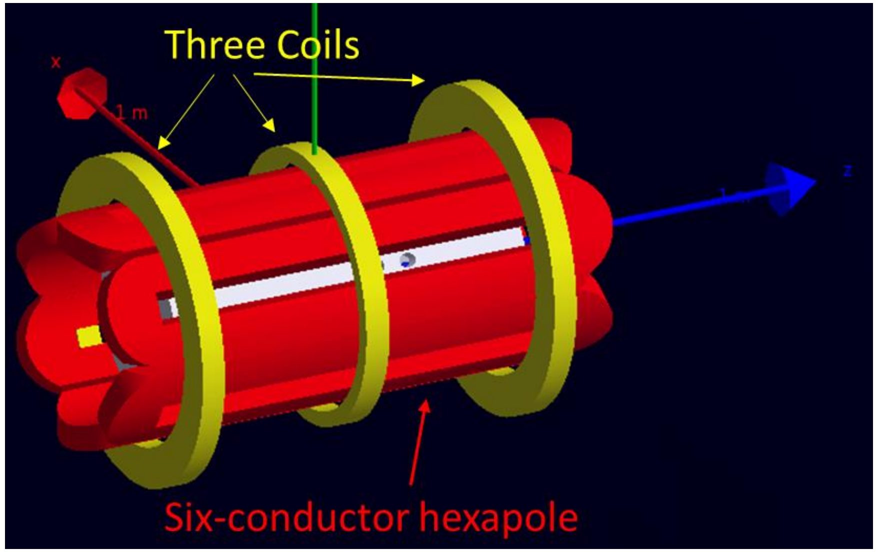

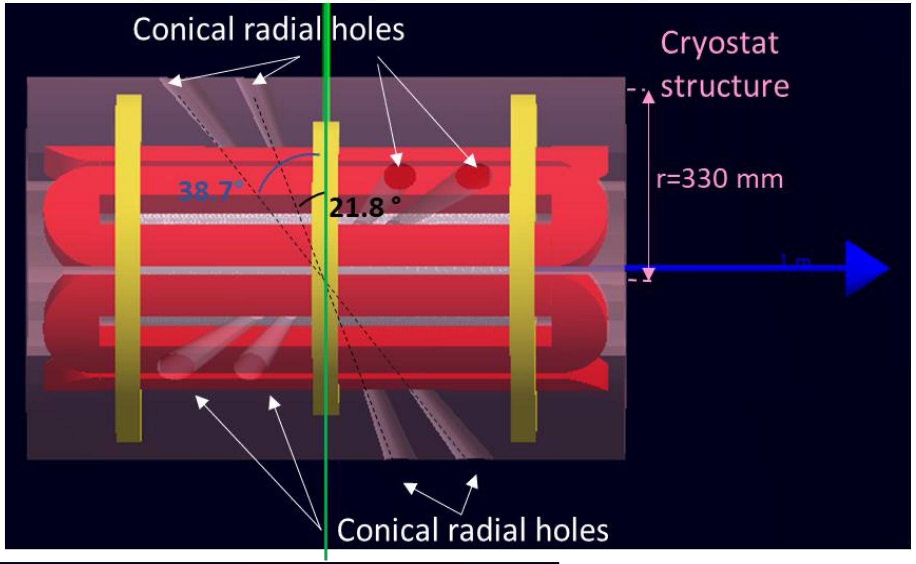

- **Stainless steel chamber**

- **Lenght: 70 cm**
- **Diameter: 30 cm**
- **Thickness: 1 cm**

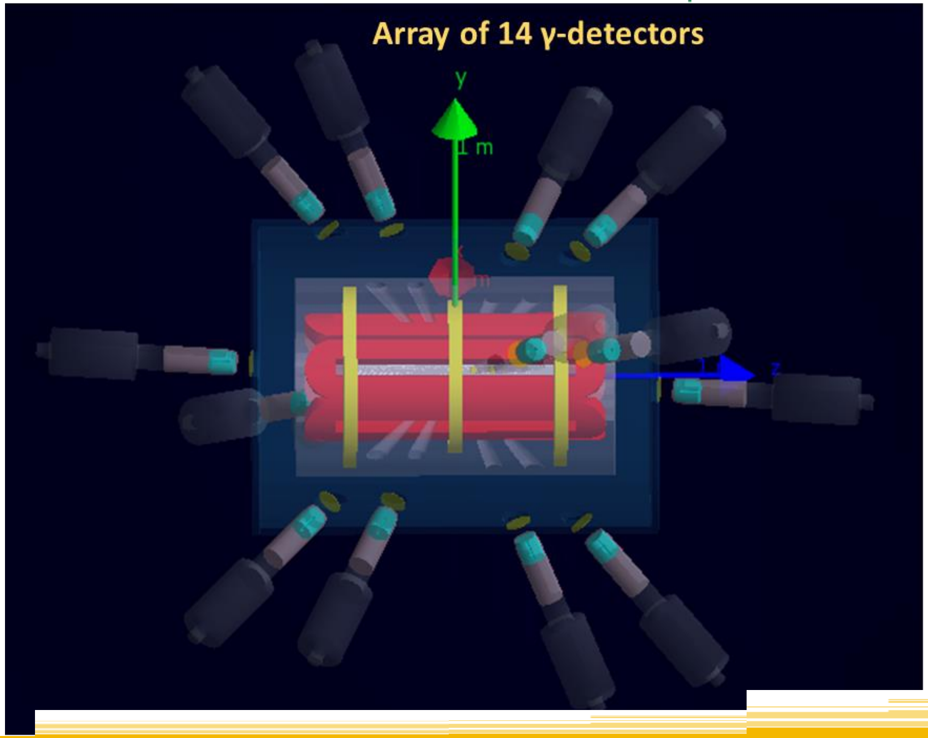

The chamber and the cryostat have been drilled with 18 holes of diameter 40mm, in order to connect long collimators for γ-rays detection and plasma diagnostic systems

2 **HPGe γ-detectors Array** → **β-decay detection by γ-rays tagging;**

E. Naselli et al., Front Phys (2022) 10:935728
A. Goasduff et al., Front. Phys. 10:936081

GEANT4 Simulations to design the HPGe array

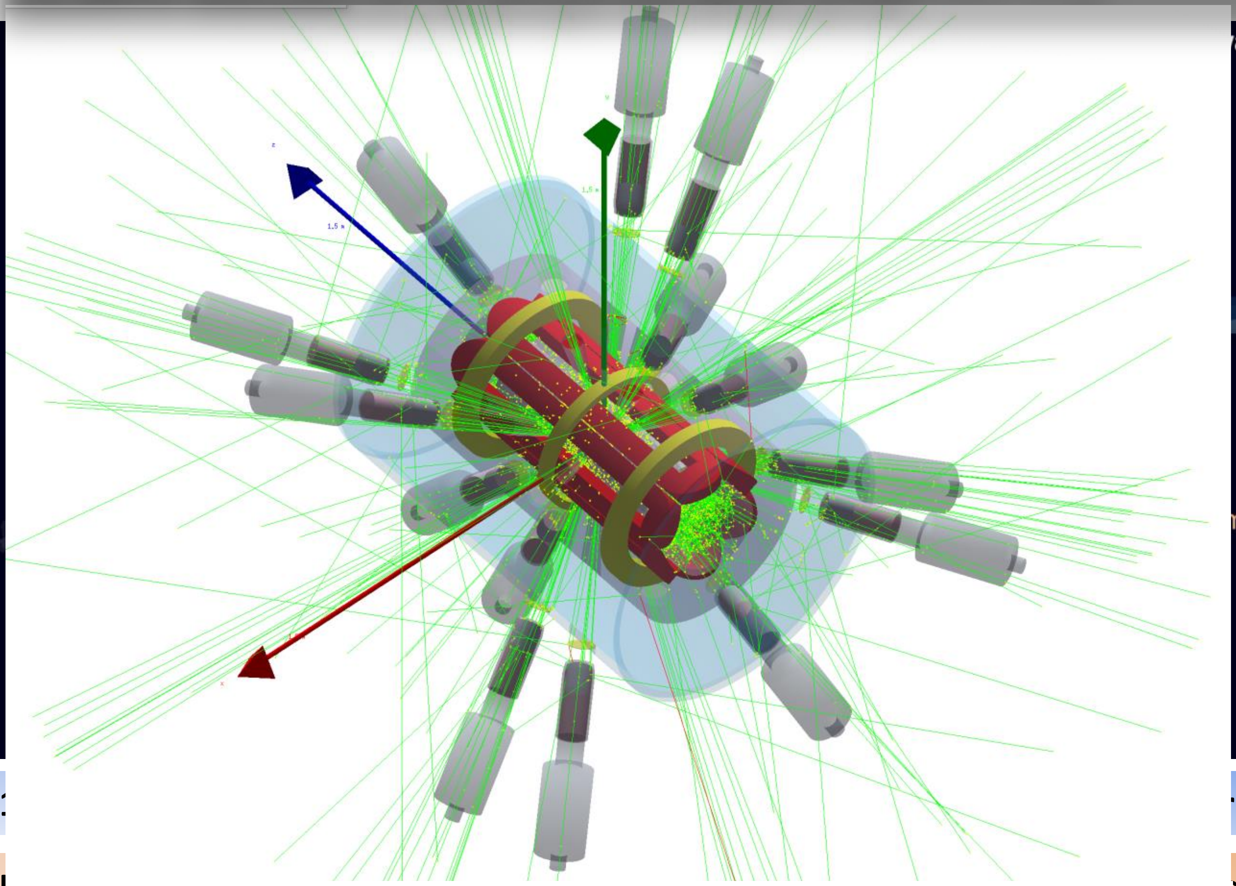

→ **Tag γ-rays** (typical energies ~ 200 keV - 1800 keV) **emitted from the «radio-product»**

Evaluation of the array efficiency by GEANT4 Simulation

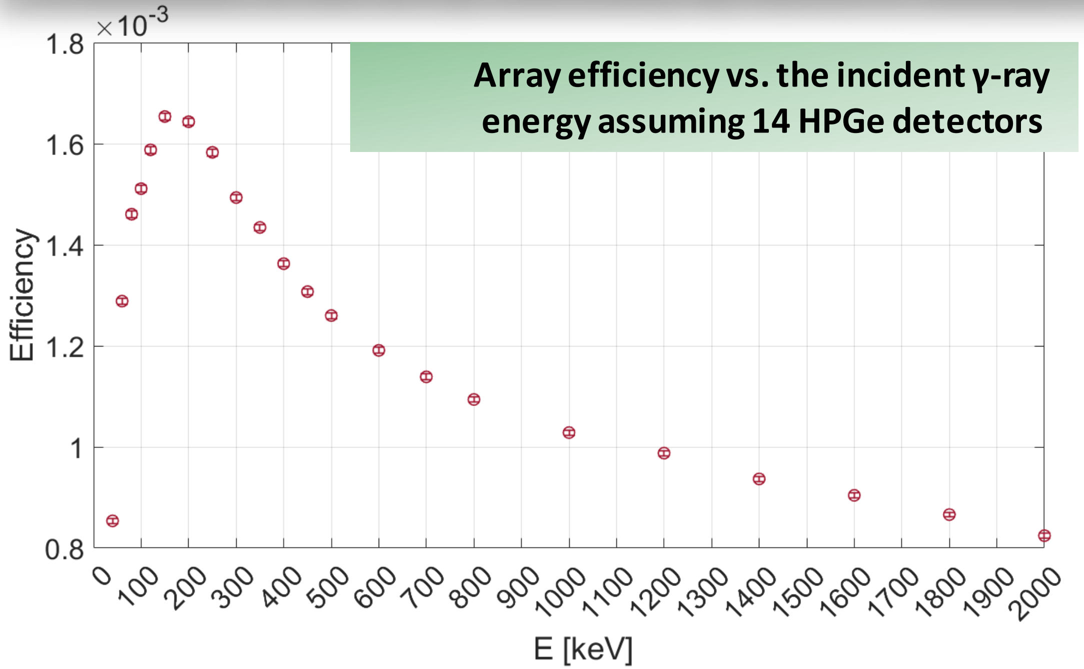

Simulations were performed considering an **isotropic ellipsoidal source** placed in the center of the plasma chamber, having semi-axis lengths of 79x79x56 mm^3 (plasma volume in the PANDORA plasma trap).

The γ-ray energy range extends from 40 keV to 2 MeV.

For the evaluation of the background due to plasma self-emission, we considered a **density of n = 10^{13} cm^{-3}, and a volume of 1500 cm^3**.

MAIN SUBSYSTEMS UPDATES: HPGE detection system

(LNS+ LNL activity)

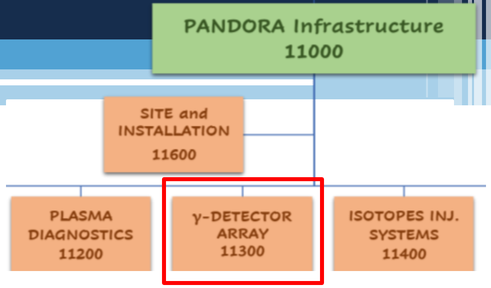

The detection setup is made of an array of 14 HPGe detectors placed around the trap

PANDORA-GAMMA Coll. Agreement signed in Oct. 2021 to use 16 HPGe detectors of GALILEO

- Time window from 2023 till the end of 2025
  - Ideal plan to move detectors to LNS in the second half of 2024
  - Really important to avoid delays in the time schedule
- It would allow to fully exploit PANDORA potentialities in the first experimental campaign
- Know-how/expertise transfer started with joint activities between LNS-LNL.
- Realization of a HPGe lab for the detectors maintenance started @LNS in mid 2023, work in progress

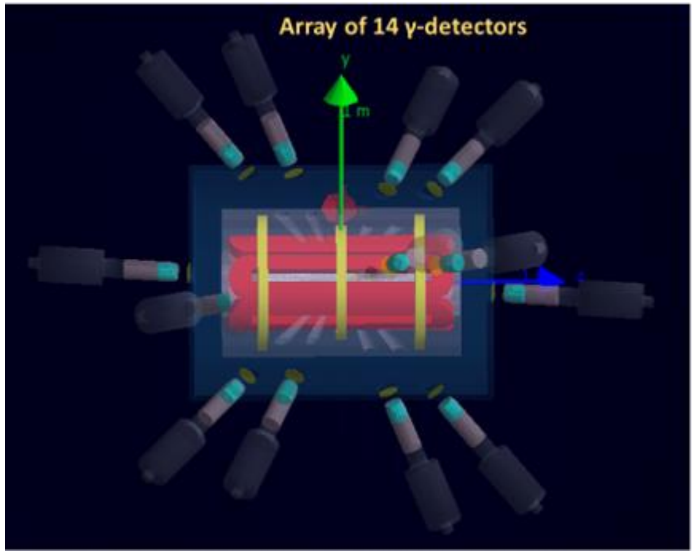

Main issues carefully evaluated:

- Photopeak detection efficiency (interplay between detector number and mechanical constraint)
- Signal to noise ratio (high background self-generated inside the trap)
- Magnetic field effects on HPGe charge collection

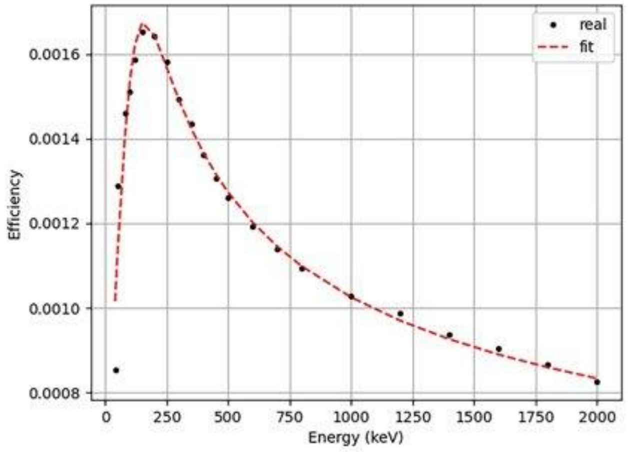

"Measurability" of ^{176}Lu lifetime from GEANT4 simulations (by an array of 14 HPGe-detectors)

In order to estimate the time needed for reaching 3σ confidence level taking into account different lifetimes, i.e. different rates in the detectors' array, we built plots showing the correlation between time measurement vs the decay-rate (or the lifetime) of the radionuclide.

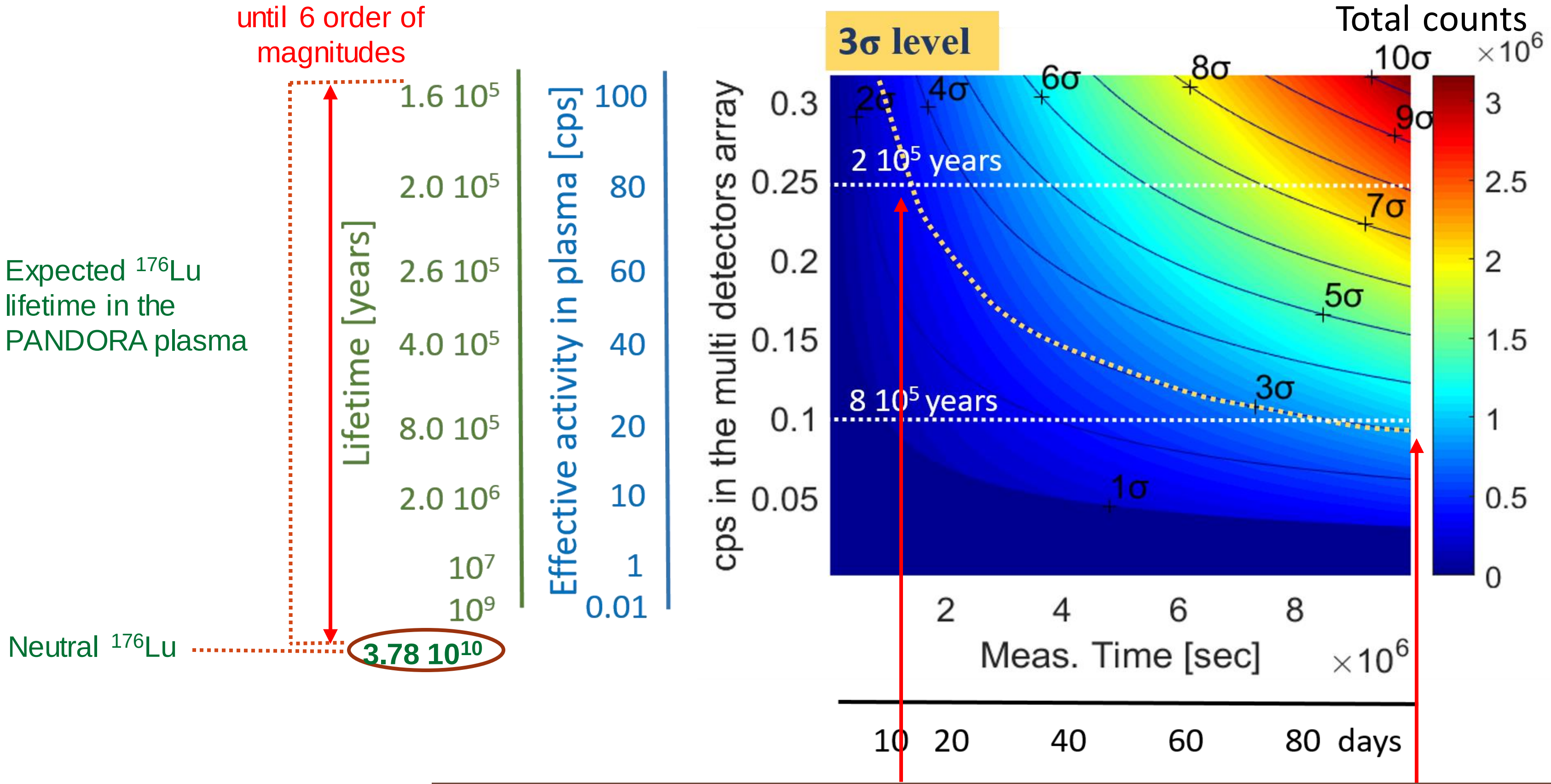

1% Lu of 10^{13} cm^{-3} (Vp=1500 cm^3)

Physics Cases

Isotope	$T_{1/2}$ [yr]	E_γ [keV]
^{176}Lu	$3.78 \cdot 10^{10}$	202.88 & 306.78
^{134}Cs	2.06	795.86
^{94}Nb	$2.03 \cdot 10^{4}$	871.09

For the variations of the lifetime expected from the theory in our laboratory plasmas, **we expect that a measure lasting from tens of days to a couple of months is needed in order to obtain a 3σ level of confidence**

E. Naselli et al., EPJ web of conferences 227, 2020, 02006
D. Mascali et al., EPJ web of conferences 227, 2020, 01013

Plasmas for Astrophysics Nuclear Decay Observation and Radiation for Archaeometry

Pro and Cons between magnetic confinement vs laser produced plasma

Magnetic confinement

PRO:
- Long-living plasma (order of weeks)
- steady state dynamical equilibrium for density and temperature,
- → hence, over days/weeks constant values for charge state distribution of in-plasma ions
- Online monitoring of plasma density, temperature, volume, eventual kinetic turbulence, at any energy domain in nLTE conditions

CONS:
- Low density/high temperature plasma: nLTE conditions
- Difficult “plasmization” of solid/metallic isotopes
- No access to nuclear excited state studies (too low T)

Scenario can be different using plasma produced by HP lasers

PRO:
- High density plasma, reaching LTE
- Online production of RIBs is in principle possible
- **Fully thermodynamical equilibrium allows, in principle, nuclear excitation**

CONS:
- Difficult to implement diagnostics following on-lime the fast time-variation of plasma parameters
- Short living plasma, with duration much shorter than typical lifetimes of isotopes involved in stellar nucleosynthesis

^{176}Lu decay rates in stellar-like high density and energetic plasma.

The intermixing between nuclear levels in ^{176}Lu has been an open topic in nuclear astrophysics for years because it has a direct impact on its treatment as a cosmochronometer.

The contribution of the isomer level will drastically modify the half-life (from years to a couple of hours) and switch its use to a cosmothermometer instead.

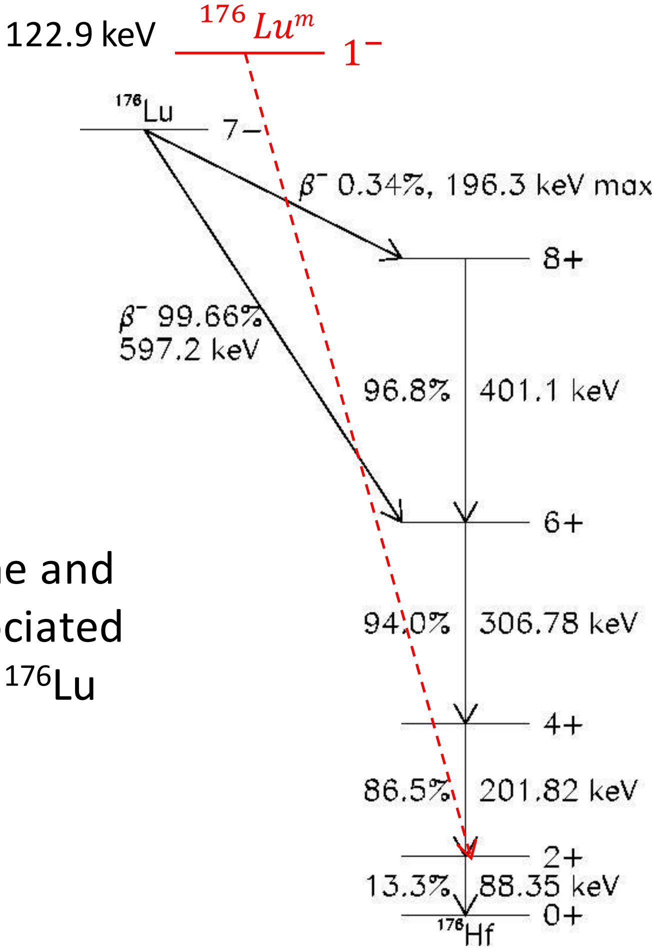

β⁻ decay scheme and γ energies associated with 7⁻ level of ^{176}Lu

assumed level scheme of ^{176}Lu

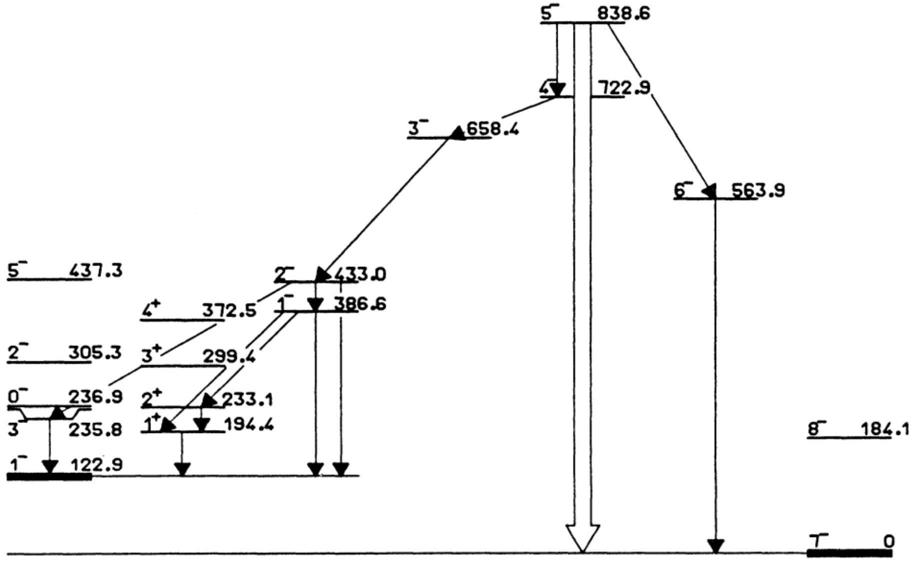

To populate 1⁻ level it is needed to populate a level at about 800 keV !

^{176}Lu decay rates in stellar-like high density and energetic plasma.

How can we populate the 1^- level ?

The intermixing depends on photoactivation rate λ^c of the nucleus through a bath of high energy X-ray photons obeying a Planck distribution in the thermal equilibrium stellar plasma.

Using a laser-plasma as a source of polychromatic high energy X-ray photon flux one could simultaneously investigate isomeric photoactivation as well as in-plasma decay rate modification of ground and isomer levels

The experimental methodology revolves around the measurement of two quantities:

- photoactivation rate $\lambda^c\,(n_e,n_i,T,s)$
- decay rates $\lambda^d\,(n_e,n_i,T,s)$ from g.s. and isomeric states

Thermalisation between the ground and isomer levels occurs when:

$\lambda^c(n_e,n_i,T,s) >= \lambda_m^d\,(n_e,n_i,T,s)$ $\longrightarrow$ the onset of equilibrium between the levels

The laser-plasma can be expected to produce X-ray spectra similar to the stellar interior, which can answer the question of equilibration more accurately than previous experiments on this topic.

^{176}Lu decay rates in stellar-like high density and energetic plasma

The naïve idea of the experiment is:

- ps lasers are directed toward a solid target composed of ^{176}Lu
- laser-generated plasma emits high energy X-ray bremsstrahlung produced from reactions between energetic electrons and buffer/^{176}Lu ions
- These X-rays are absorbed by the ^{176}Lu nuclei which get photoactivated to the 1^- isomer level according to a cross section σ(E) ➡ photoactivation rate $\lambda^c(n_e,n_i,T,s)$
- ^{176}Lu nuclei undergo β^- decay to ^{176}Hf from both the 7^- and 1^- levels
- Daughter nuclei will decay emitting specific gamma-rays
- Assuming the plasma remains active and stable LTE for a time *T*, the total number of specific γ-photons recorded can be correlated to the aforementioned rates
- The yield of 88.25 keV photons can be correlated to $\lambda_m^d(n_e,n_i,k_BT,s)$ if the photoactivation rate $\lambda^c(n_e,n_i,k_BT,s)$ is known
- Same considerations works for decay from g.s.
- The in-plasma photoactivation rate is the common factor in both the above cases.
- One of the photons in the cascade of 176Lu can serve as a fingerprint of the isomer population and hence $\lambda^c(n_e,n_i,T,s)$.

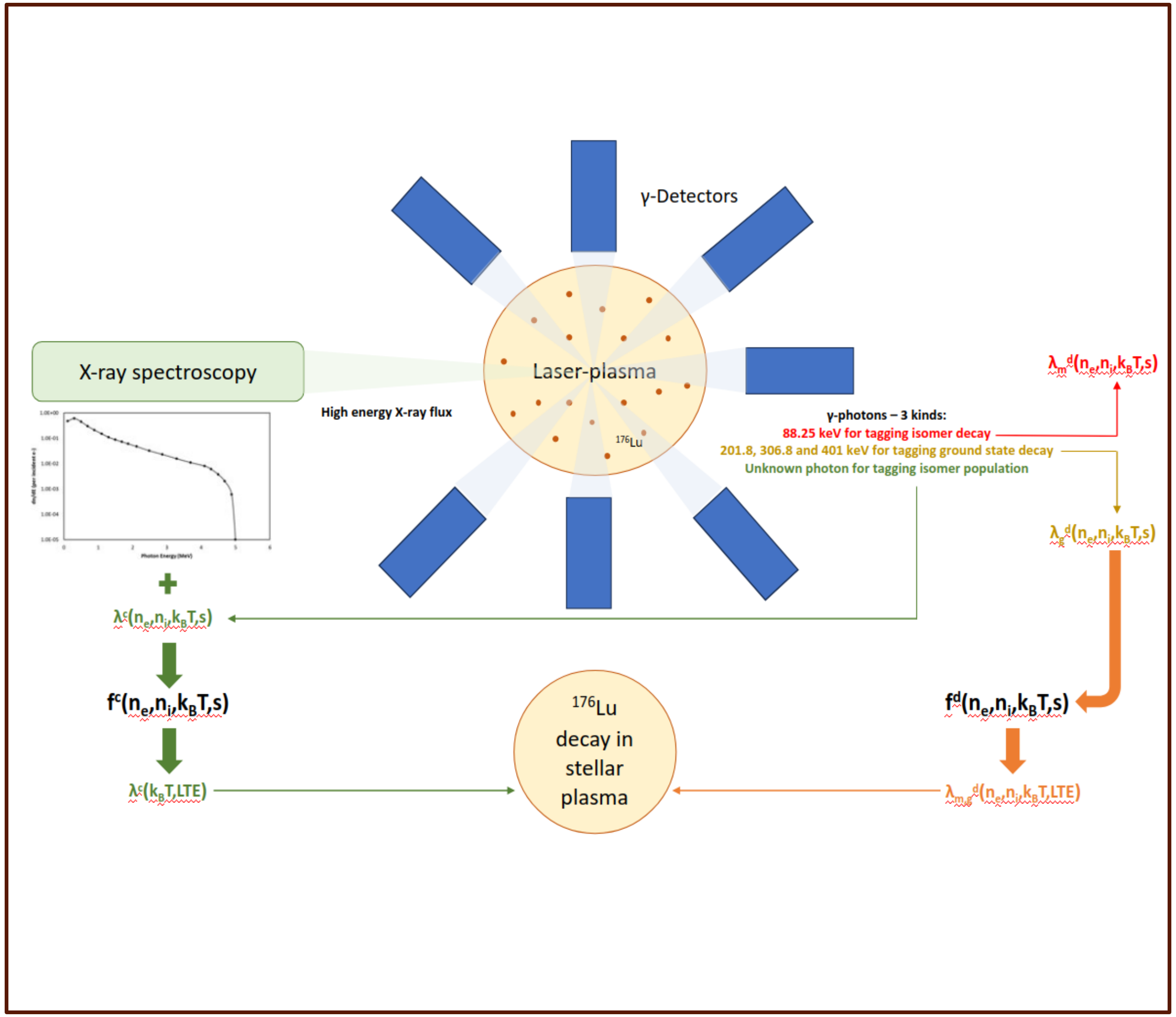

Multiphysics Simulations, Theory and Modelling of PANDORA

- **Plasma kinetics:** stationary PIC-Particle-In-Cell simulation by Relativistic Boris Leap-Frog Method implemented in MATLAB

- **Plasma Collisions:** Monte-Carlo approach embedded in the PIC-code

- **Electromagnetic interaction with plasma:** self-consistent evaluation of the field by FEM code with tensorial computation (attuated in COMSOL)

- **Beta-dacay rate evaluation:** generalization of the Fermi-Golden Rule to LTE and nLTE multi-ionized media (laboratory and astrophysical plasmas)

- **Gamma-ray detection:** GEANT4 simulation including the plasma source, magnets, cryostat and HPGe detectors array

- **Isotope Injection:** evaporation dynamics and coupling to the plasma of metallic isotope → blending COMSOL diffusion tool with our PIC-Code

Plasma heating modelling

Solving the time-independent Vasov equation, including single particle collisions

$$\frac{\partial f_\alpha}{\partial t} + \vec{v}\cdot\vec{\nabla} f_\alpha + \frac{q_\alpha}{m_\alpha}\left(\vec{E} + \frac{\vec{v}\times\vec{B}}{c}\right)\cdot\vec{\nabla}_{\vec{v}} f_\alpha = 0$$

$$\frac{d\vec{v}}{dt} = \frac{q}{m_0\gamma}\left[\vec{E} + \vec{v}\times B - \frac{\vec{v}\cdot\vec{E}}{c^2}\vec{v}\right]$$

Step-by-step current

Step-by-step plasma density

$$\begin{aligned}
\vec{\nabla}\cdot\vec{E} &= 4\pi\sum_\alpha \overline{n}_\alpha q_\alpha \boxed{\int f_\alpha d\vec{v}} + 4\pi\rho_{ext} \\
\vec{\nabla}\times\vec{B} &= \frac{1}{c}\frac{\partial\vec{E}}{\partial t} + \frac{4\pi}{c}\sum_\alpha \overline{n}_\alpha q_\alpha \boxed{\int \vec{v} f_\alpha d\vec{v}} + \frac{4\pi}{c}\vec{J}_{ext} \\
\vec{\nabla}\times\vec{E} &= -\frac{1}{c}\frac{\partial\vec{B}}{\partial t}
\end{aligned}$$

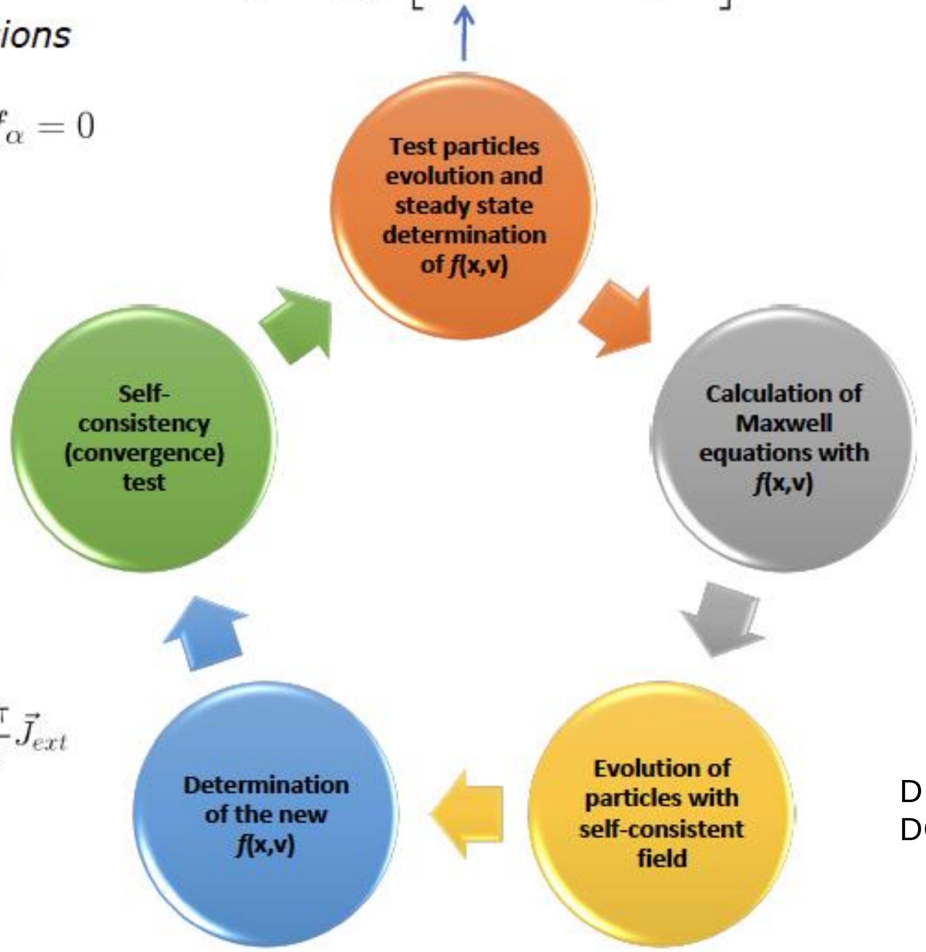

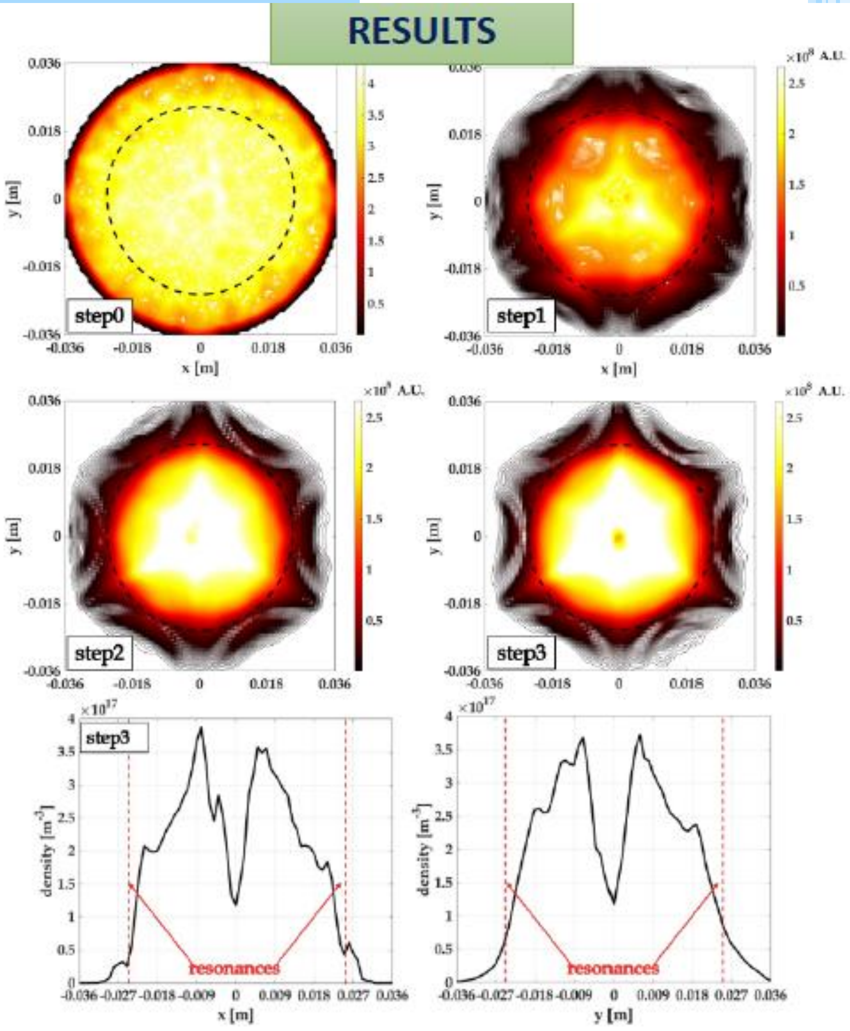

D Mascali et al Eur. Phys. J. D (2015) 69: 27
DOI: 10.1140/epjd/e2014-50168-5

ECR Plasma Simulations: Pipeline

PIC SIMULATIONS FOR ELECTRONS

3D, steady-state maps of n_e and E_e

First level input to all codes and therefore precision needed

Observables: **Soft X-ray spectroscopy**, interferometry, polarimetry, profilometry, Thomson scattering

PIC-MC SIMULATIONS FOR PLASMA IONS

3D, steady-state maps of $\langle Z \rangle$ and n_i

Second level input to in-plasma decay code

Observables: **Faraday cup**, optical emission spectroscopy, X-ray fluorescence

PIC-MC SIMULATIONS FOR ISOTOPE IONS

3D, steady-state maps of $\langle Z \rangle$ and λ^*

Observables: **PANDORA**

Particle-in-Cell Simulations

PIC is a technique to simulate plasma.

Self-consistent, steady-state solution

***N* macroparticles**, each representing a certain number of real particles, are initialised and transported according to **equations of motion**

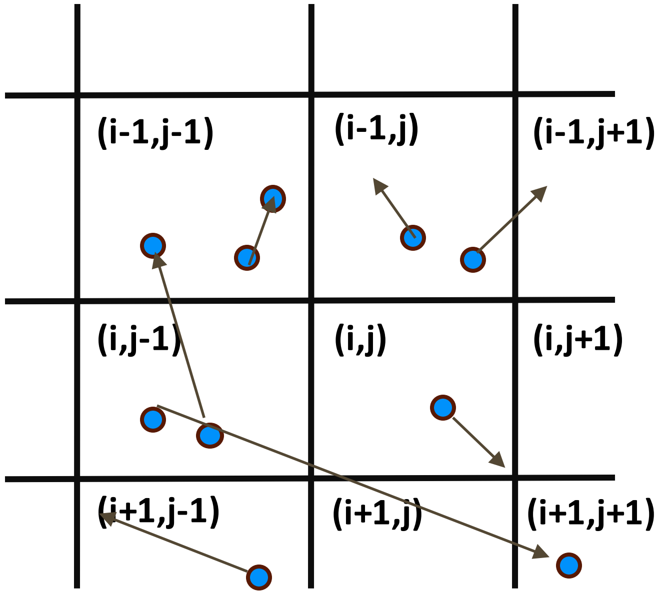

The simulation domain is divided into a grid, and particle trajectories leaves **traces at grid points** which leads to an **occupation map**

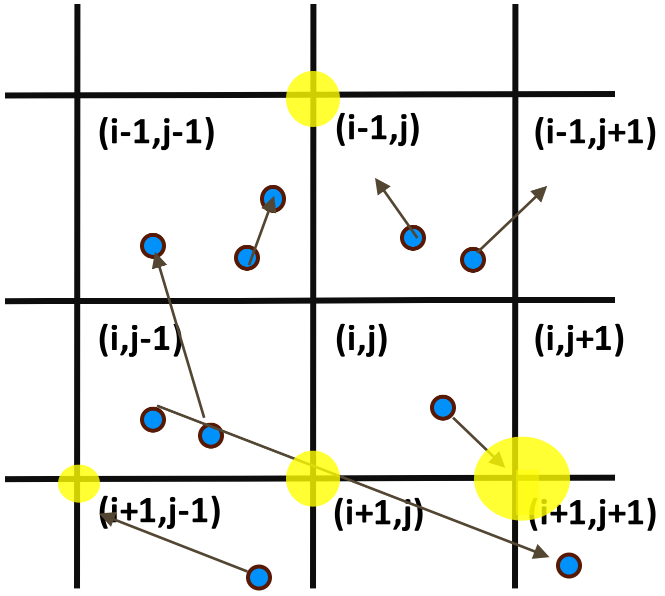

Occupation maps are **scaled to density maps** according to some physical law, and fields are calculated on grid points using **FEM/FDM**

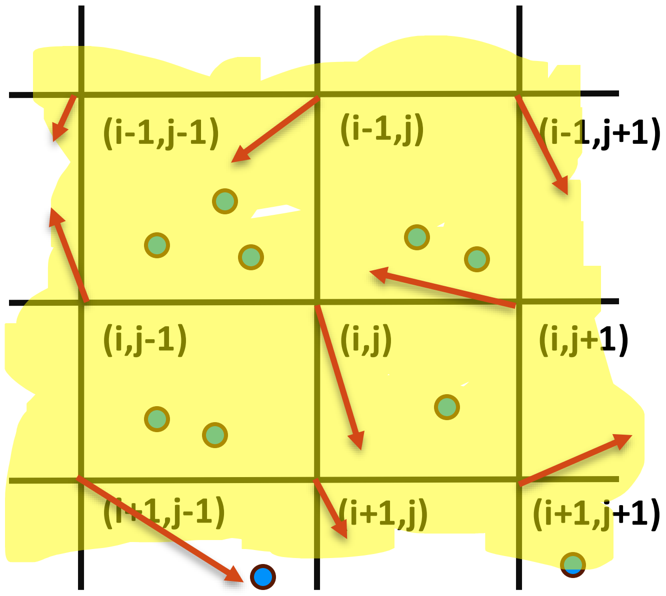

Simulation of stationary system

Simulation of a river

1° Simulation of all involved particles
+
Continuous creation and destruction of particles

2° Simulation of well defined statistical sample
+
Accumulation and statistical information for
all the life of the sample

Modeling of electron and ion dynamics with Monte-Carlo calculations:

$$B_x = -B_1 xz + 2Sxy$$

$$B_y = -B_1 yz + 2S(x^2 - y^2)$$

$$B_z = \begin{cases} -B_0 + B_{inj} z^2 & \forall z < 0 \\ -B_0 + B_{ext} z^2 & \forall z > 0 \end{cases}$$

Hexapolar field

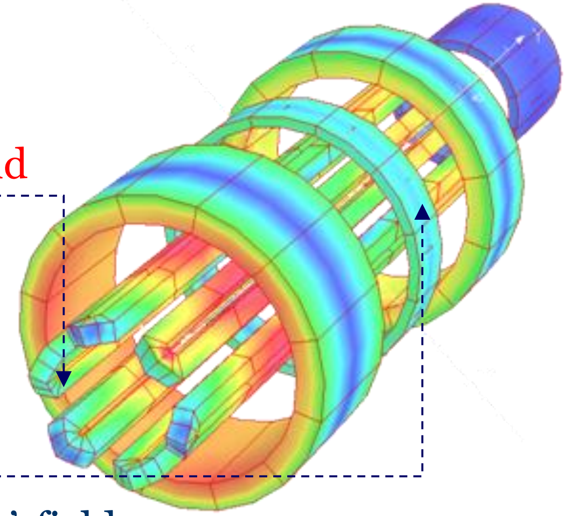

Solenoids' field

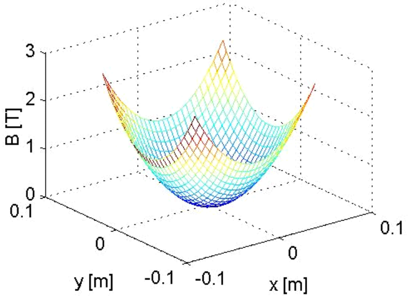

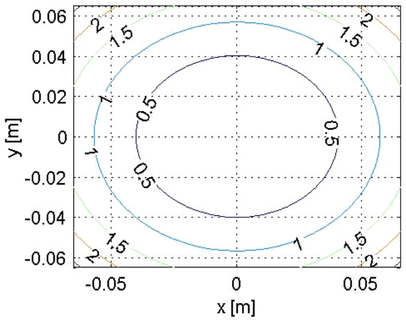

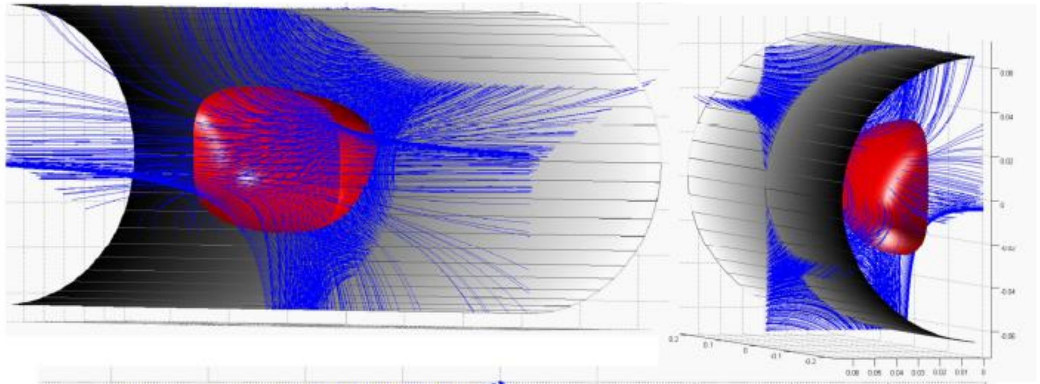

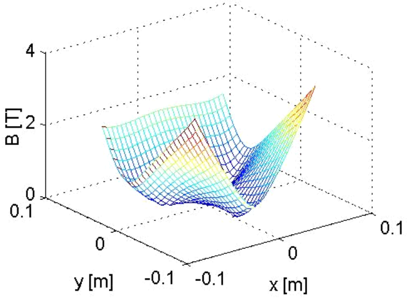

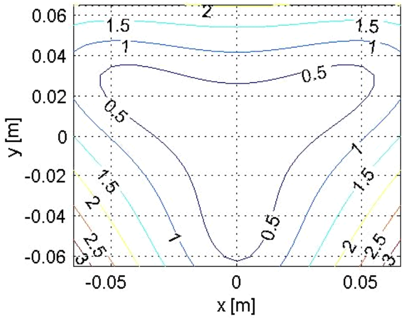

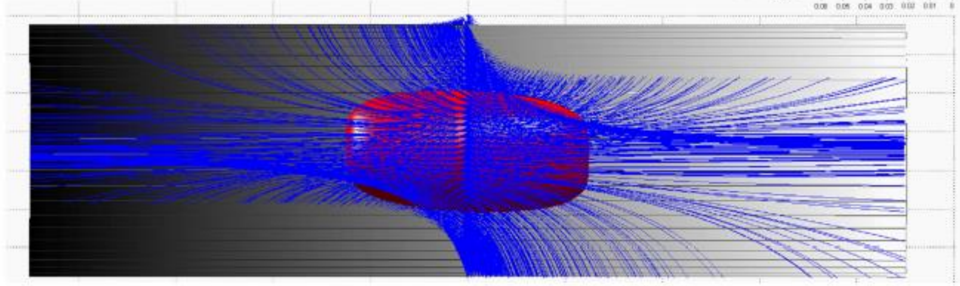

Electromagnetic Field

Inner "empty-cavity" electric field distribution for the $TE_{4\ 4\ 23}$ mode close to 14 GHz

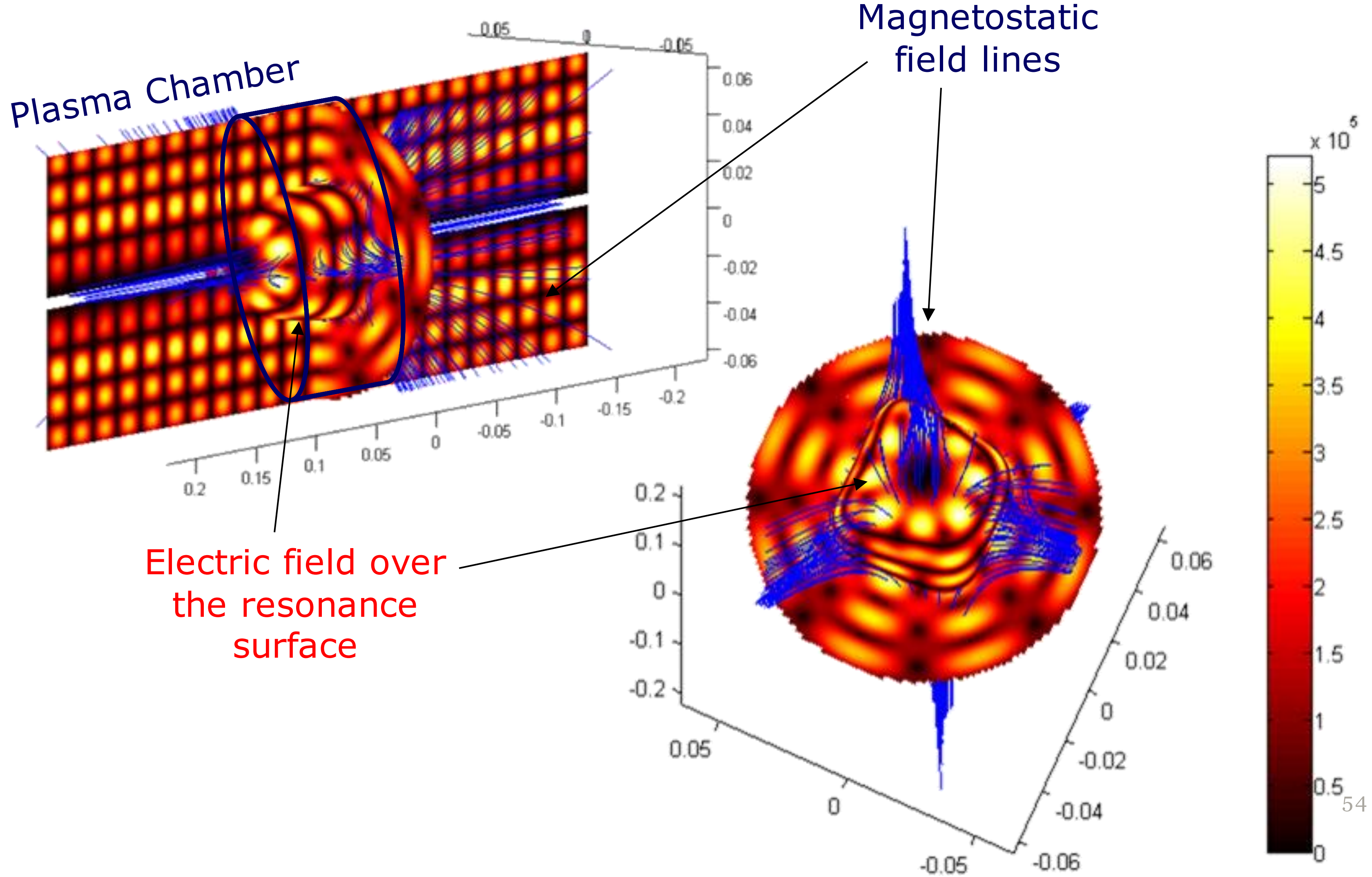

Example of a mesh in a FEM (Finite Element Method) simulator (***Ansoft HFSS)***
tetraedres are used to approximate the curved surfaces.

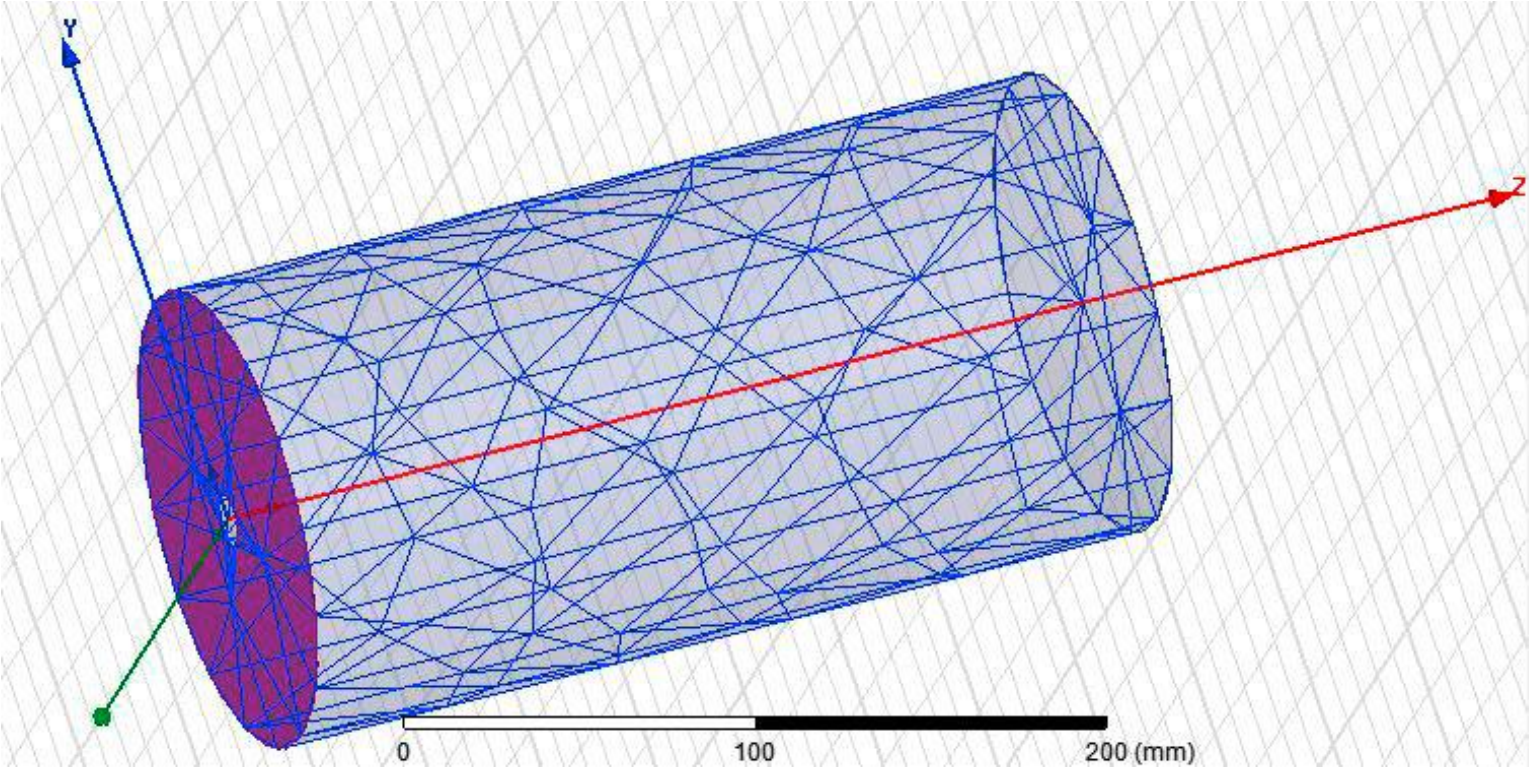

ECRIS cavities

- FEM Simulators

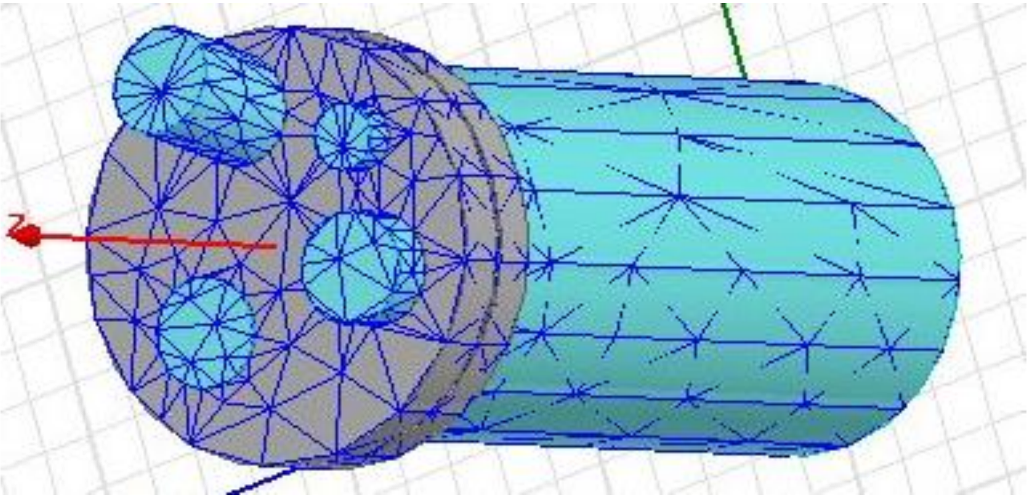

Solutions Approaches: why full-wave simulations?

Ray tracing modeling has several critical issues:

- WKB approximation requires $\frac{\nabla k}{k} << 1$ that is not valid in ECRIS plasmas scenario

Full-wave modeling allows:

- Direct evaluation of Electric field (also in cutoff region) in presence of plasma and RF waveguide excitation.

Finite Elements method (FEM)

- Tends to make numerically **sparse matrix**
- Can handle **complicated geometry**
- Inclusion of **dissimilar material properti**
- Capture of local effects
- Good application suite (GUI, CAD import, Visualization) are available

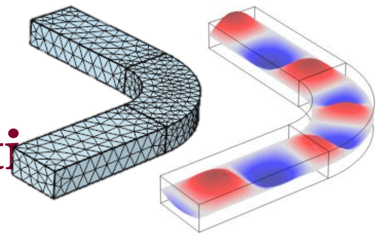

...With COMSOL

Non-uniform, anisotropic dielectric tensors

Non-uniform dielectric tensor

Non-symmetric 3D magnetostatic field Equations

$$\begin{cases} B_x = B_1 xz + 2S_{ex}xy \\ B_y = -B_1 yz + S_{ex}(x^2 - y^2) \\ B_z = B_0 + B_1 z^2 \end{cases}$$

Assuming a non uniform magnetostatic field the ***dielectric tensor*** *is:*

$$\overline{\overline{\epsilon}} = \epsilon_0 \overline{\overline{\epsilon}}_r = \epsilon_0 \left(\overline{\overline{\mathrm{I}}} + \frac{\mathrm{i}\overline{\overline{\sigma}}}{\omega\epsilon_0} \right) = \epsilon_0 \left(\overline{\overline{\mathrm{I}}} + \frac{\mathrm{i}\omega_p^2 \overline{\overline{\mathrm{T}}}^{-1}}{\omega} \right) =$$

$$= \epsilon_0 \begin{bmatrix} 1 + \frac{\mathrm{i}\omega_p^2}{\omega} \frac{(-\mathrm{i}\omega+\omega_{\mathrm{eff}})^2 + B_{0x}^2 (\frac{q}{m})^2}{\Delta} & \frac{\mathrm{i}\omega_p^2}{\omega} \frac{B_{0z}\frac{q}{m}(-\mathrm{i}\omega+\omega_{\mathrm{eff}}) + B_{0x}B_{0y}(\frac{q}{m})^2}{\Delta} & \frac{\mathrm{i}\omega_p^2}{\omega} \frac{-B_{0y}\frac{q}{m}(-\mathrm{i}\omega+\omega_{\mathrm{eff}}) + B_{0x}B_{0z}(\frac{q}{m})^2}{\Delta} \\ \frac{\mathrm{i}\omega_p^2}{\omega} \frac{-B_{0z}\frac{q}{m}(-\mathrm{i}\omega+\omega_{\mathrm{eff}}) + B_{0x}B_{0y}(\frac{q}{m})^2}{\Delta} & 1 + \frac{\mathrm{i}\omega_p^2}{\omega} \frac{(-\mathrm{i}\omega+\omega_{\mathrm{eff}})^2 + B_{0y}^2 (\frac{q}{m})^2}{\Delta} & \frac{\mathrm{i}\omega_p^2}{\omega} \frac{B_{0x}\frac{q}{m}(-\mathrm{i}\omega+\omega_{\mathrm{eff}}) + B_{0y}B_{0z}(\frac{q}{m})^2}{\Delta} \\ \frac{\mathrm{i}\omega_p^2}{\omega} \frac{B_{0y}\frac{q}{m}(-\mathrm{i}\omega+\omega_{\mathrm{eff}}) + B_{0x}B_{0z}(\frac{q}{m})^2}{\Delta} & \frac{\mathrm{i}\omega_p^2}{\omega} \frac{-B_{0x}\frac{q}{m}(-\mathrm{i}\omega+\omega_{\mathrm{eff}}) + B_{0z}B_{0y}(\frac{q}{m})^2}{\Delta} & 1 + \frac{\mathrm{i}\omega_p^2}{\omega} \frac{(-\mathrm{i}\omega+\omega_{\mathrm{eff}})^2 + B_{0z}^2 (\frac{q}{m})^2}{\Delta} \end{bmatrix}$$

$$\overline{\overline{\sigma}} = \epsilon_0 \omega_p^2 \overline{\overline{\mathrm{T}}}^{-1}$$

Off-diagonal Elementes due to 3D Magnetic field

Tools for modelling 3D e.m. interaction with magnetized plasmas for fundamental research and Fusion

Non-symmetric 3D magnetostatic field

$$\begin{cases} B_x = B_1 xz + 2S_{ex}xy \\ B_y = -B_1 yz + S_{ex}(x^2 - y^2) \\ B_z = B_0 + B_1 z^2 \end{cases}$$

Assuming a non uniform magnetostatic field the ***dielectric tensor*** *is:*

$$\frac{\overline{\overline{\varepsilon}}}{\varepsilon_0} = \begin{bmatrix} 1 + j\dfrac{\omega_p^2}{\omega}\dfrac{A_x}{\Delta} & j\dfrac{\omega_p^2}{\omega}\dfrac{C_z + D_{xy}}{\Delta} & j\dfrac{\omega_p^2}{\omega}\dfrac{-C_y + D_{xz}}{\Delta} \\ j\dfrac{\omega_p^2}{\omega}\dfrac{-C_z + D_{xy}}{\Delta} & 1 + j\dfrac{\omega_p^2}{\omega}\dfrac{A_y}{\Delta} & j\dfrac{\omega_p^2}{\omega}\dfrac{C_x + D_{yz}}{\Delta} \\ j\dfrac{\omega_p^2}{\omega}\dfrac{C_y + D_{xz}}{\Delta} & j\dfrac{\omega_p^2}{\omega}\dfrac{-C_x + D_{zy}}{\Delta} & 1 + j\dfrac{\omega_p^2}{\omega}\dfrac{A_z}{\Delta} \end{bmatrix}$$

$$\boxed{\omega_p^2 = \frac{n_e e^2}{m\varepsilon_0}}$$

$$\boxed{A_i(x,y,z,B_0,n_e,\omega_{eff}) = C_i(x,y,z,B_0,n_e,\omega_{eff}) = D_i(x,y,z,B_0,n_e,\omega_{eff}) = \Delta(x,y,z,B_0,n_e,\omega_{eff})}$$

Off-diagonal Elements due to 3D Magnetic field

ECR-surface-based mesh to create a fine mesh on the ECR surface

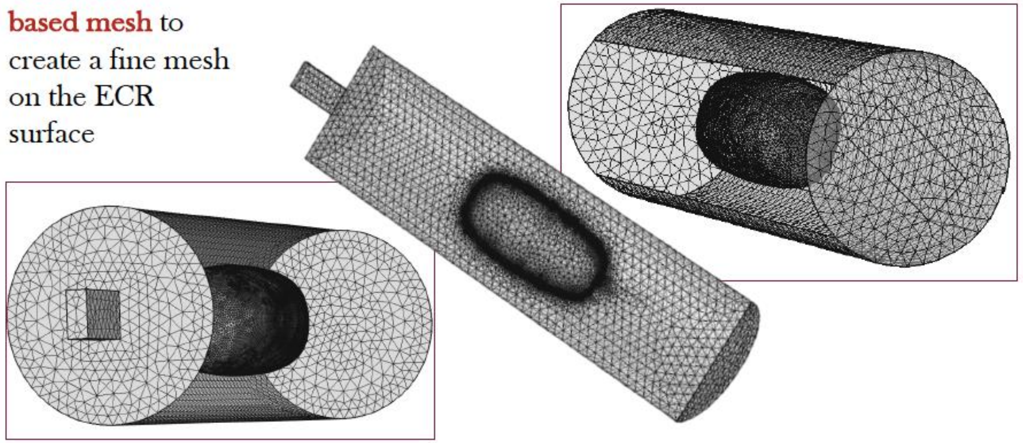

The mesh is very fine on the ECR surface and relatively coarser away from the resonance zone.

$$P_{diss} = \vec{J}\cdot\vec{E} = \left(\overline{\overline{\sigma}}\cdot\vec{E}\right)\cdot\vec{E}$$

The largest fraction of energy is absorbed at the ECR

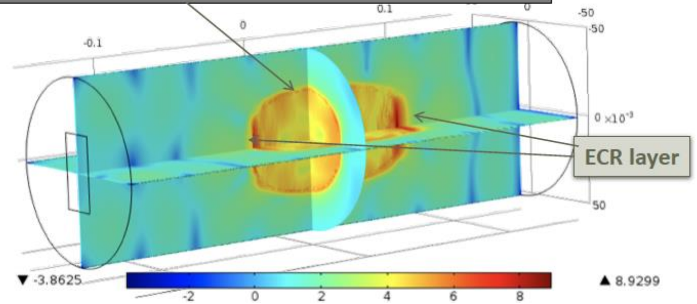

G. Torrisi et al. Journal of Electromagnetic Waves and Applications, 28:9, 1085-1099, DOI:10.1080/09205071.2014.905245

Cold plasma simulations in COMSOL with Matlab

Solution of Maxwell's equations in **COMSOL** using MUMPS direct solver

Full anisotropic dielectric tensor for the magnetized plasma computed in **MATLAB**

Electromagnetic field in ECRIS Plasma

Solution of the wave equation

$$\nabla \times \nabla \times \vec{E}(\vec{r}) + \frac{\omega^2}{c^2} \overleftrightarrow{\varepsilon} \cdot \vec{E}(\vec{r}) = 0$$

Conventional PDE which can be solved by **COMSOL**

NUMERICAL RESULTS

COMPARISON OF ELECTRIC FIELD IN VACUUM VS PLASMA FILLED CAVITY

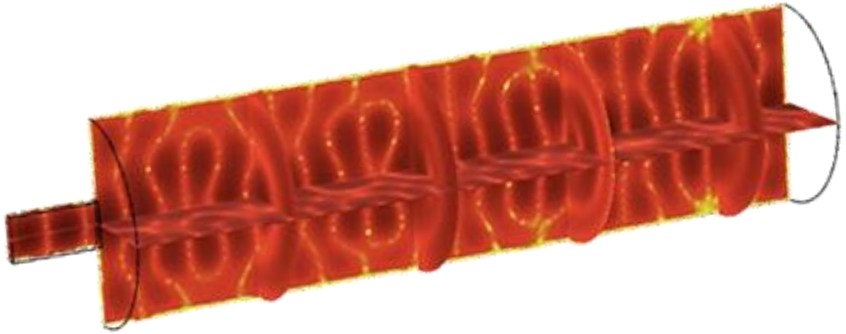

Vacuum field in the cavity

Areas where the electric field is more intense:
the plot is in log colour map

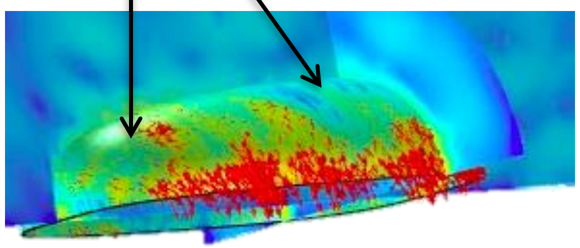

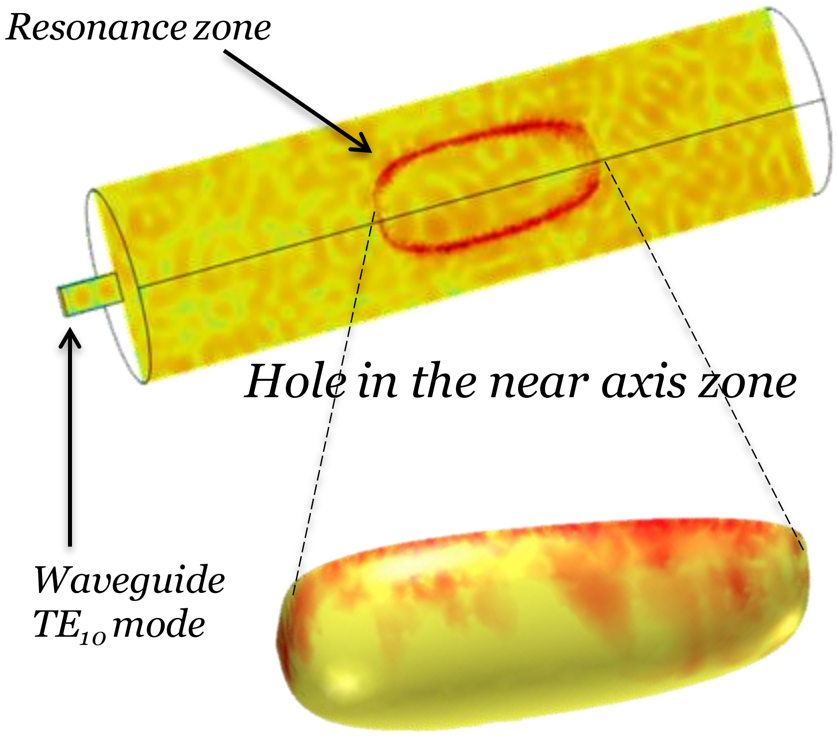

Full-wave solution: densification of the electromagnetic field in the near resonance zone

Electrons and Ions Simulations: Transport Module

Ion Transport: Boris Method

Being charged particles, ions in an ECR plasma move under the influence of EM fields (self-generated and external)

EM transport

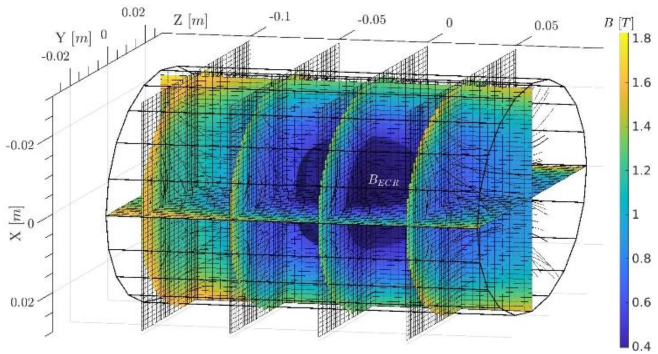

Magnetostatic field profile in A-HPC ECRIS

$$\frac{\mathbf{dr}}{\mathbf{d}t} = \mathbf{v}$$

$$m\frac{\mathbf{dv}}{\mathbf{d}t} = q(\mathbf{E} + \mathbf{v} \times \mathbf{B})$$

Equation of motion for charged particles under Lorentz force

Numerical implementation of Lorentz force using Boris method, with correction by Zenitani and Umeda

r — n — n+1

$\mathbf{B}^n$
$\mathbf{E}^n$

$$\mathbf{u}^- = \gamma \mathbf{v}^{n-1/2} + \frac{q}{2m}\mathbf{E}^n T_{step}$$

$$\theta = \frac{qT_{step}}{m\gamma}|\mathbf{B}^n|$$

$$\mathbf{u}^+ = R_{rot}\mathbf{u}^-$$

$$\mathbf{v}^{n+1/2} = \frac{1}{\gamma}(\mathbf{u}^+ + \frac{q}{2m}\mathbf{E}^n)$$

$$\mathbf{r}^{n+1} = \mathbf{r}^n + \mathbf{v}^{n+1/2} T_{step}$$

$$R_{rot} = \begin{pmatrix} R_{11} & R_{12} & R_{13} \\ R_{21} & R_{22} & R_{23} \\ R_{31} & R_{32} & R_{313} \end{pmatrix}$$
$$R_{11} = \cos\theta + b_x^2(1-\cos\theta)$$
$$R_{22} = \cos\theta + b_y^2(1-\cos\theta)$$
$$R_{33} = \cos\theta + b_z^2(1-\cos\theta)$$
$$R_{12} = R_{21} = b_x b_y(1-\cos\theta) + b_z\sin\theta$$
$$R_{13} = R_{31} = b_z b_x(1-\cos\theta) + b_y\sin\theta$$
$$R_{23} = R_{32} = b_y b_z(1-\cos\theta) + b_x\sin\theta$$

v — n-1/2 — n+1/2

J.P. Boris, Proc. 4th Naval Conf. on Numerical Simulation of Plasmas
S. Zenitani and T. Umeda, Phys. Plasmas ***25*** *(2018)*

Electrons maps and Stepwise ionization

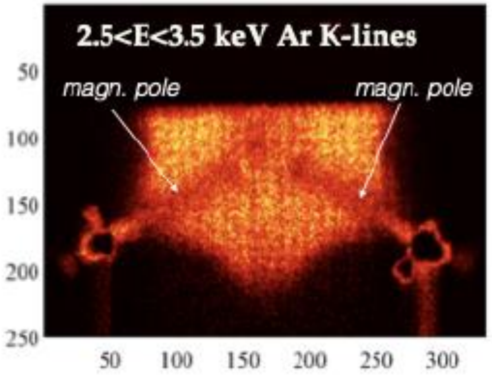

X-ray fluorescence from Ar ions in the plasma

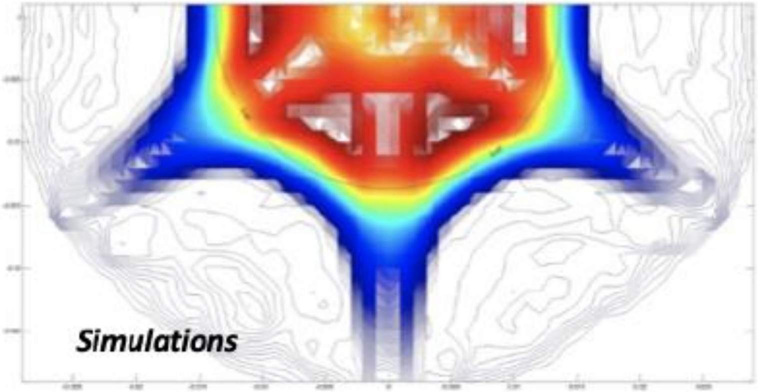

3D self-consistent simulations very well reproduce energy content distribution of the plasma, which in turn fits with experimental detected displacement of Argon ions

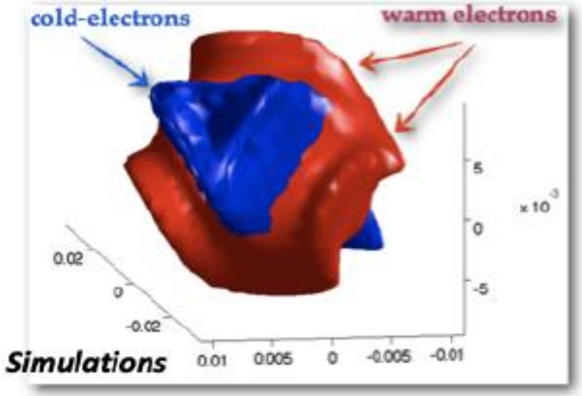

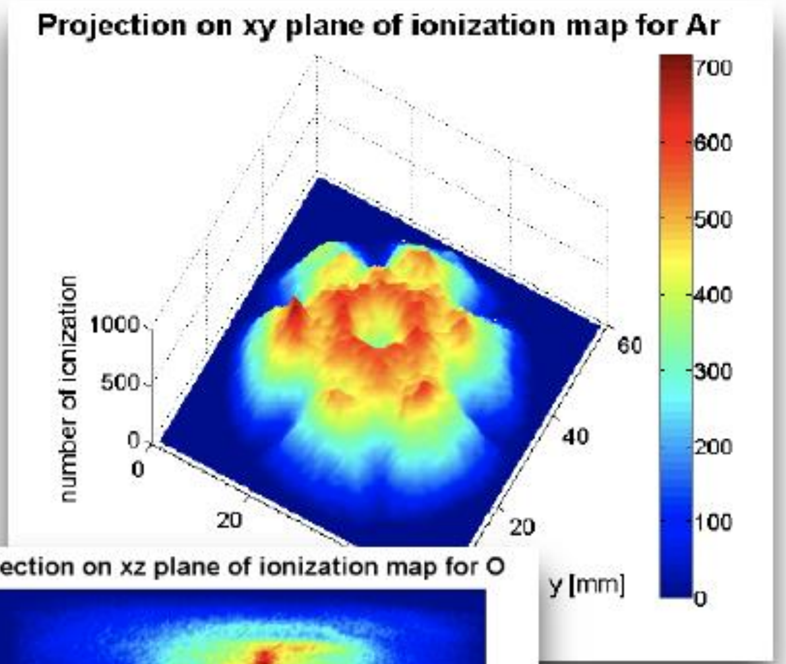

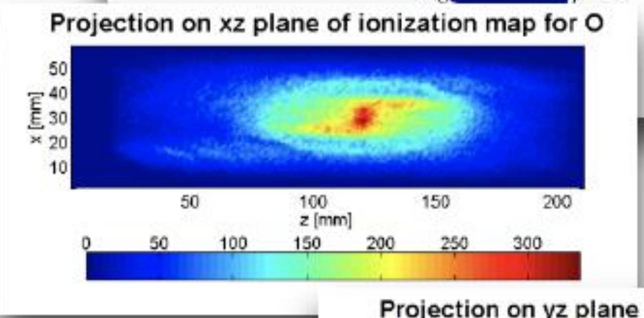

Starting from 3D distribution of electrons in the plasma, maps of ions distribution can be obtained

$$\frac{\nu_{ion\,i\to i+1}}{n_e} = \sum_{j=1}^{N} \frac{a_{ij}q_{ij}}{T_e^{3/2}}\left\{\frac{1}{P_{ij}/T_e}E_1(P_{ij}/T_e) - \frac{b_{ij}e^{c_{ij}}}{P_{ij}/T_e+c_{ij}}E_1(P_{ij}/T_e+c_{ij})\right\}$$

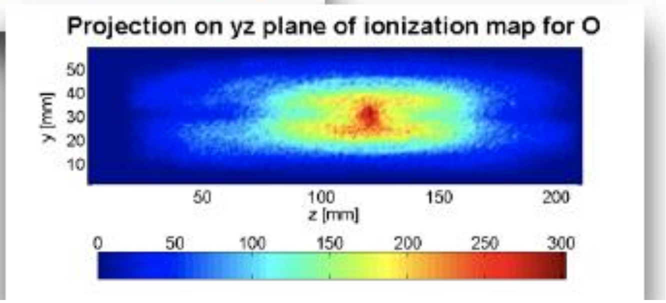

SIMULATED 3D STRUCTURE OF THE PLASMA

Simulations based on a 3D Monte-Carlo collisional approach reveal that the plasma almost totally accumulates inside the ECR surface (**PLASMOID GENERATION**).

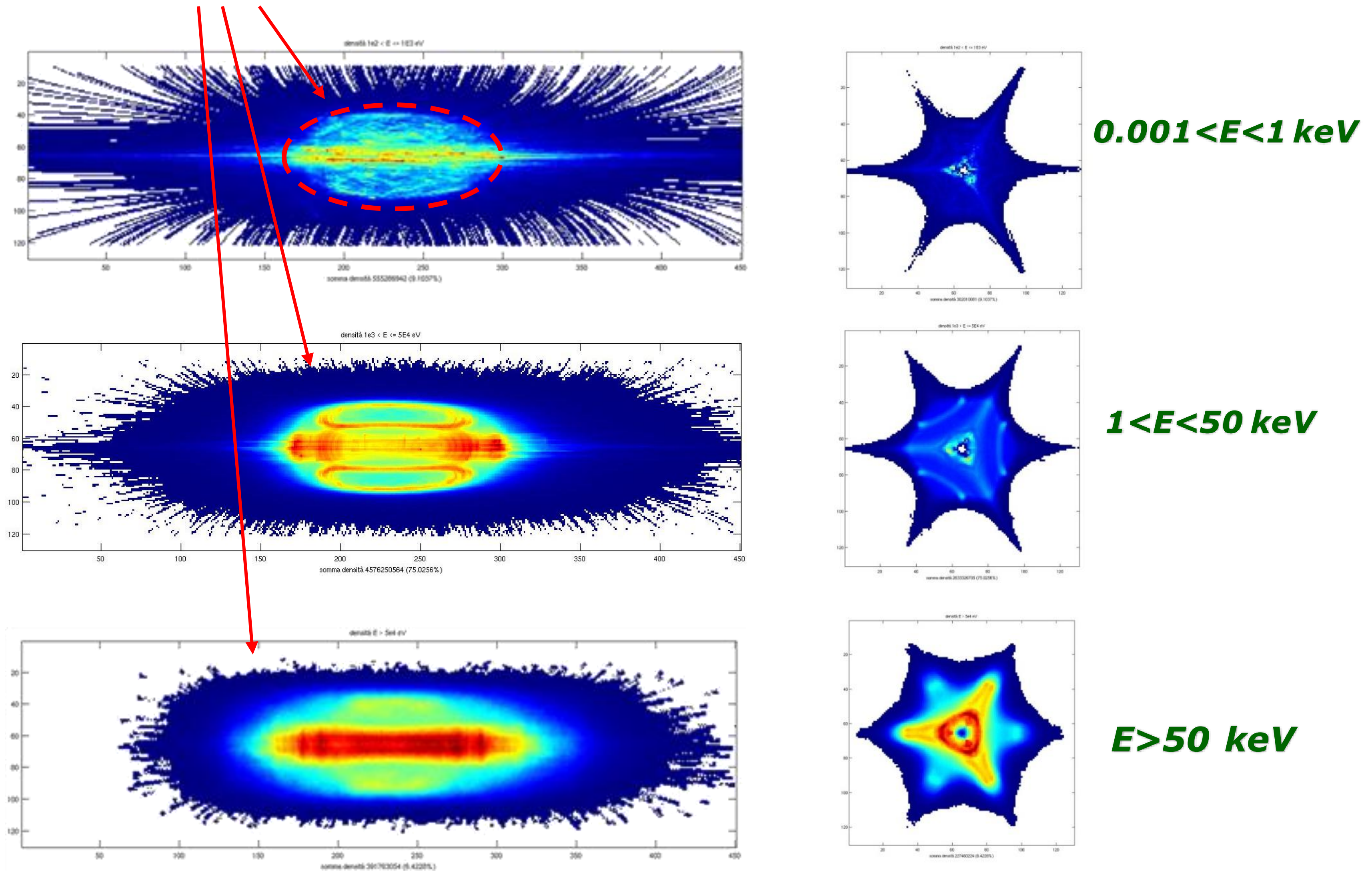

Electron Simulations: Overview

PIC simulation for ECR plasma electrons
- Description: Vlasov-Maxwell equation
- Scaling: Plasma cutoff density
- Self-consistency: Microwave EM field

D. Mascali, G. Torrisi et al , Eur. Phys. J. D. ***69****, 27 (2015)*
G. Torrisi, D. Mascali et al, JEWA ***28****, 9 (2014)*
A. Galatà et al, Front. Phys. ***10****, 947194 (2022)*

ECRIS	ω	P_{inj}	Gas	P	r	L
A-HPC	14.25 GHz	200 W	Ar	10^{-6} mbar	29 mm	210 mm

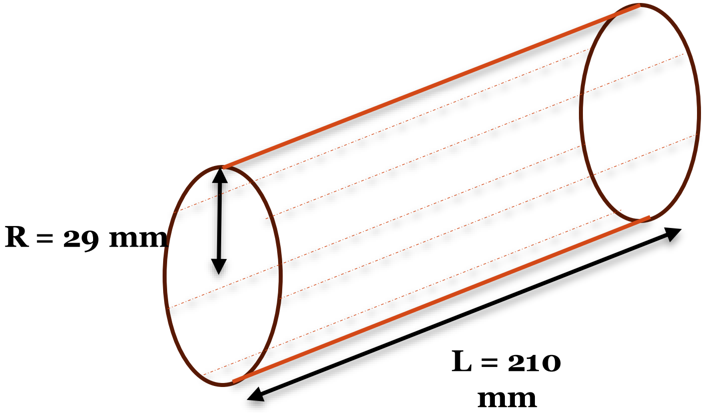

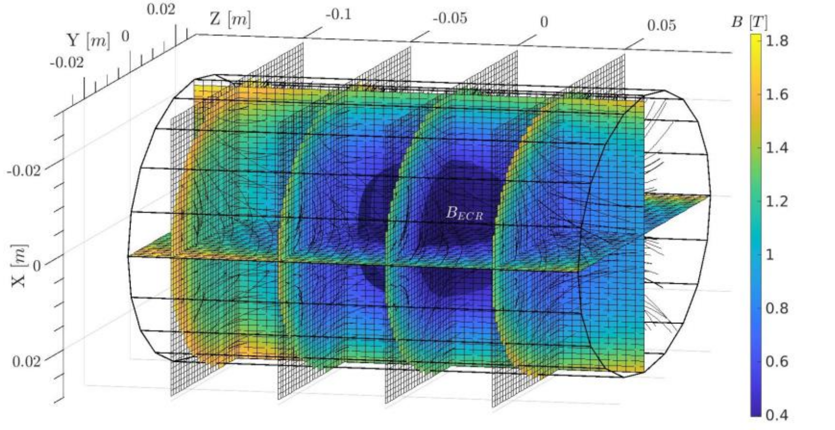

B-field distribution in A-HPC ion source. The ellipsoidal surface nestled in the middle represents the ECR surface

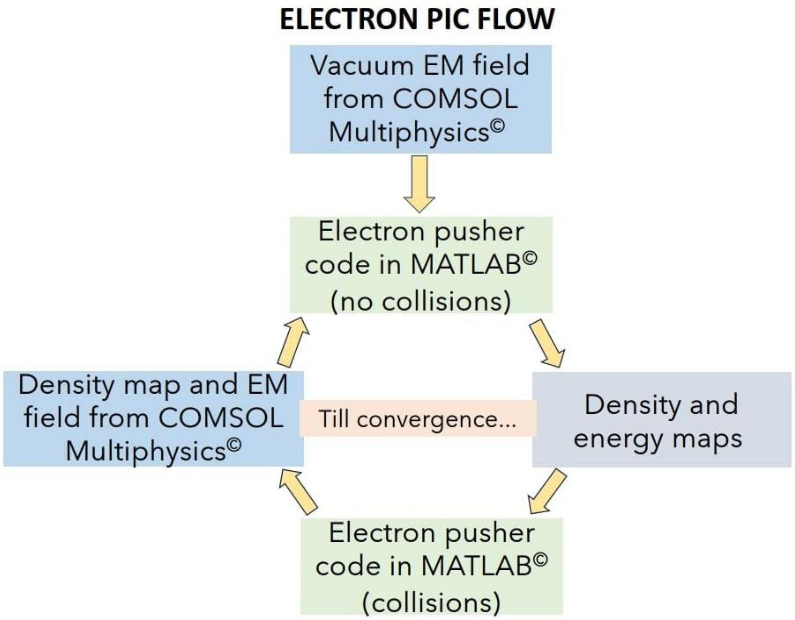

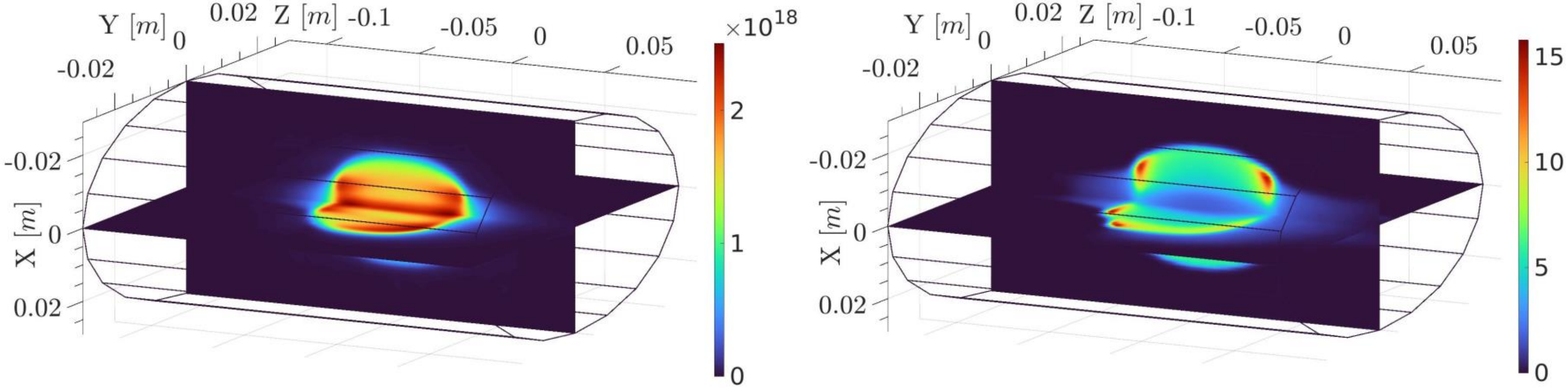

Electron density n_e (m^{-3}) and mean energy E_e (keV) maps for A-HPC obtained from PIC simulations.

Ion Simulations: Overview

PIC simulations for ECR plasma ions:

- Description: Vlasov-Maxwell equations + Balance equation
- Scaling: Quasineutrality with electron density
- Self-consistency: Electron density and energy maps

$$\frac{\mathrm{d}n_i}{\mathrm{d}t} = n_{i-1}n_e\gamma_{i-1,i} - n_i n_e \gamma_{i,i+1} + n_{i+1}n_0E_{i+1,i} - n_i n_0 E_{i,i-1} - \frac{n_i}{\tau_i}$$

B. Mishra et al, Front. Phys. ***10****, 932448 (2022)*

B. Mishra, EPJ WoC ***275****, 02001 (2023)*

3 core modules

Ion Transport

Transport in EM fields under Lorentz force

Collisions by Fokker-Planck equation

MC Sampling

$$\frac{\mathrm{d}n_i}{\mathrm{d}t} = n_{i-1}n_e\gamma_{i-1,i} - n_i n_e \gamma_{i,i+1} + n_{i+1}n_0E_{i+1,i} - n_i n_0 E_{i,i-1} - \frac{n_i}{\tau_i}$$

Electron impact ionization (EI) — Ion impact charge exchange (CEX)

Density Scaling

Iterative scaling of ion occupation map

$$\int_V n_e \mathrm{d}V = K \int_V w_i n_i$$

Ion Simulations: Self-Consistent Loop

ECR plasma ions can be simulated PIC-MC codes, which evolve the density maps of successive ionization stages self-consistently with electron density and energy maps given as input

B. Mishra et al, Front. Phys. ***10****, 932448 (2022)*
B. Mishra, EPJ WoC ***275****, 02001 (2023)*

BUFFER IONS BALANCE EQUATION:

$$\frac{\mathrm{d}n_i}{\mathrm{d}t} = n_{i-1}n_e\gamma_{i-1,i} - n_i n_e \gamma_{i,i+1} + n_{i+1}n_0 E_{i+1,i} - n_i n_0 E_{i,i-1} - \frac{n_i}{\tau_i}$$

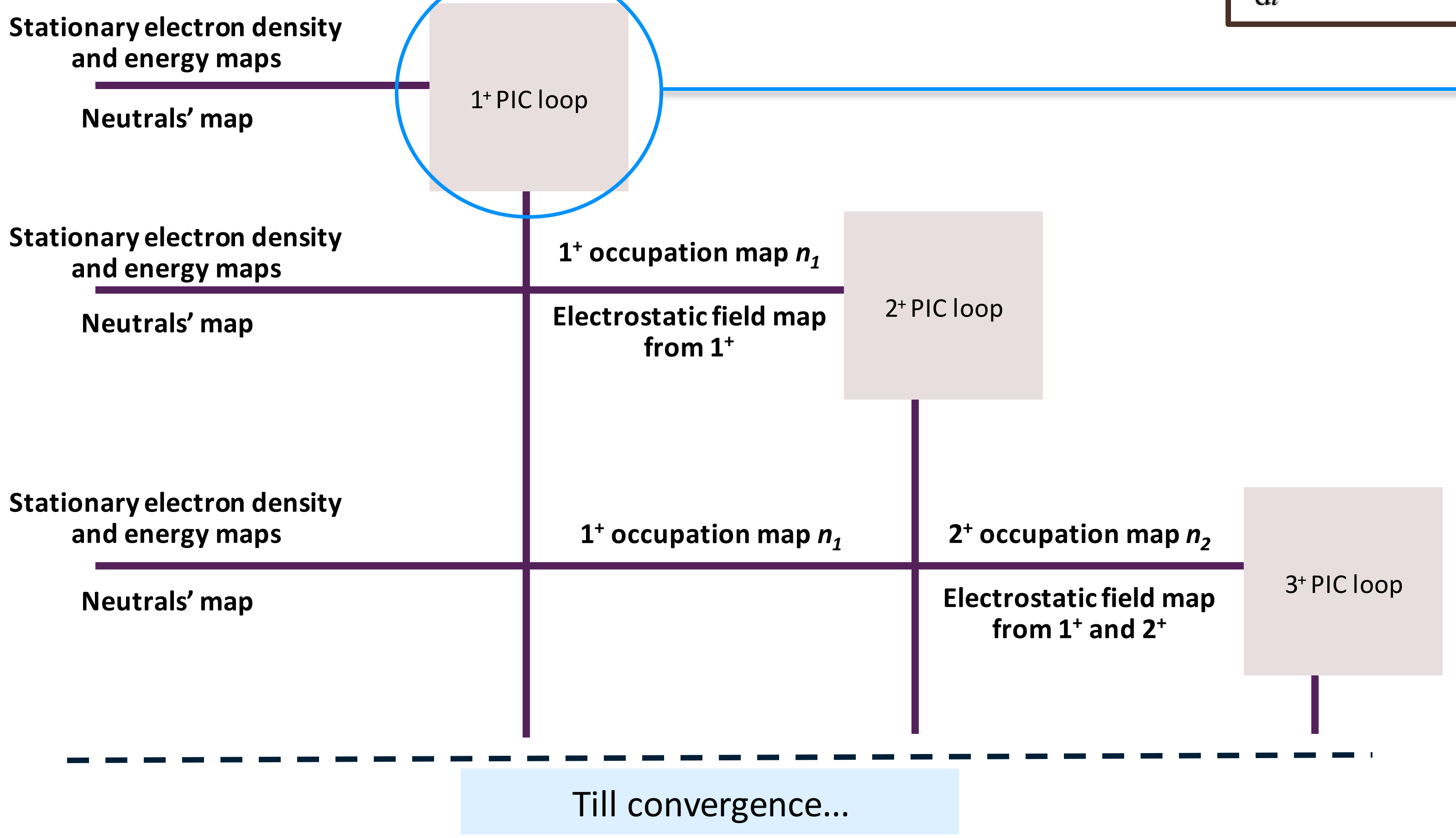

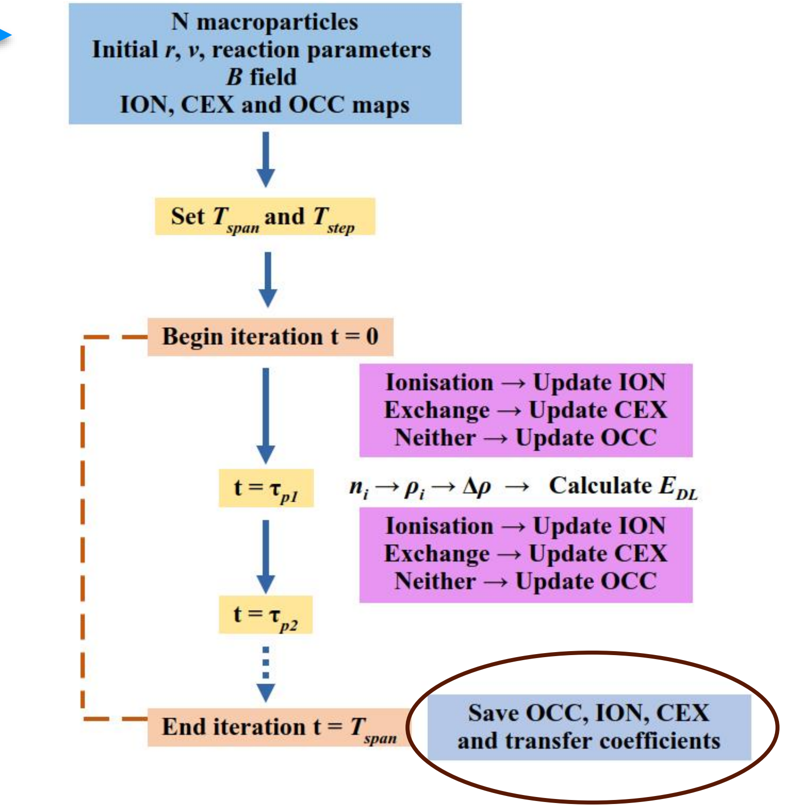

Ion Simulations: Transport Module

Ion Transport: Collisions

Ions in an ECR plasma also undergo collisions with other plasma species

Collisions

Numerical implementation of Fokker-Planck equation using superpotential formalism by MacDonald and Rosenbluth

*W.M. MacDonald, M.N. Rosenluth and W. Chuck, Phys. Plasmas **107**, 350 (1957)*
*A. Galatà et al, Plasma Sources Sci. Technol. **25** (2016)*

Test particle *p* enters a field of plasma particles of density n_s and temperature *kT* along a magnetic field line. It interacts with the field through numerous long-range Coulomb interaction, which change its momentum

$$A_D = \frac{(ZZ')^2 e^4 n_s \ln\Lambda}{2\pi\epsilon_0^2 m^2}$$

$$\boxed{\nu_s = \left(1+\frac{m}{m_s}\right)\frac{A_D}{c_s^3}\frac{G(\frac{|\mathbf{v}^{n-1/2}|}{c_s})}{\frac{|\mathbf{v}^{n-1/2}|}{c_s}}}$$

Friction frequency

$$\boxed{D_{||} = \langle \mathbf{v}_{||}^2 \rangle = \frac{A_D}{|\mathbf{v}^{n-1/2}|} G\left(\frac{|\mathbf{v}^{n-1/2}|}{c_s}\right)}$$

Parallel diffusion coefficient

$$\boxed{D_{\perp} = \langle \mathbf{v}_{\perp}^2 \rangle = \frac{A_D}{|\mathbf{v}^{n-1/2}|}\left\{\Phi\left(\frac{|\mathbf{v}^{n-1/2}|}{c_s}\right) - G\left(\frac{|\mathbf{v}^{n-1/2}|}{c_s}\right)\right\}}$$

Perpendicular diffusion coefficient

$$\mathbf{v}^{n+1/2} = \frac{1}{\gamma}\left(\mathbf{u}^+ + \frac{q}{2m}\mathbf{E}^n\right) + \mathbf{v}_{fric} + \mathbf{v}_{rand}$$

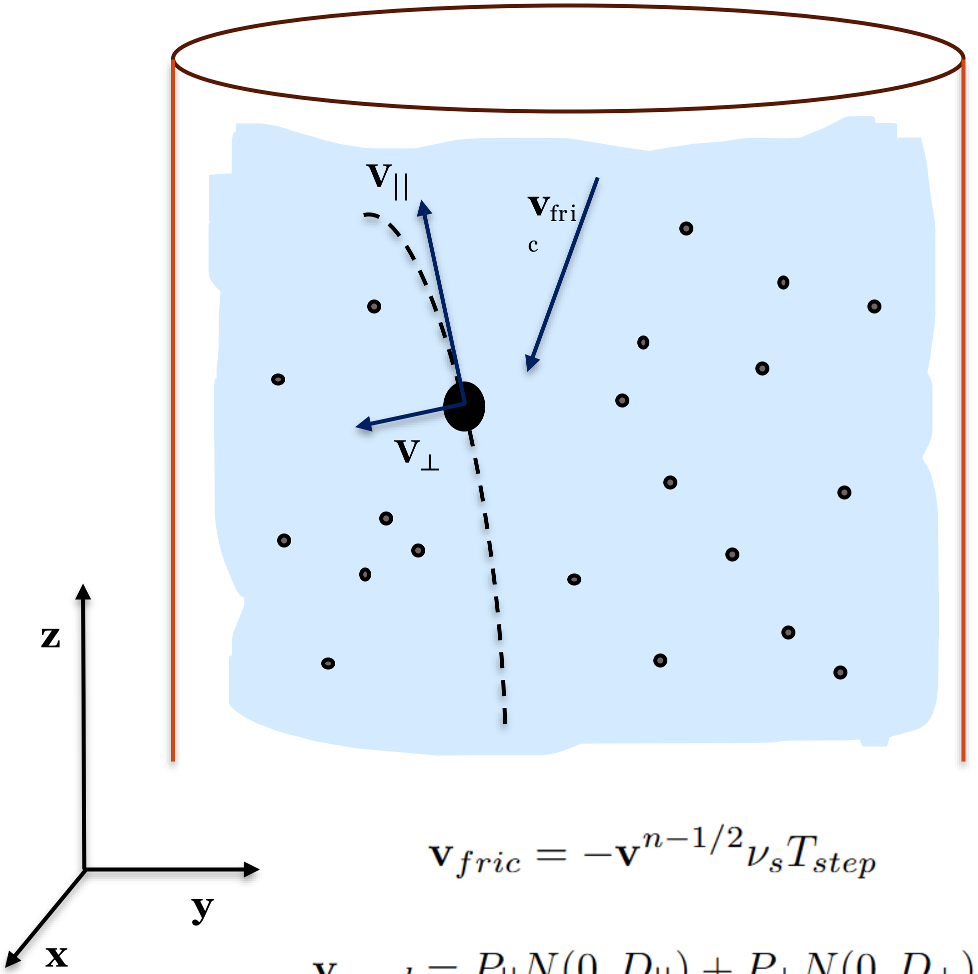

$$\mathbf{v}_{fric} = -\mathbf{v}^{n-1/2}\nu_s T_{step}$$

$$\mathbf{v}_{rand} = P_{||}N(0, D_{||}) + P_{\perp}N(0, D_{\perp})$$

Ion Simulations: Reaction Module

MC Sampling

Ions in a plasma can interact with each other and electrons to undergo competing reactions.

Ion transport occurs simultaneously with reactions, which can be sampled using MC methods

$$\frac{dn_i}{dt} = n_{i-1} n_e \gamma_{i-1,i} - n_i n_e \gamma_{i,i+1} + n_{i+1} n_0 E_{i+1,i} - n_i n_0 E_{i,i-1} - \frac{n_i}{\tau_i}$$

<u>**Electron impact ionization (EI)**</u>

<u>**Ion impact charge exchange (CEX)**</u>

$$\nu_{ion} = n_e \sigma_{ion,i\to i+1} v_{e,rel}$$

$$\nu_{CEX} = n_0 \sigma_{CEX,i\to i-1} v_{i,rel}$$

$$\sigma_{ion,i\to i+1} = \frac{10^{-17}}{I_i E_e}\left[\sum_{n=1}^{6} A_n \left(1 - \frac{I_i}{E_e}\right)^n + B \ln\left(\frac{E_e}{I_i}\right)\right]$$

$$\sigma_{CEX,i\to i-1} = A i^{\alpha} (I_0)^{\beta}$$

$$\begin{aligned} P_{tot}(T_{step}) &= 1 - e^{-\nu_{tot} T_{step}} = \frac{\nu_{ion} + \nu_{CEX}}{\nu_{tot}}(1 - e^{-\nu_{tot} T_{step}}) \\ &= \frac{\nu_{ion}}{\nu_{tot}}(1 - e^{-\nu_{tot} T_{step}}) + \frac{\nu_{CEX}}{\nu_{tot}}(1 - e^{-\nu_{tot} T_{step}}) \\ &= P_{ion}(T_{step}) + P_{CEX}(T_{step}) \end{aligned}$$

- Ionisation if $0 <= r < P_{ion}$
- CEX if $P_{ion} <= r < (P_{ion} + P_{CEX})$
- Nothing if $(P_{ion} + P_{CEX}) <= r < 1$

The plots comparing the frequencies of the various processes offer insight into the dynamics of atomic processes as a function of ionisation stage.

Under conditions of perfect confinement, the simulated EI and CEX coefficients would resemble these plots

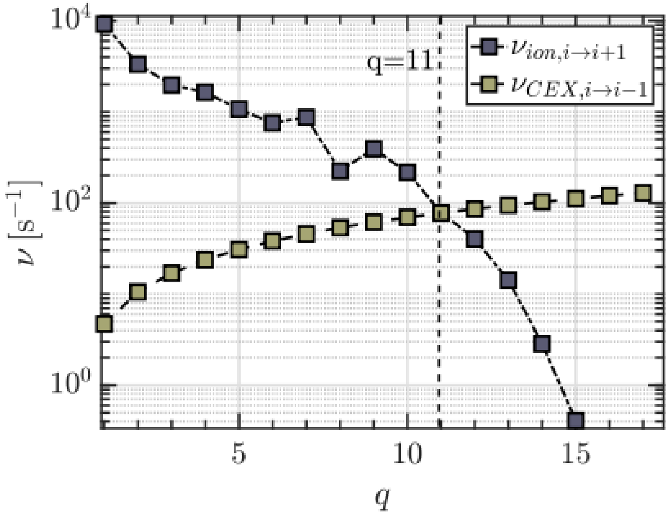

Comparison between EI and CEX frequencies in A-HPC with argon (top) and LEGIS with oxygen (bottom)

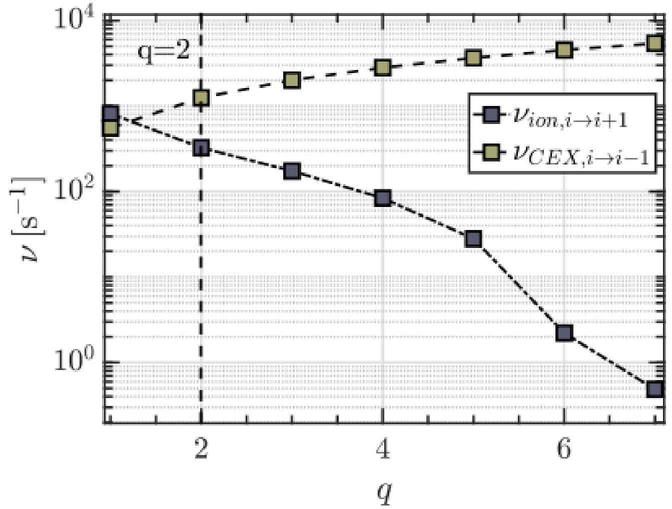

Ion Simulations: Results

The main results of the PIC-MC simulations are 3D steady-state maps of ion density in for each ionisation stage and <*Z*>

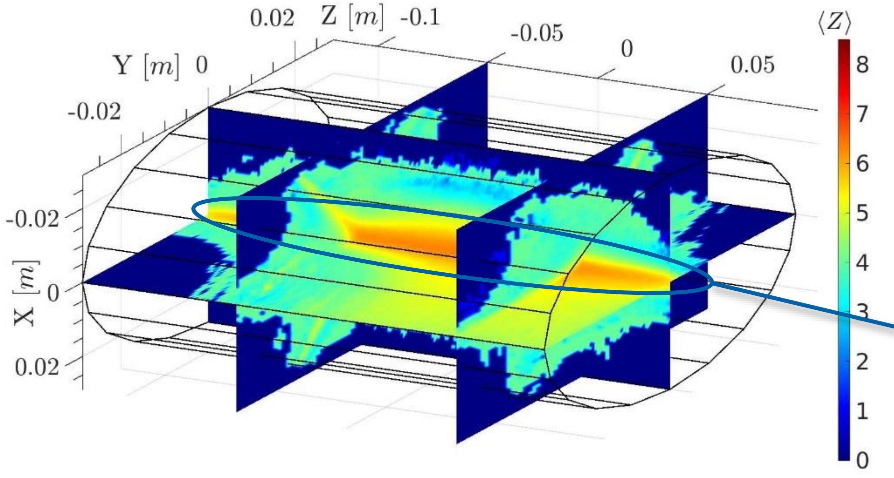

<Z> of argon plasma in A-HPC ECRIS as calculated using PIC-MC code (top) and of oxygen plasma in LEGIS (bottom)

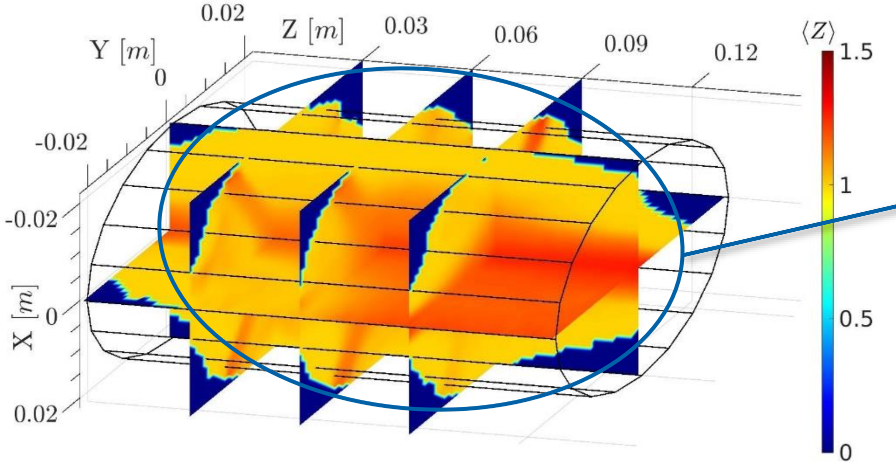

Higher charge states tend to accumulate in the near-axis region because they are generated from lower charge states through EI in those same regions with high E_e, and they are strongly confined by E_{DL} and diffusion

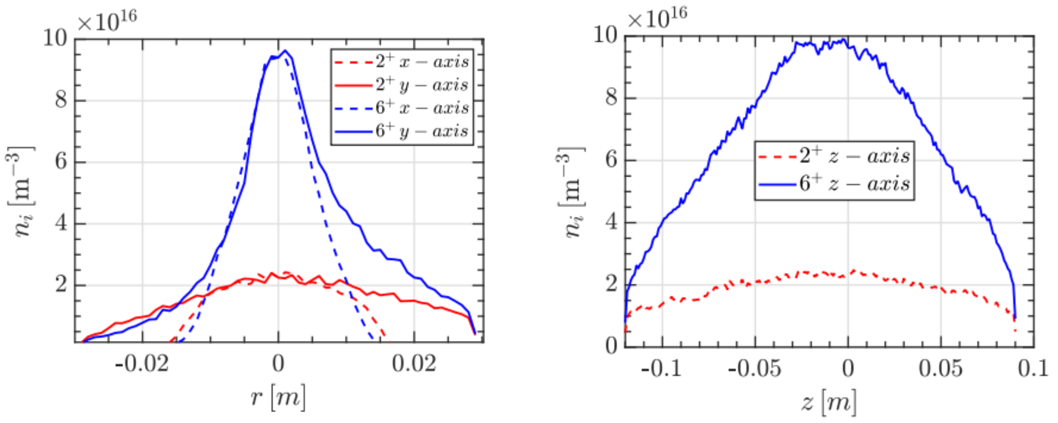

n_i of Ar^{2+} and Ar^{6+} in A-HPC ECRIS along the radius and axis in A-HPC (top) and same for O^{2+} and O^{6+} in LEGIS (bottom)

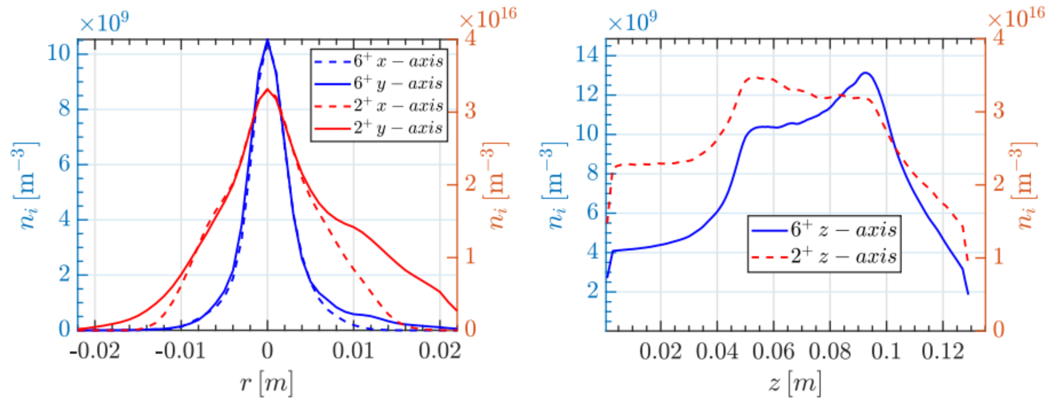

Results may vary according to the geometry of the system, the magnetostatic field and type of ions (which govern particle transport), and steady state n_e, k_BT_e maps

Stepwise ionization: from electron energy-density 3D maps to charge state distribution

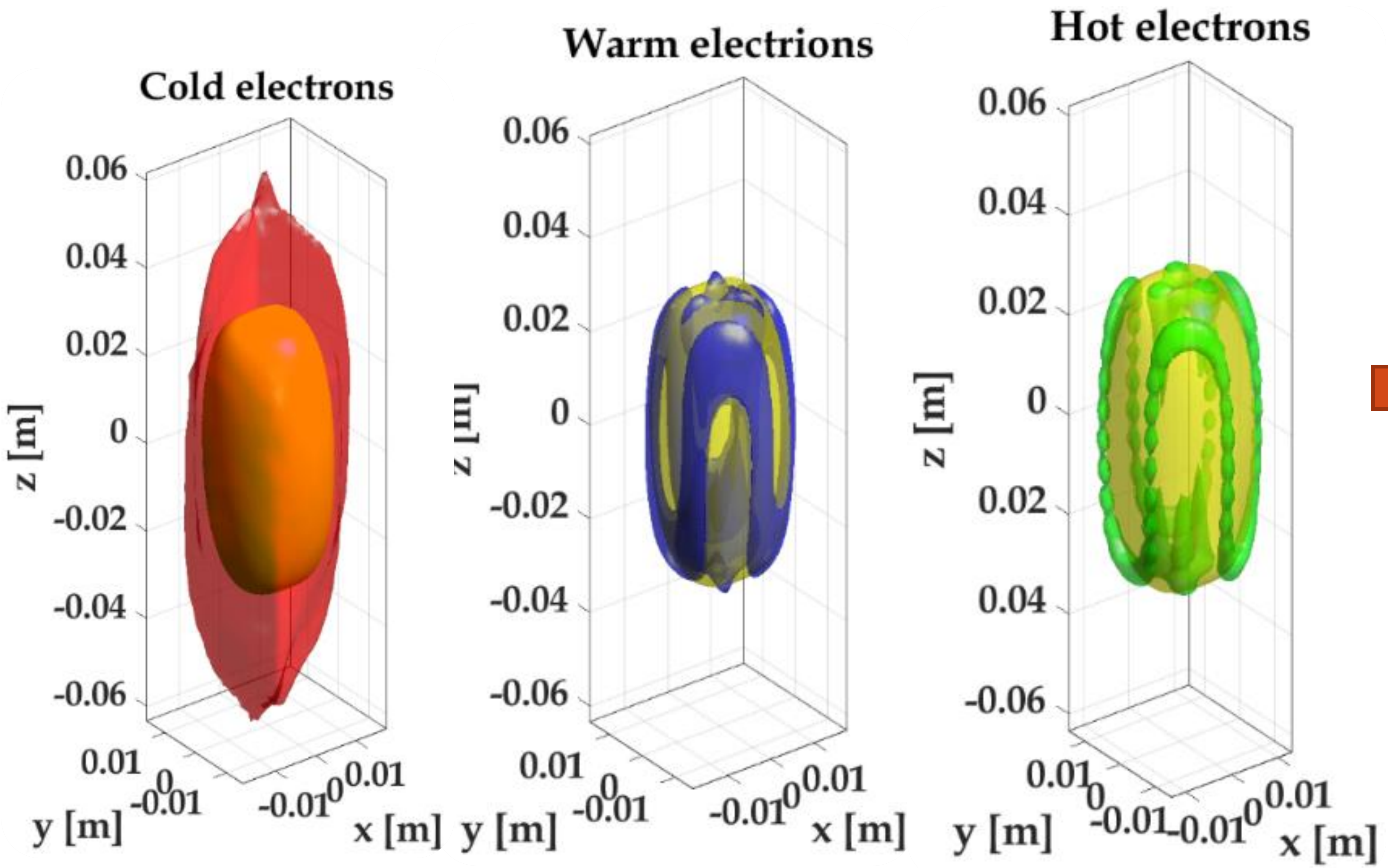

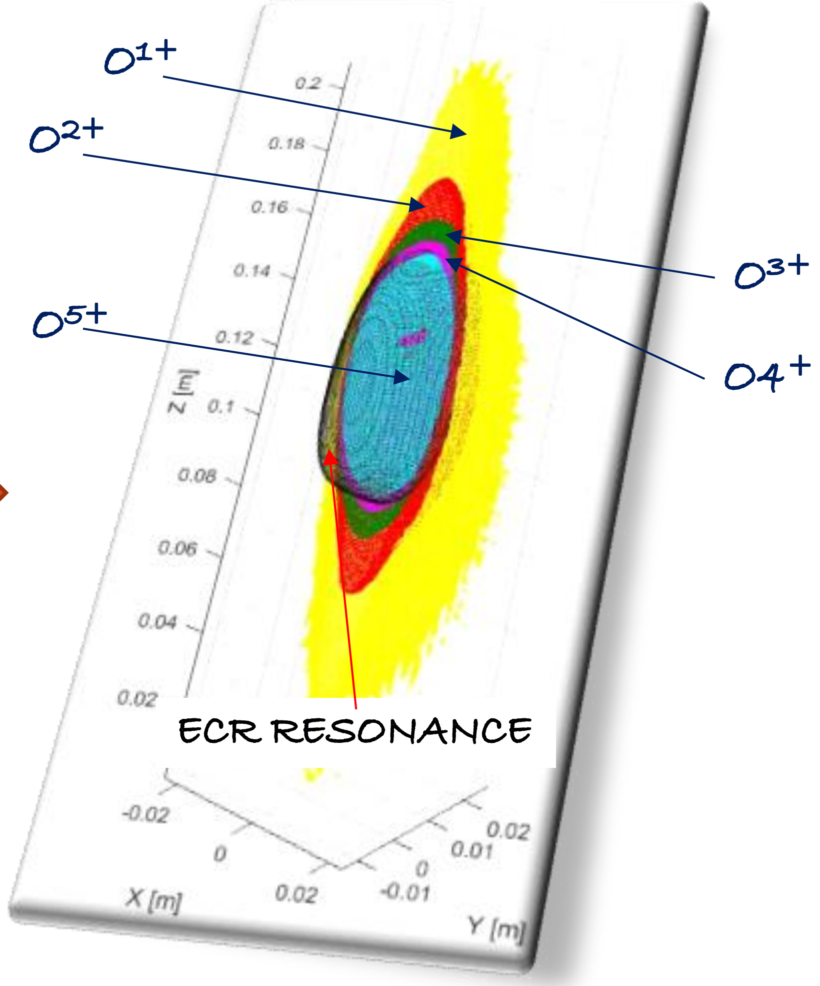

Orbital Electron Capture Decay in ^{7}Be in uniform plasma

Configuration-Dependent Decay Rate

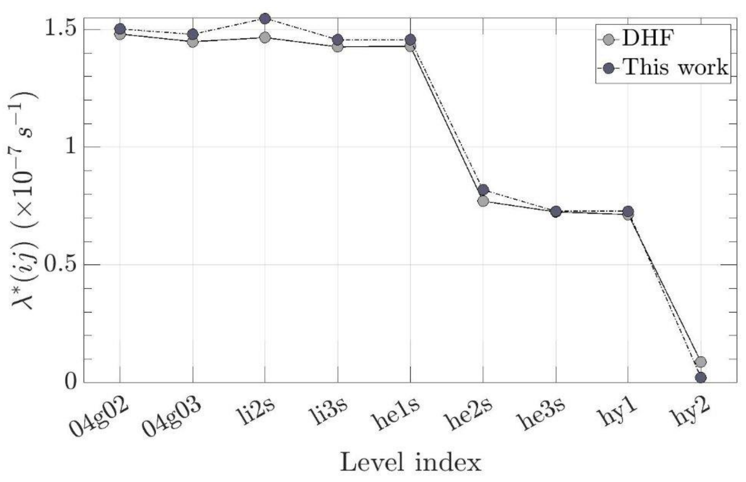

Ion CSD in uniform plasma with n_e=10^{12} cm^{-3} and varying $k_B T_e$

Calculated with FLYCHK under LTE and NLTE conditions

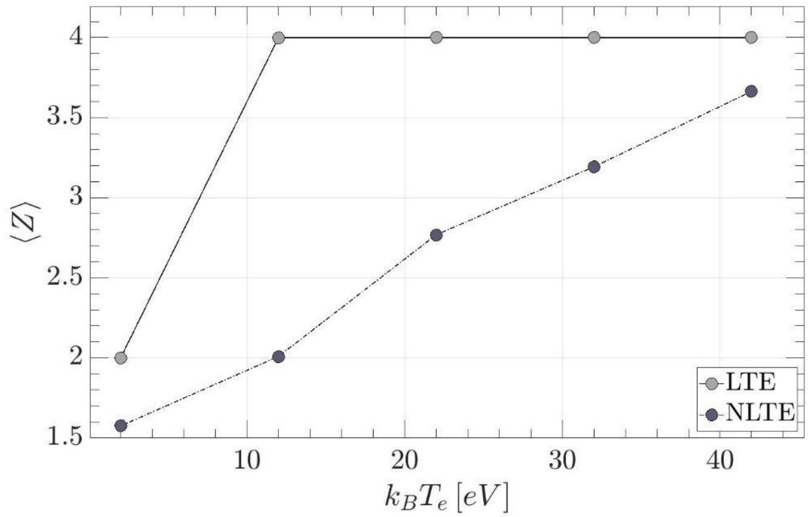

In-plasma orbital EC rate

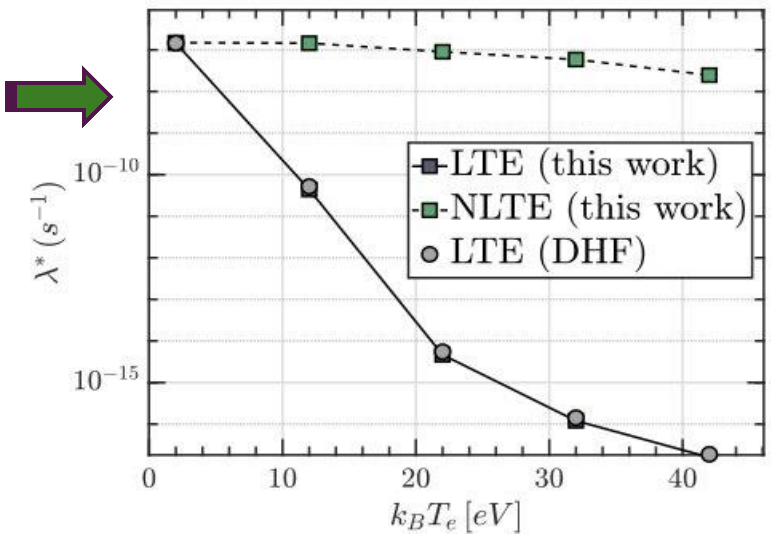

Results highlight that in-plasma decay models designed for LTE plasmas (ex. DHF) will predict wrong values in NLTE plasmas like PANDORA. The new model is universal and can be applied to both systems.

Orbital Electron Capture Decay in ^{7}Be in uniform plasma

Configuration-Dependent Decay Rate

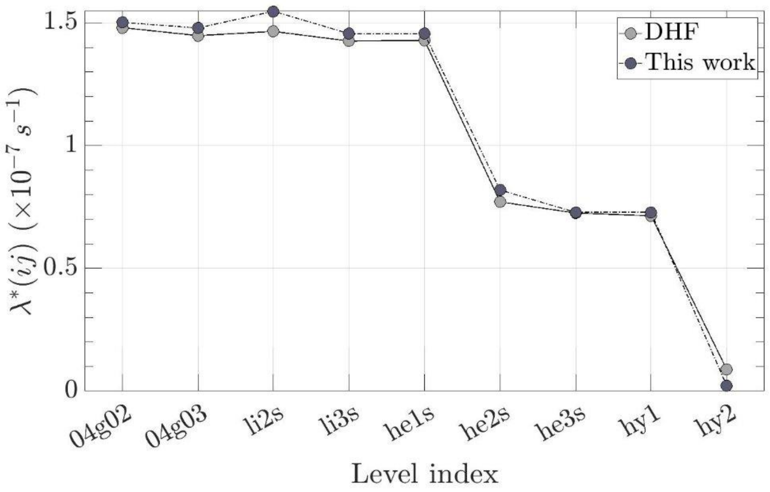

Ion CSD in ECR plasma with space-resolved n_e and $k_B T_e$
Simulated with PIC-MC code

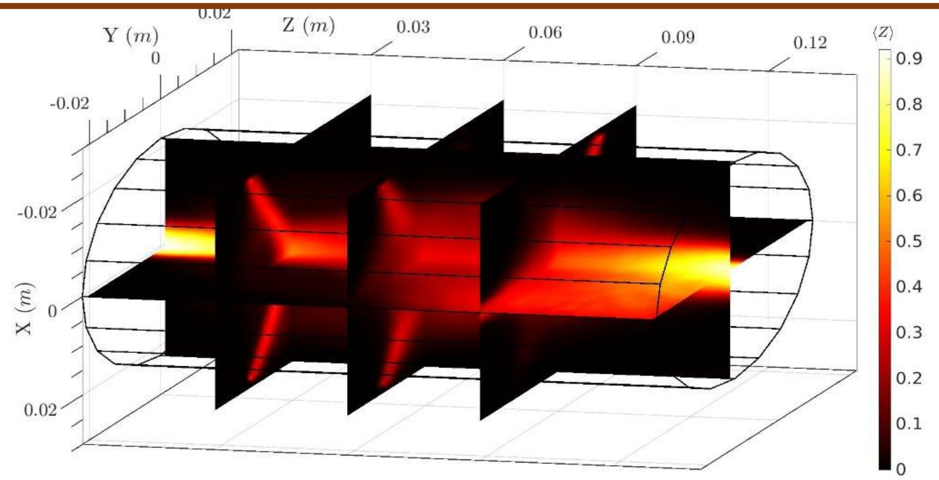

Orbital EC rate in ECR plasma

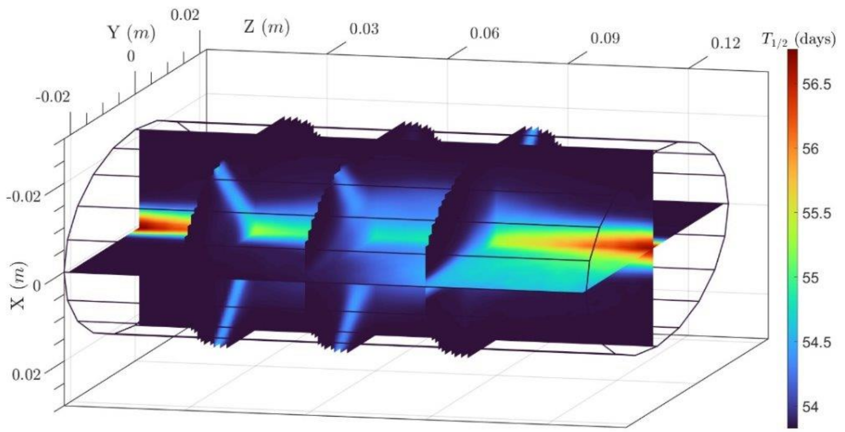

Simulation has been tested on low power configuration (and hence low degree of ionisation) but can be applied to PANDORA now

→ GOAL: to study if and how the lifetimes is affected by the atomic charge state and by the plasma "*environment*"

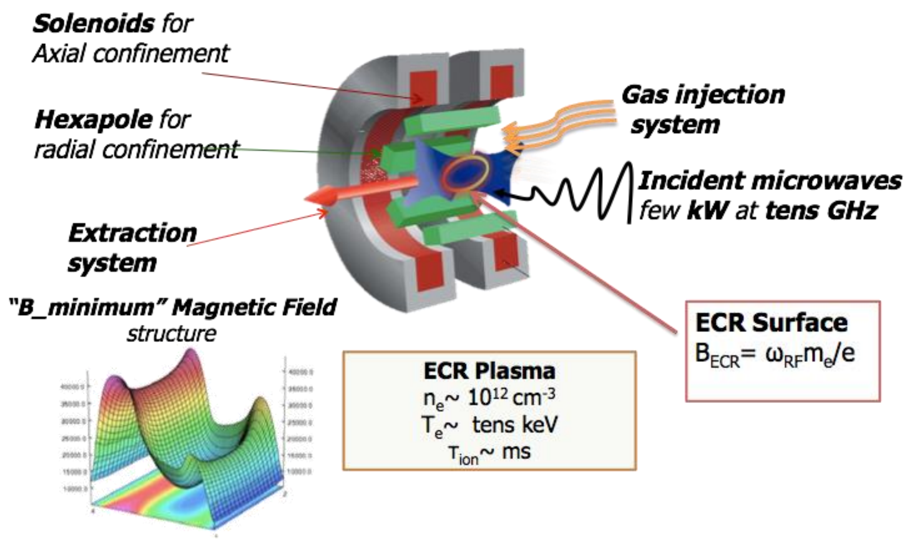

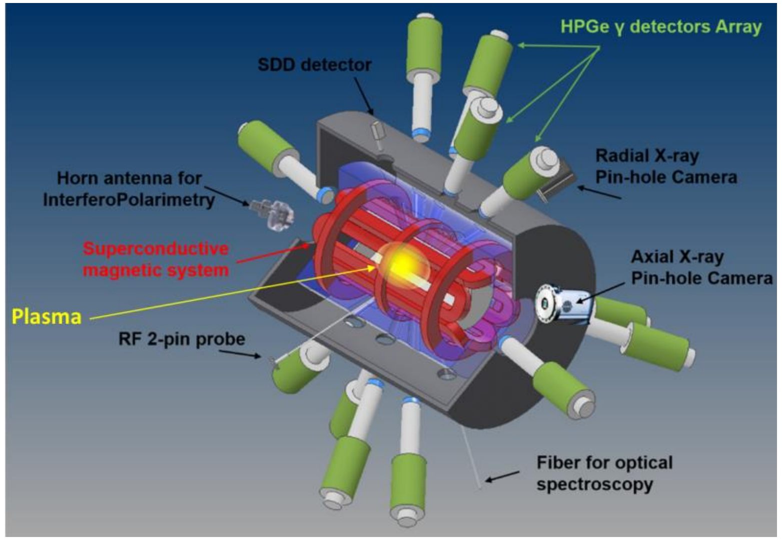

D. Mascali et al., Universe, 2022, 8(2), 80
D. Mascali et al., EPJ-A, 53, 2017, 7

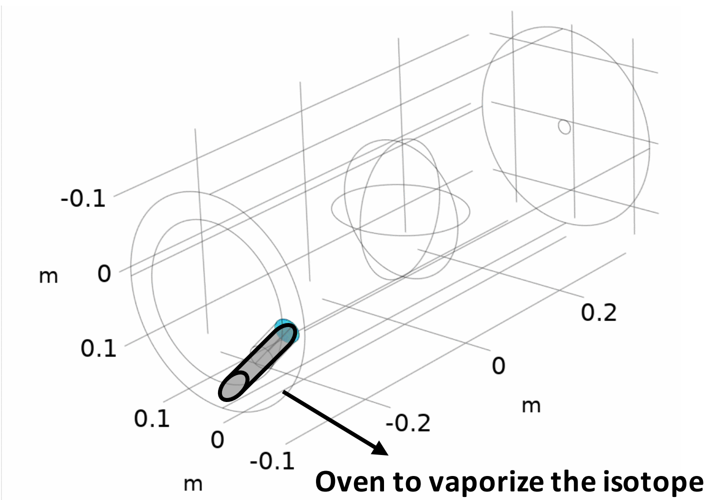

Oven to vaporize the isotope into the chamber

- Electron Density: $10^{12} - 10^{14}$ cm^{-3}
- Electron Temperature: 0.01 – 100 keV
- Ion Temperature: ~1 eV
- Ion Density: 10^{6} - 10^{11} cm^{-3} (this density relies to the radiactive isotope concentration in plasma)

PANDORA proposes an innovative experimental approach which includes 5 steps:

I. A buffer plasma is created from He, O or Ar up to density of 10^{13} cm^{-3} by **Electron-Cyclotron-Resonance heating** and confined by **magnetic field**;

II. The **isotope is vaporized by proper ovens** into the chamber **to be transformed into plasma-state** (with a given relative abundance of buffer vs isotope densities)

III. The plasma is maintained in **MHD equilibrium** for days or even weeks: **the number od decays per unit of times can be written as**:

$$\boxed{\frac{dN}{dt} = \lambda n_i V} \Longrightarrow \boxed{N(T_{meas}) = \lambda n_i V_{plasma} T_{meas}}$$

$\lambda n_i V$ is constant

Plasma volume (const.)

Isotope activity: λ ≡ λ(T, n) *Density of the isotope in the plasma (const.)*

First Physics Cases

Isotope	$T_{1/2}$ [yr]	E_γ [keV]
^{176}Lu	$3.78 \cdot 10^{10}$	202.88 & 306.78
^{134}Cs	2.06	795.86
^{94}Nb	$2.03 \cdot 10^{4}$	871.09

IV. While the isotopes decay, the confined **daughter nuclei emit γ-rays of hundreds of keV, which are detected by a HPGe detector array**;

V. In-plasma radioactivity can be correlated to plasma parameters monitored by an **innovative non-invasive multi-diagnostics setup**;

Plasmas for Astrophysics Nuclear Decay Observation and Radiation for Archaeometry
INFN LNS Istituto Nazionale di Fisica Nucleare Laboratori Nazionali del Sud
samothrace Sicilian Micro and Nano Technology Research and Innovation Center

MAIN SUBSYSTEMS UPDATES: Plasma modelling

(LNL + LNS activity)

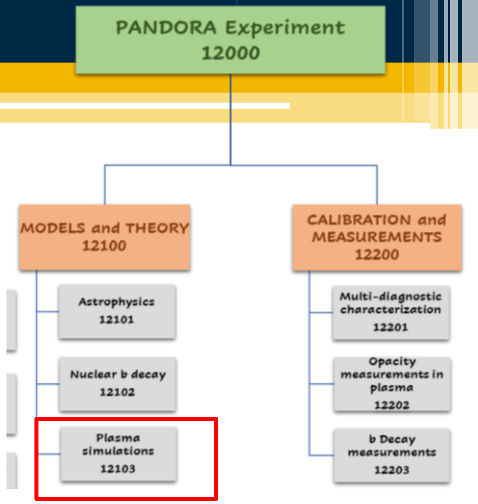

First self-consistent calculation of a high power, high density plasma

Simulation of the distribution of the different electron populations in plasma

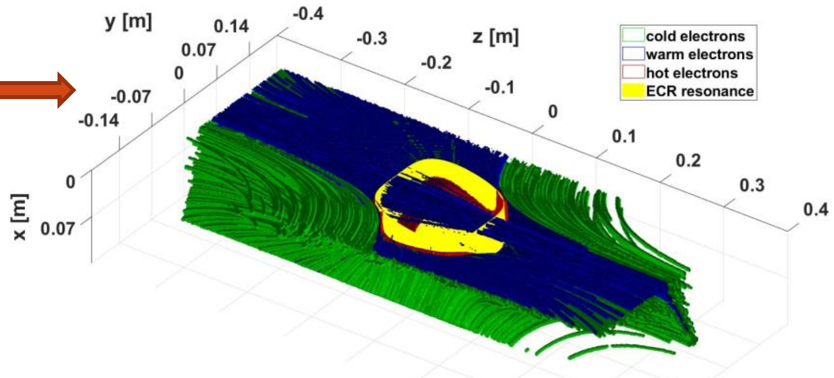

Prediction of global electrons energy and density distribution

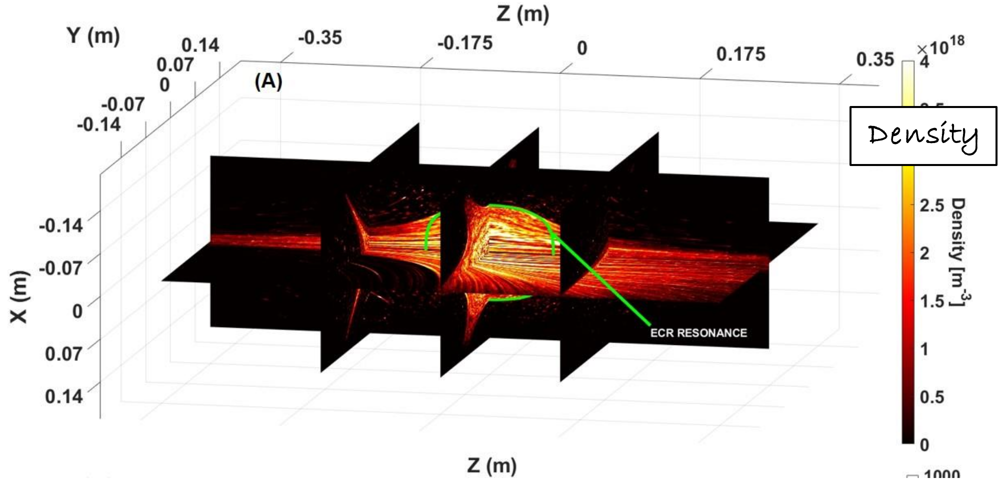

HPGe detectors positioning vs. the warm electrons distribution !

Correct positioning

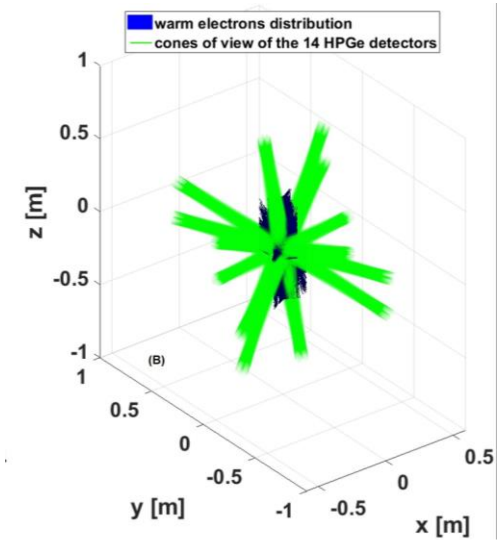

A. Galatà *et al.*, ***Front. Phys.*** *DOI 10.3389/fphys.2022.947194*

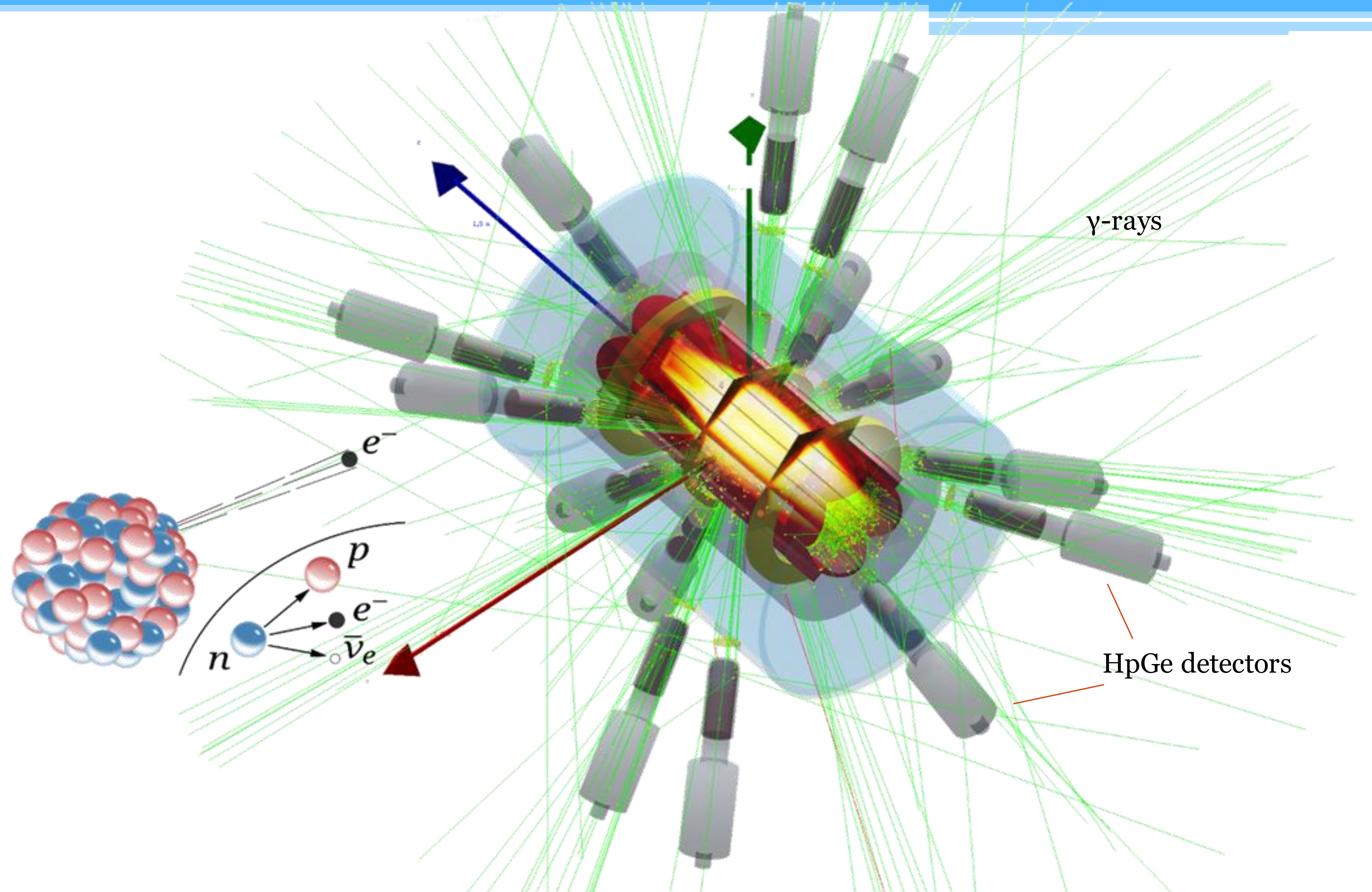
γ-rays
e^-
p
e^-
n
$\bar{\nu}_e$
HpGe detectors

Many thanks to the ***#LNSplasmateam*** members contributing to this presentation: *G. Finocchiaro, V. Francalanza, E. Naselli, G. Mauro, B. Mishra, B. Peri, A. Pidatella, C. Salvia, D. Santonocito, G. Torrisi and many others (researchers, technologist, technicians)*

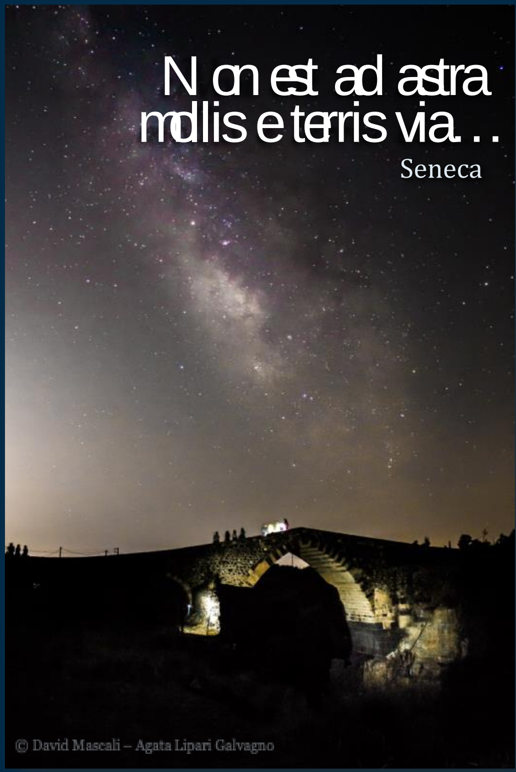

Grazie per la vostra attenzione!

https://www.lns.infn.it/it/apparati/pandora.html

Contacts:

davidmascali@lns.infn.it
david.mascali@unict.it

INFN LNS Istituto Nazionale di Fisica Nucleare Laboratori Nazionali del Sud

Università di Catania

MAIN SUBSYSTEMS UPDATES: Trap procurement

Competitor #2-Executive Design

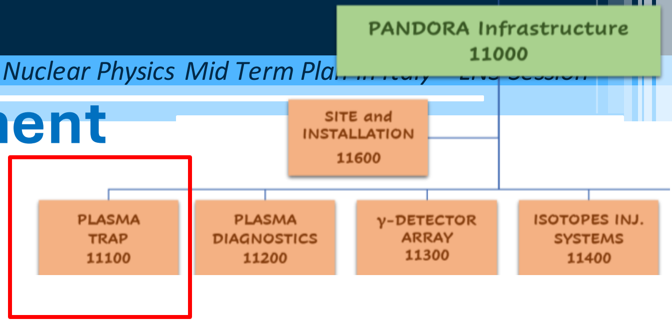

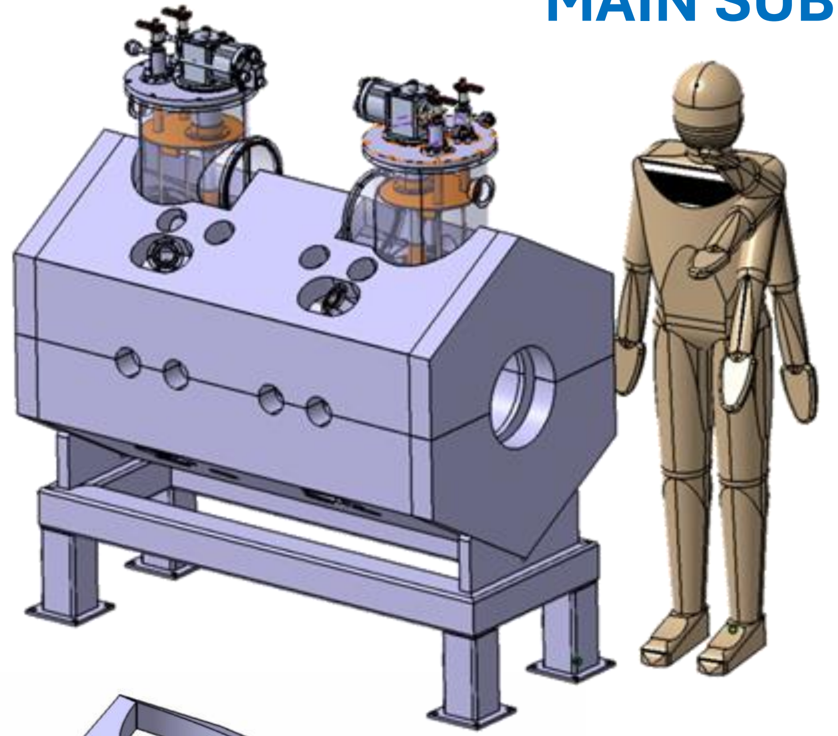

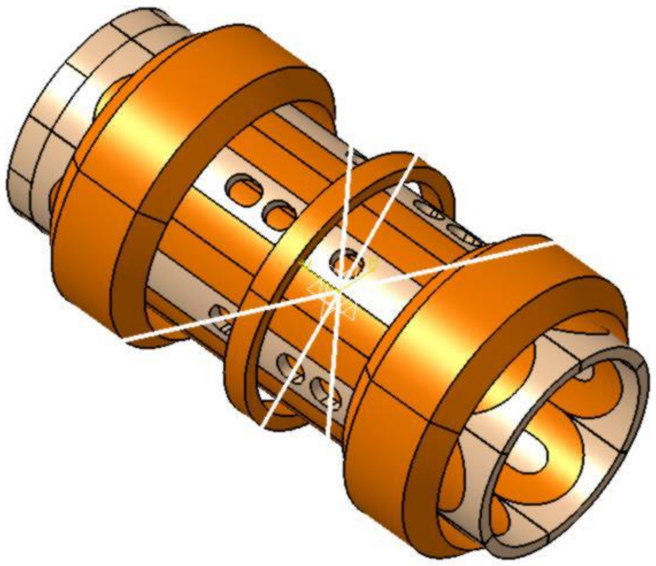

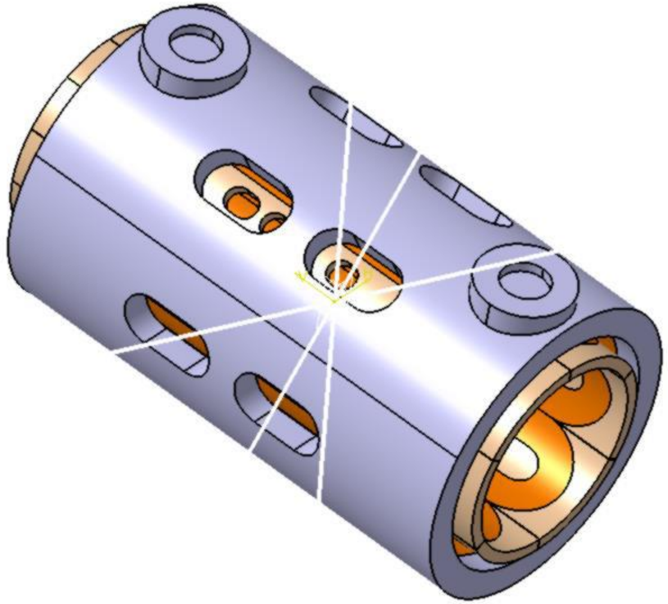

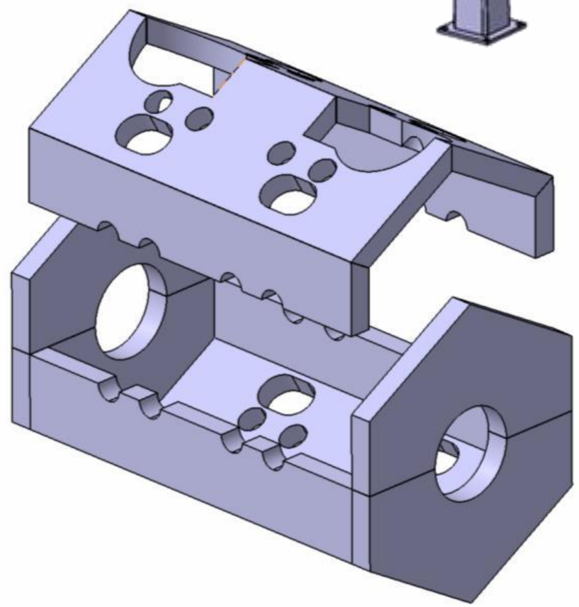

Detail of radial containment cylinders

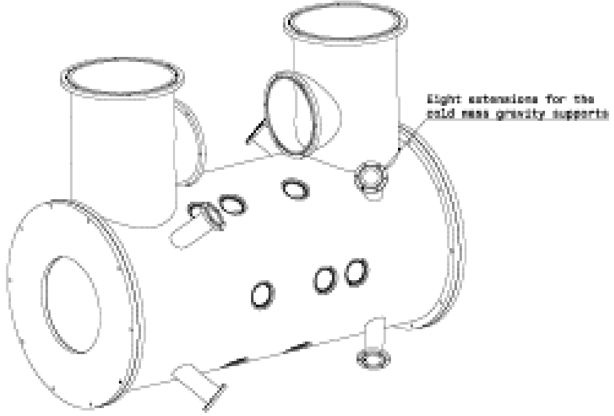

Figure 2. Isometric view of the cryostat

MAIN SUBSYSTEMS UPDATES: plasma chamber

(LNS + PD ACTIVITY)

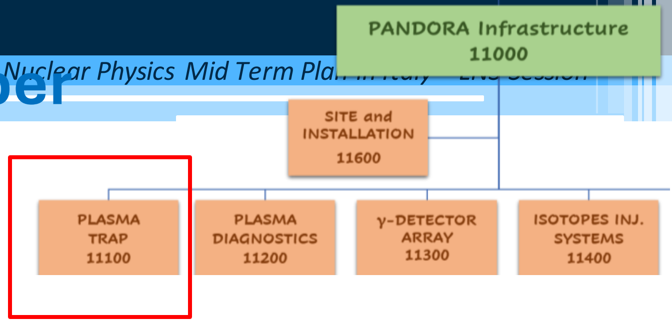

The design of the main plasma chamber is ongoing

The end caps, through several flanges and feedthroughs, allow to connect the vacuum pipe, the RF injection waveguides, the gas inlet, the oven, and several diagnostic devices.

Many aspects concerning the positioning of different diagnostic tools on the injection side of the chamber were defined but still work needs to be done to complete the design.

The completion of the design will be possible only when the technical specifications (dimensions) of the magnetic trap will be know

With INFN-PD we have already ordered 120 kg of Inconel (Nickel alloy) for the chamber fabrication by Additive Manufacturing - Dec. 2023
Delivery at INFN-PD in April 2024

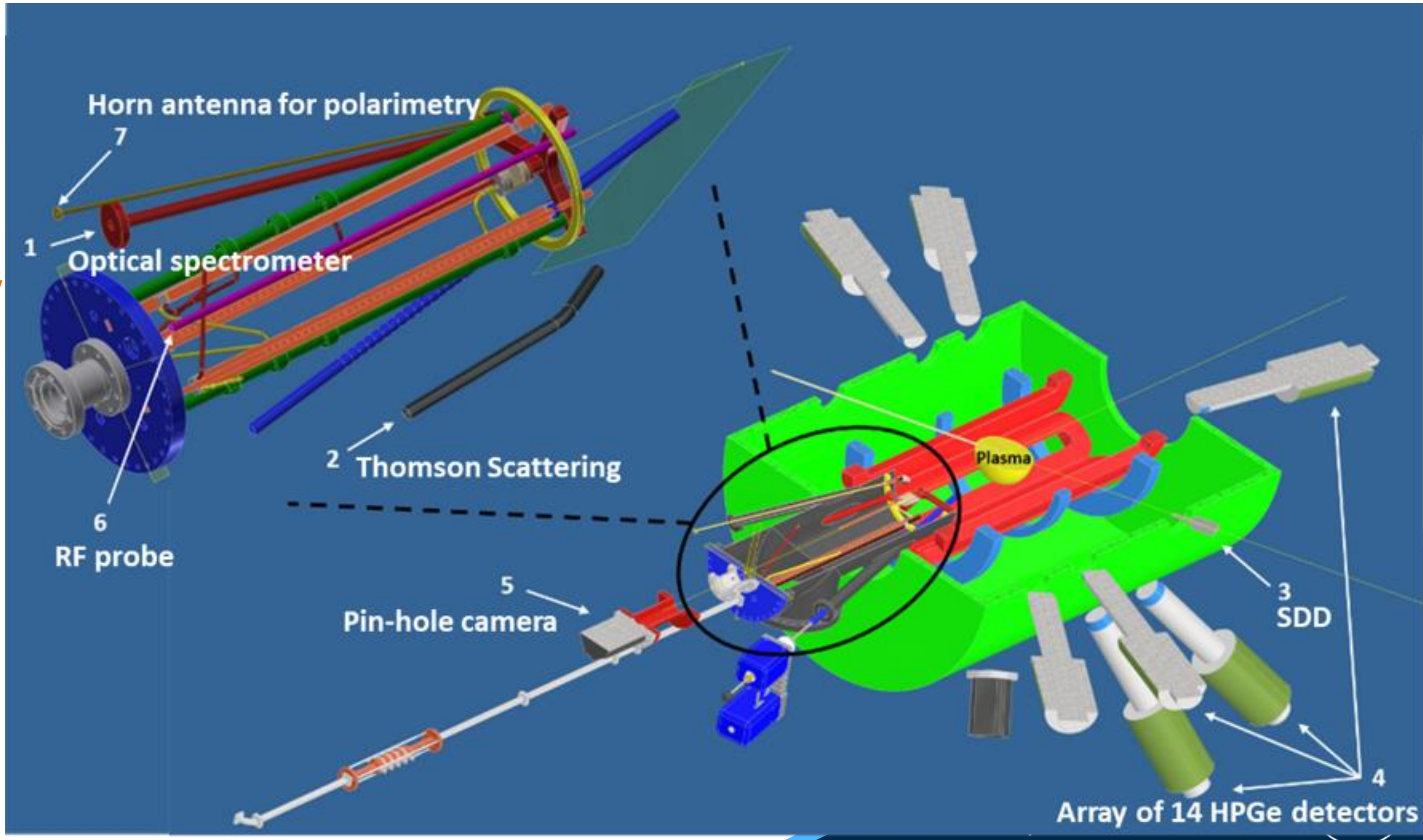

MAIN SUBSYSTEMS UPDATES: plasma chamber

(LNS + PD ACTIVITY)

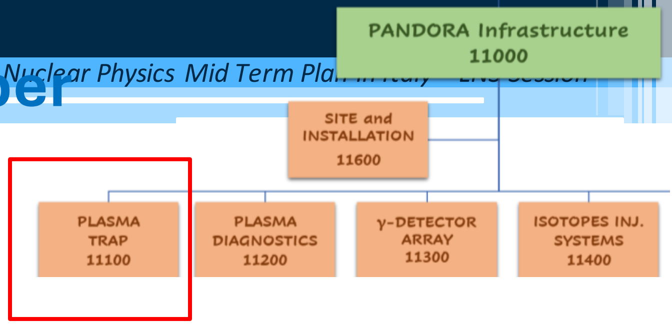

The design of the main plasma chamber is ongoing

The end caps, through several flanges and feedthroughs, allow to connect the vacuum pipe, the RF injection waveguides, the gas inlet, the oven, and several diagnostic devices.

Many aspects concerning the positioning of different diagnostic tools on the injection side of the chamber were defined but still work needs to be done to complete the design.

The completion of the design will be possible only when the technical specifications (dimensions) of the magnetic trap will be know

With INFN-PD we have already ordered 120 kg of Inconel (Nickel alloy) for the chamber fabrication by Additive Manufacturing - Dec. 2023
Delivery at INFN-PD in April 2024

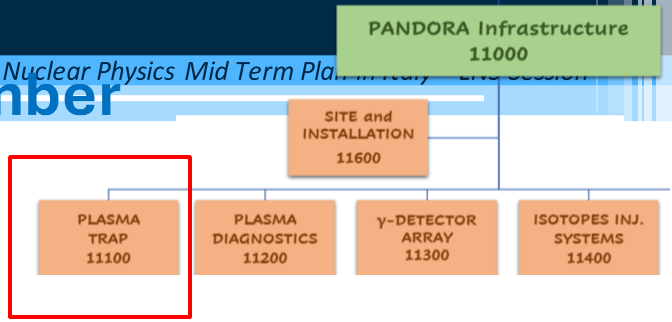

MAIN SUBSYSTEMS UPDATES: plasma chamber

(INFN-BO ACTIVITY)

The main plasma chamber is equipped with an Inner Chamber which forms a thin mechanical coating and provides an electrical segmentation of the cylinder's wall.

It will be used to measure plasma leakage currents based on axial segmentation and to minimize radial losses.

The mechanical and electrical design of the Plasma Inner Chamber prototype in reduced scale (~1:3) **has been completed.**

Test planned for 2022 has been postponed to late 2024, as the installation of AISHa in the new experimental room has been delayed for over a year.

To mitigate the effects of this delay, a pre-test of the Plasma Inner Chamber prototype has been conducted at the Bologna Section in the second **part of 2023 using a dummy chamber** identical to that of AISHa, specially built for this purpose.

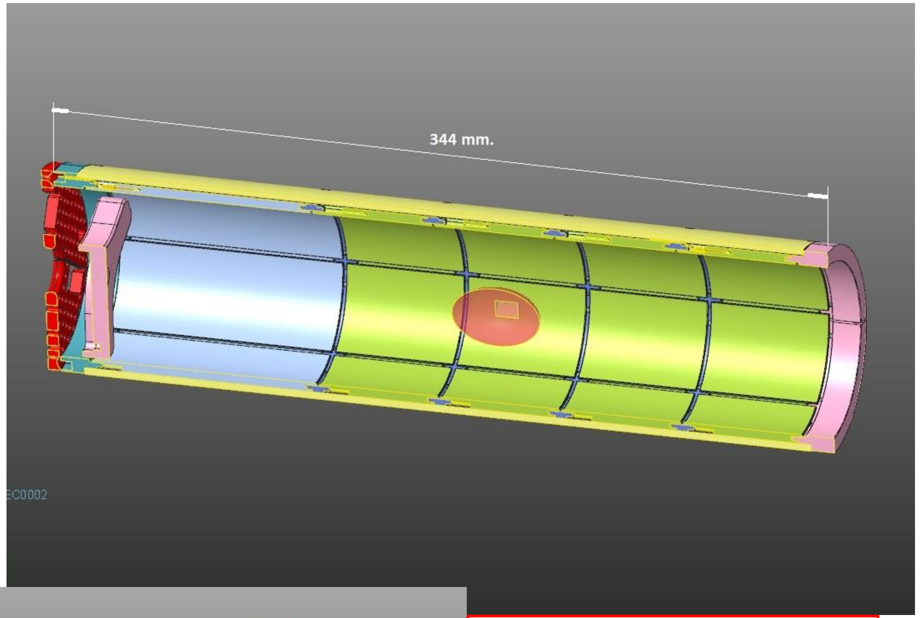

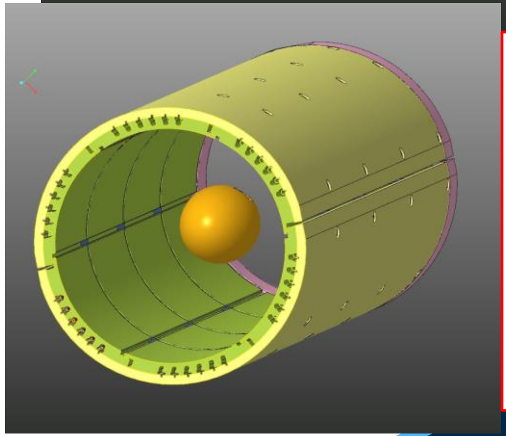

Channels (6x6) for electrical contacts via copper wires (insulated with ceramic coating) and thermocouples to monitor the tiles' temperature.

MAIN SUBSYSTEMS UPDATES: plasma chamber

(INFN-BO ACTIVITY)

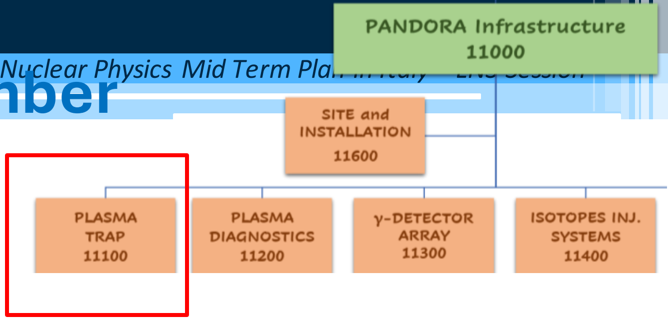

«Coppi» and anodized rings

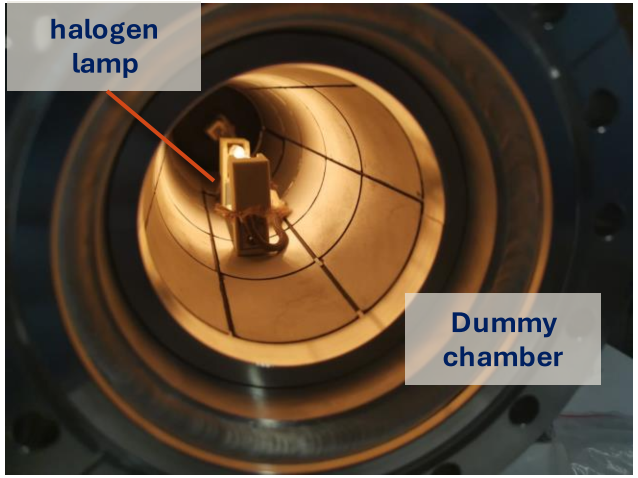

Pressure (mbar):

- 1x10E-4 in 90'
- 7.4x10E-6 after 17h
- After baking con alogena @ 77W

➔ 8.6x10E-4 @ **Tmax coppo 212°C**

Baking	Tmax	Pressure (mbar)
30 W	115°C	2.5x10E-6
38 W	127°C	1.0x10E-6
42 W	135°C	8.6x10E-7
51-61 W	145-155°C	7.4x10E-7
51-61 W	145-155°C	4.6x10E-7 after 3h pumping

Goal: to investigate Electron-Cyclotron-Resonance plasma thermodynamical proprieties (electron density and temperature) in compact trap;

→ A gas or a metallic material vaporized by an oven is fluxed inside a plasma chamber

→ Plasma is excited by Electron-Cyctron-Resonance by microwaves and confined by magnetic fields

→ A multidiagnostic system surrounding the plasma chamber was developed to measure plasma parameters

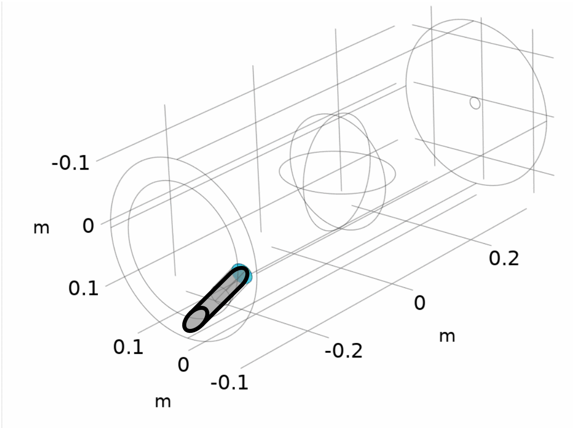

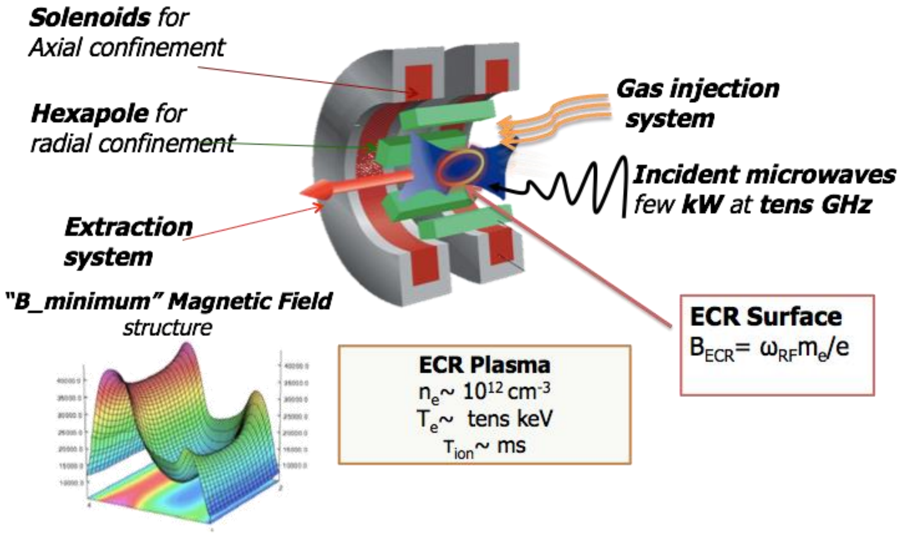

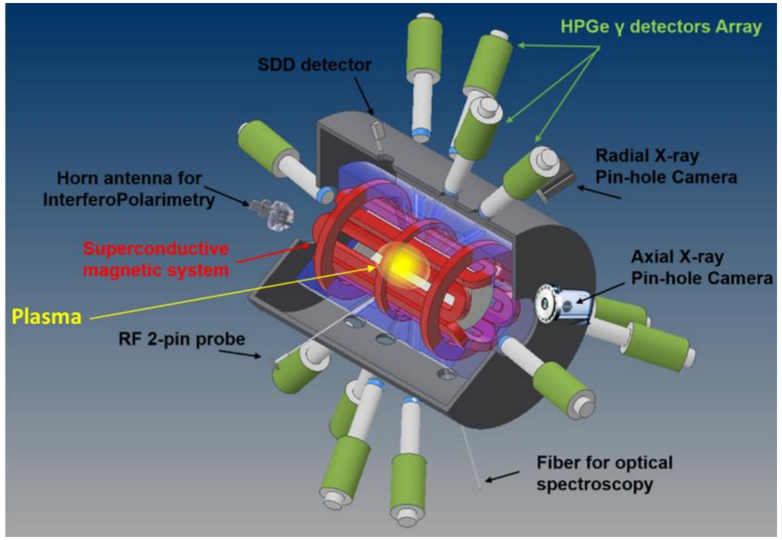

Method: ECR plasmas emit radiation from microwave to hard X-rays and this radiation can be used to investigate plasma parameters in different regimes;

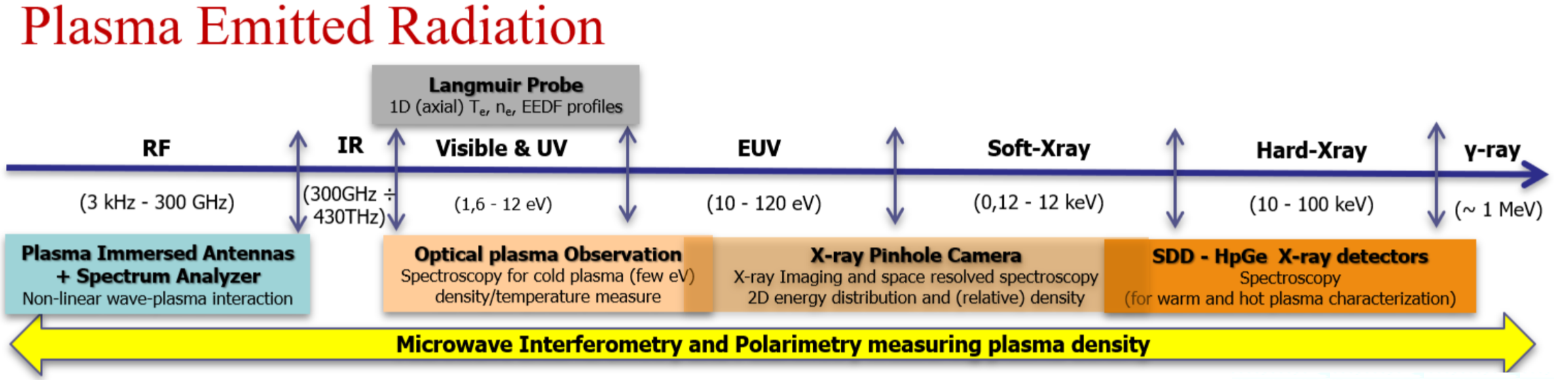

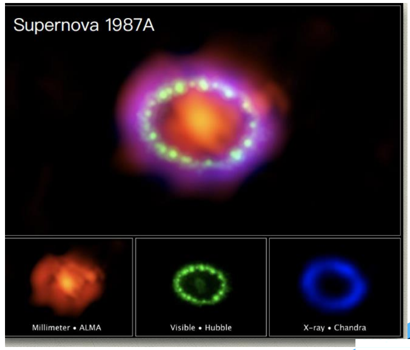

Multimessenger Astronomy Era:
→ Exploring the Universo across the EM spectrum

Testbench (operating at down-frequency domain) of the VESPRI 2.0 mm-wave polarimeter prototype:

- The **goal** is to detect the plasma-induced Faraday rotation and measure the plasma line-integrated electron density;
- The **innovative approach** is based on the super-heterodyne scheme;

Detectors and Technologies for Fusion Plasmas: towards a sub-mm wave polarimeter for plasma parameters remote sensing

Two W-band horn antennas, the receiving one connected to **an orthomode transducer** (OMT),

Rotating RX horn antenna

TX horn antenna

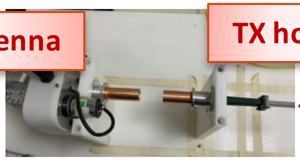

Orthomode transducer (OMT) is a waveguide component which serves to combine or separate two orthogonally polarized microwave signal paths.

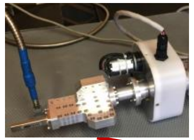

Detection the Lissajous figure from a **two channels scope** of a direct probing RF signals crossing the magnetoplasma

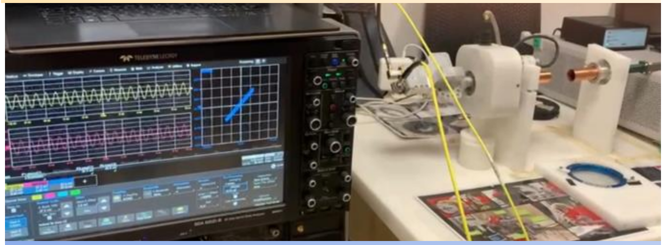

Rotation of the Lissajous figures in free-space (rotating the RX antenna) and with polarizer (for different polarizer angles)

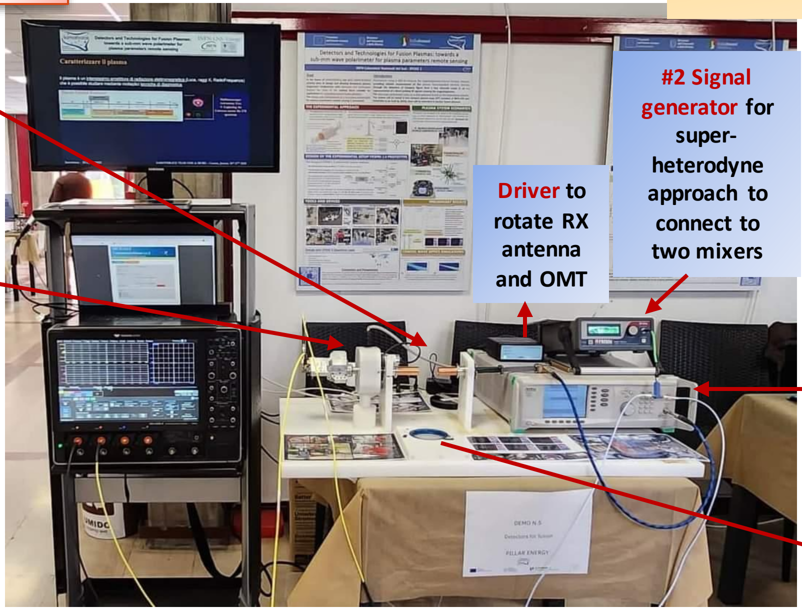

#2 Signal generator for super-heterodyne approach to connect to two mixers

Driver to rotate RX antenna and OMT

The prototype can be installed on the **Flexible-Plasma-Trap installed at INFN-LNS** for **in-plasma measurements**

The **Super-Heterodyne scheme** allows to down-shift the detected frequency (1 GHz) compared to the probing one (20 or 100 GHz) in order to be detected in a scope. It can be done by using **mixers**.

Mixers which convert the mm-wave of the wave received by the antenna **to intermediate frequency:** the signal on the output of an ideal RF mixer contain the sum and difference frequencies of the two input signals.

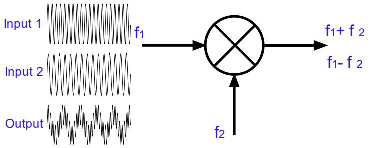

#1 Signal generator (probing wave @ 20 GHz)

Wire-grid polarizer:
Rotation angle can be arbitrarily fixed by properly rotating the grid polarizer.
Tungsten wires phi = 40 μm;
Wire spacing d = 100 μm;
Aperture a = 80 mm;

Preliminary Results @ down-frequency domain

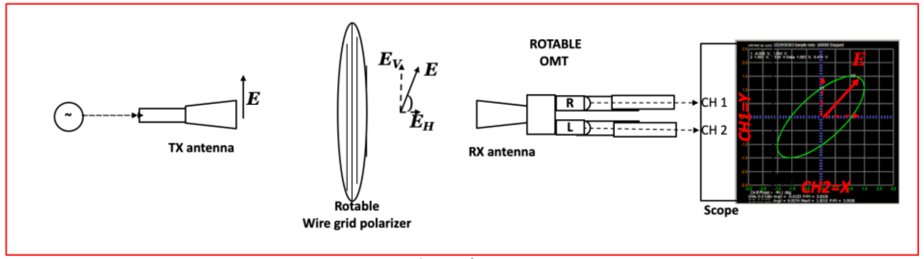

experimental arrangement

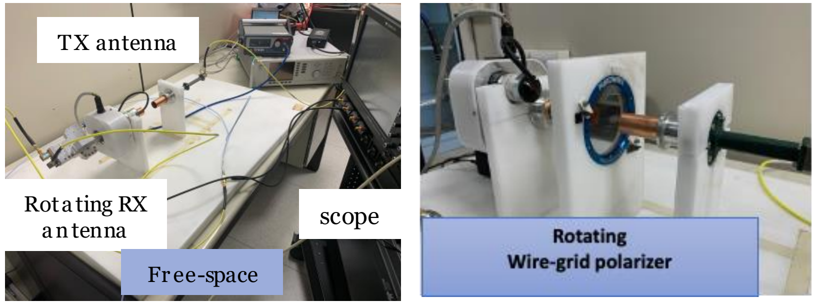

Lissajous figures in free-space and with polarizer for different polarizer angles

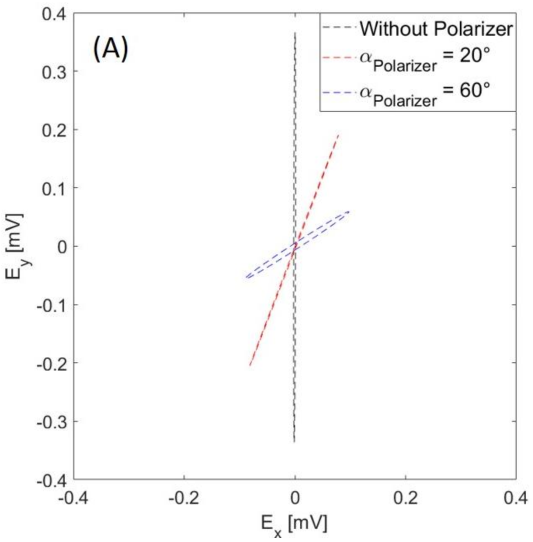

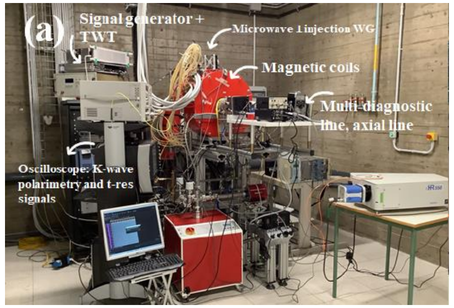

In-plasma measurements on FPT vs. 3 RF pumping power values: 0, 20, 60 W

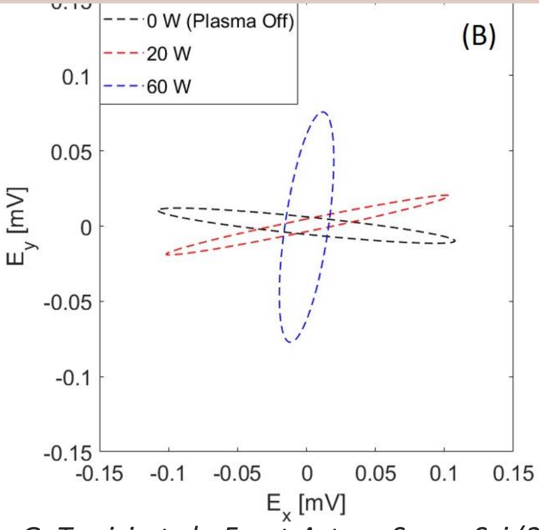

G. Torrisi et al., Front Astron Space Sci (2022) 9:949920

- The polarization ellipse detected after the plasma ignition (20 W) is well distinguishable from that of the switched off plasma (0 W).
- A rotation of around 90° at 60 W of RF power was observed, in agreement to the gradually increasing of the optical emission vs. the pumping power observed by visual inspection.

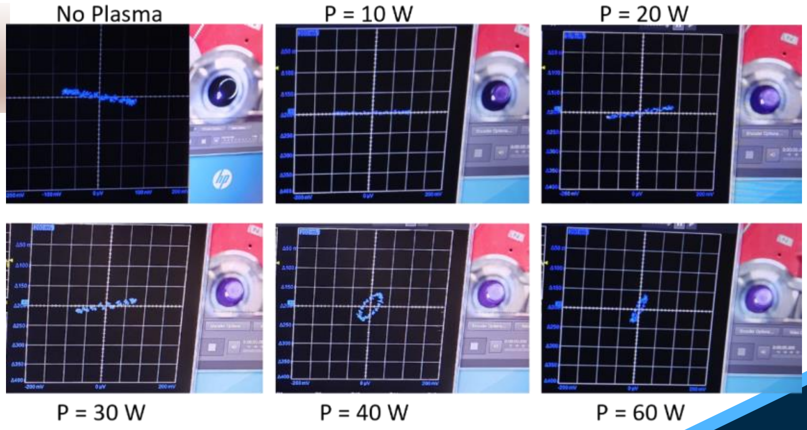

Emission by an isotropic source placed in the center of the plasma chamber, changing the energy of the source in the range from 100 keV to 2 MeV

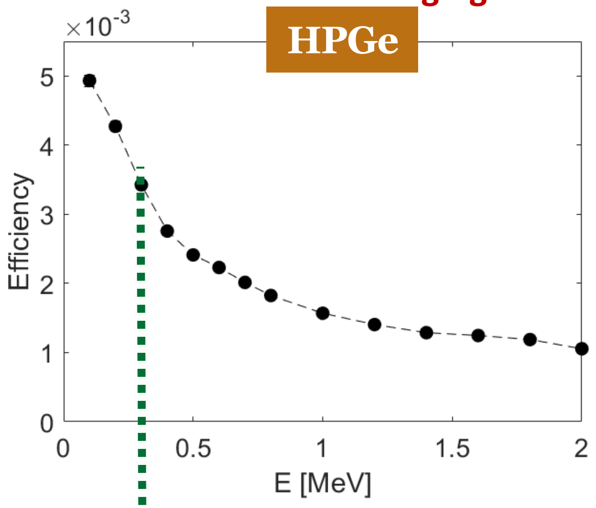

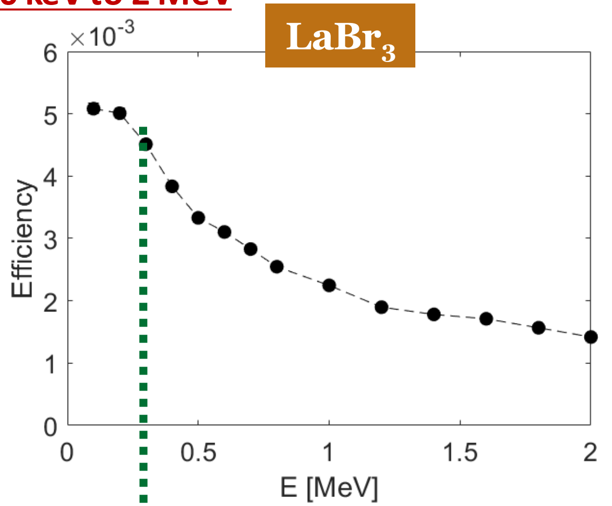

By simulations we estimated the **total efficiency** for two different type of detectors: HPGe and $LaBr_3$ (Lanthanum Bromide)

Typical resolution trend versus the energy for HPGe (on the left) and $LaBr_3$ (on the right) detectors

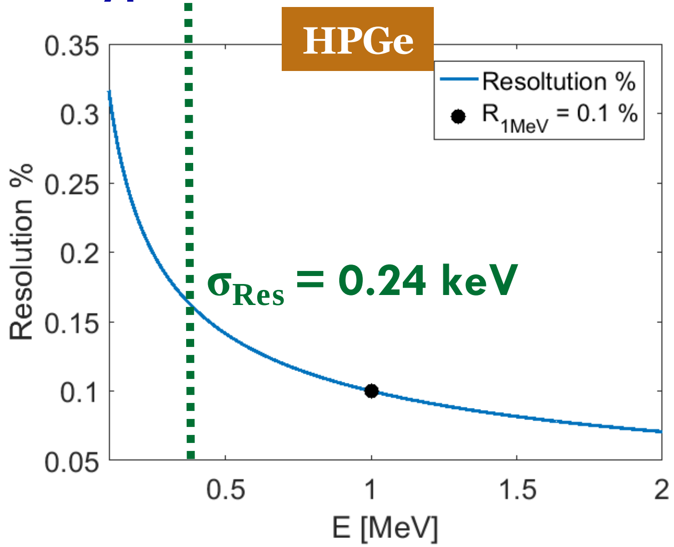

Physics case of ^{176}Lu: γ @ 306.78 keV

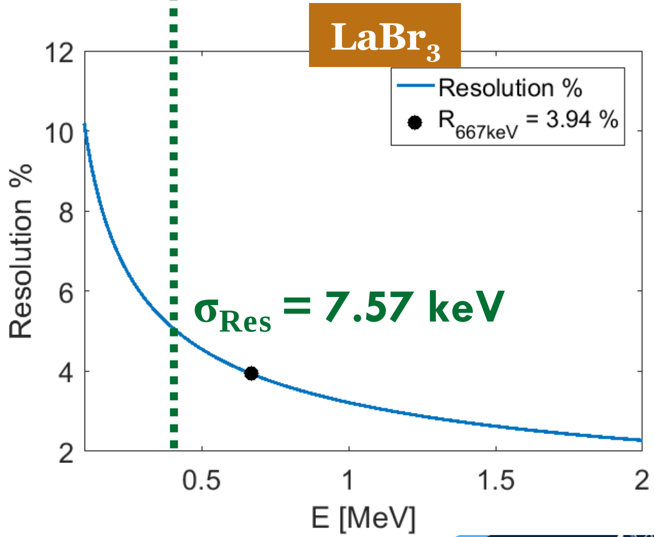

E. Naselli et al., EPJ web of conferences 227, 2020, 02006

The noise (consisting, especially, in the plasma self emission) affects the detection of the signal

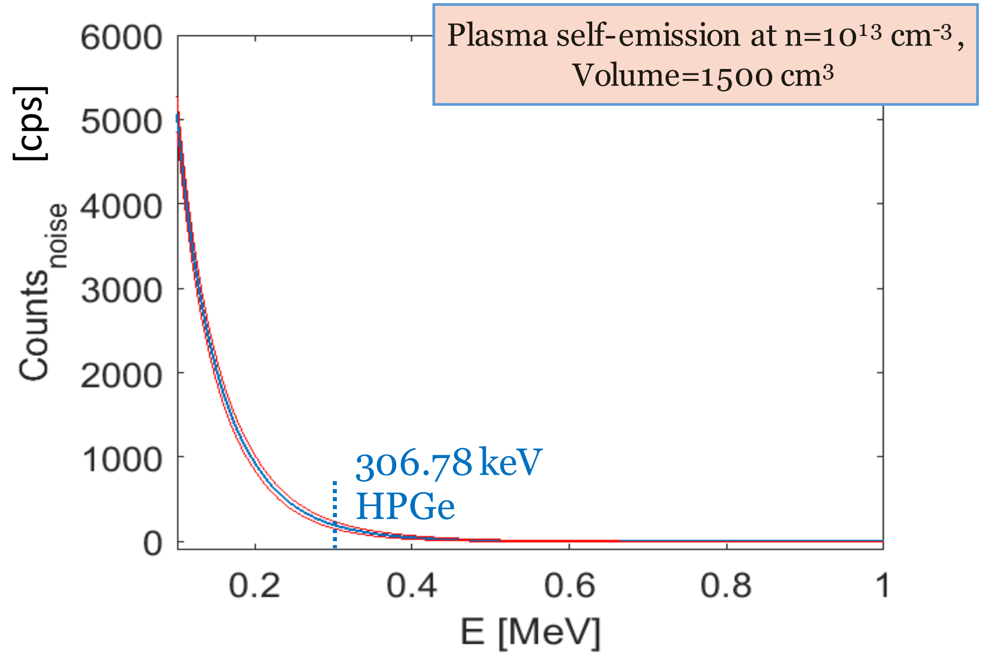

The noise spectrum was used to evaluate the time needed to have a significative 3 level signal

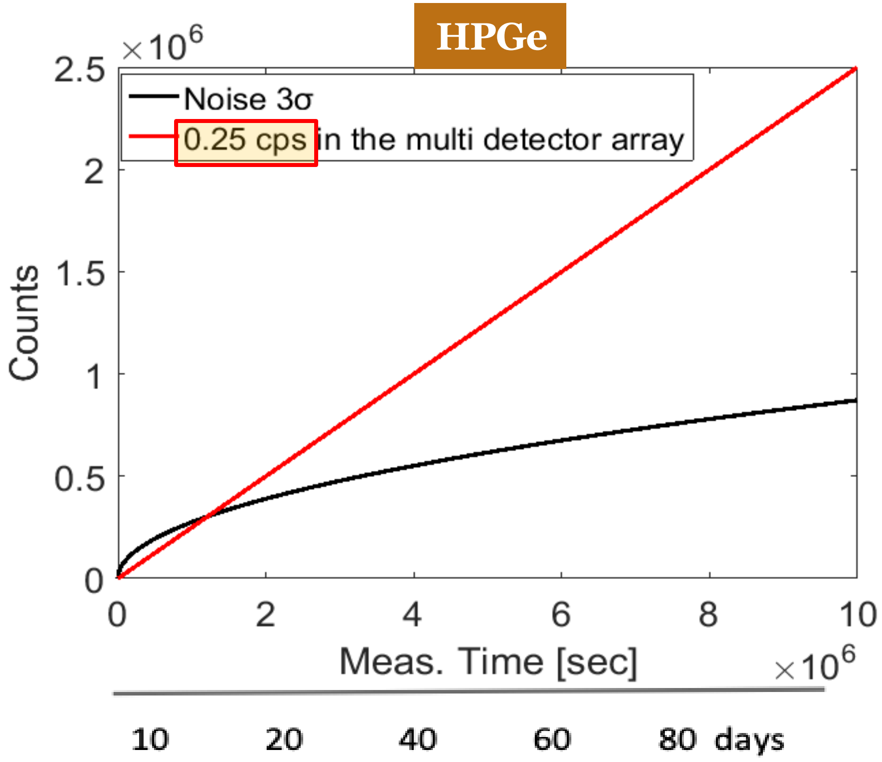

The intersection from the two lines shows the point where the signal over comes the 3 noise level, and the correspondent abscissa is the measurement time needed to have a 3 level of confidence

Trend of the **signal counts** (in red) compared to the **3 times the noise** (in black)

$$\text{Noise}_{3\sigma} = 3\sqrt{Noise_{cps} \cdot Tmeas}$$

$$N(T_{meas}) = \lambda n_i V_{plasma} T_{meas}$$

E. Naselli et al., EPJ web of conferences 227, 2020, 02006

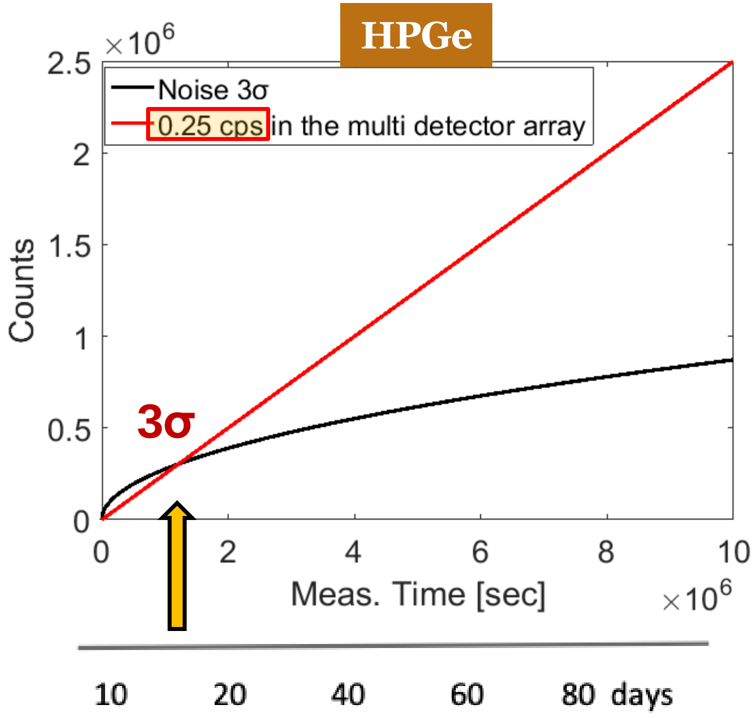

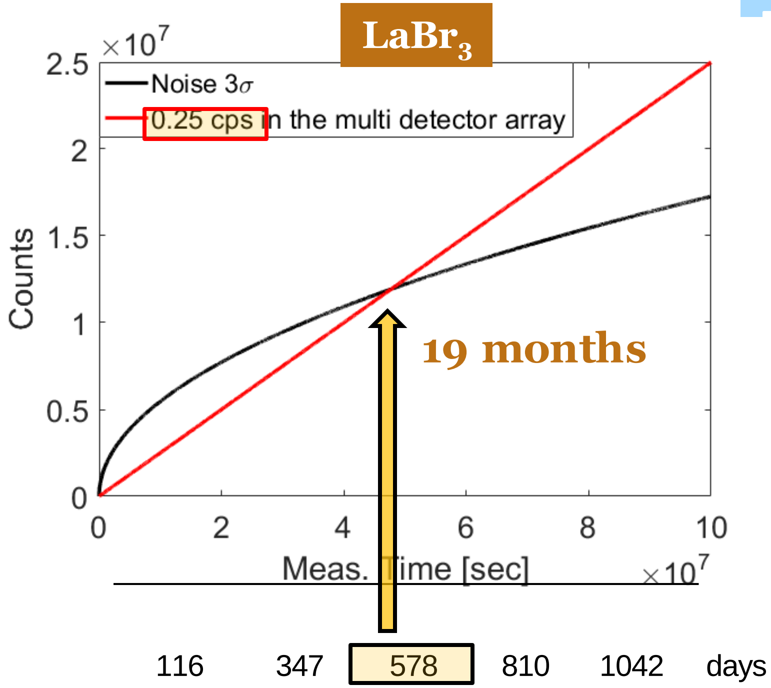

After about **several days** it is possible to obtain a **3σ** level using the array of **HPGe detectors**;

Whilst in the case of the array of **LaBr$_3$** a much longer time is needed: the measurement resulting **very challenging** or, eventually, **not-feasible**.

E. Naseli et al., EPJ web of conferences 227, 2020, 02006

^{176}Lu decay rates in stellar-like high density and energetic plasma

The naïve idea of the experiment is:

- ps lasers are directed toward a solid target composed of ^{176}Lu
- laser-generated plasma emits high energy X-ray bremsstrahlung produced from reactions between energetic electrons and buffer/^{176}Lu ions
- These X-rays are absorbed by the ^{176}Lu nuclei which get photoactivated to the 1^- isomer level according to a cross section σ(E) ➡ photoactivation rate $\lambda^c(n_e,n_i,T,s)$
- ^{176}Lu nuclei undergo β^- decay to ^{176}Hf from both the 7^- and 1^- levels
- Daughter nuclei will decay emitting specific gamma-rays
- Assuming the plasma remains active and stable LTE for a time T, the total number of specific γ-photons recorded can be correlated to the aforementioned rates
- The yield of 88.25 keV photons can be correlated to $\lambda_m^d(n_e,n_i,k_BT,s)$ if the photoactivation rate $\lambda^c(n_e,n_i,k_BT,s)$ is known
- Same considerations works for decay from g.s.

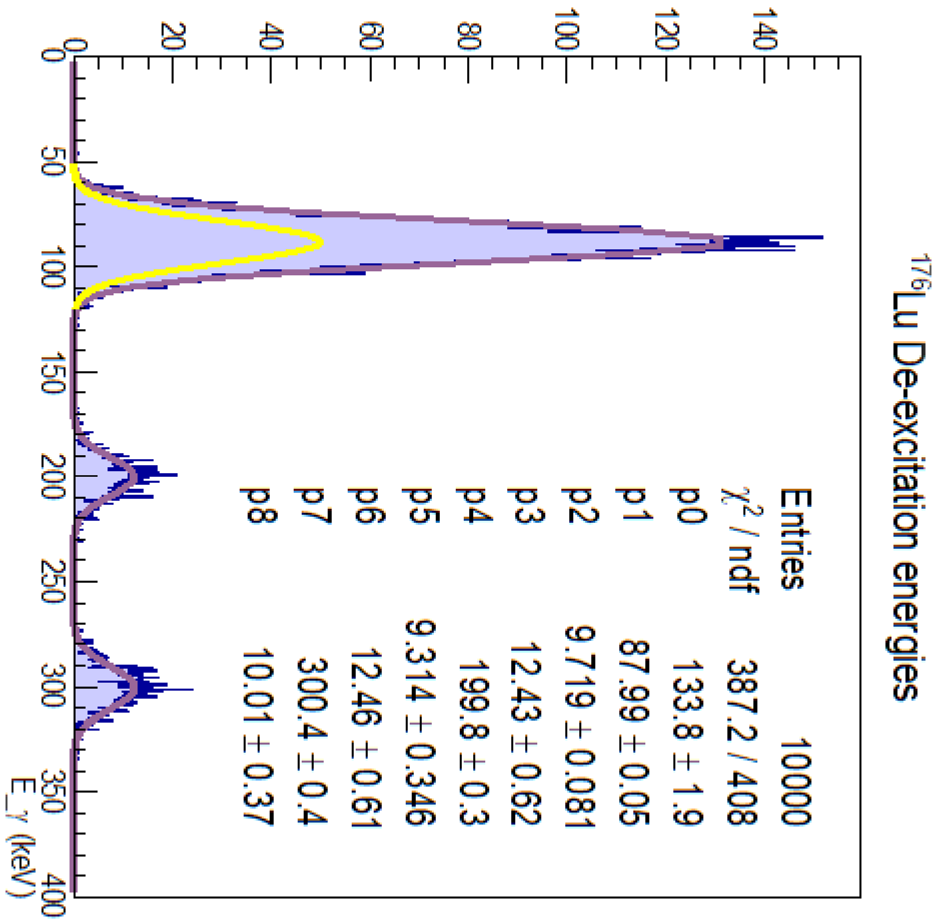

Ion Simulations: Scaling Module

Density Scaling and CSD

The results of ion transport + MC sampling are 3D accumulation maps which denote relative particle occupation in each simulation cell, and transfer coefficient which weigh the accumulation maps according to EI and CEX reactions.

The accumulation maps can be scaled by considering global charge neutrality with electrons

Example: After simulating first 3 charge states…

$$\oint_V n_e \mathrm{d}V = K_3 \Big[(1 - k_{1\to2} + 2k_{1\to2}k_{2\to1} + k_{1\to2}k_{2\to3}k_{3\to2}) \oint_V N_1 \mathrm{d}V + 2k_{1\to2}(1 - k_{2\to3} - k_{2\to1} + k_{2\to3}k_{3\to2}) \oint_V N_2 \mathrm{d}V + 3k_{1\to2}k_{2\to3}(1 - k_{3\to4} - k_{3\to2}) \oint_V N_3 \mathrm{d}V + 4k_{1\to2}k_{2\to3}k_{3\to4} \oint_V N_{3\to4} \mathrm{d}V \Big]$$

Transfer coefficients

Scaling coefficient

$$n_1 = K_3(1 - k_{1\to2} + 2k_{1\to2}k_{2\to1} + k_{1\to2}k_{2\to3}k_{3\to2})n_1$$
$$n_2 = K_3k_{1\to2}(1 - k_{2\to3} - k_{2\to1} + k_{2\to3}k_{3\to2})n_2$$
$$n_3 = K_3k_{1\to2}k_{2\to3}(1 - k_{3\to4} - k_{3\to2})n_3$$

Scaling the density also helps evaluating self-consistently the electrostatic double layer field

D. Mascali et al, Rev. Sci. Instrum. ***83*** *(2012)*
K. Takahashi, T. Kaneko and R. Hatakeyama, Phys. Plasmas ***15*** *(2008)*

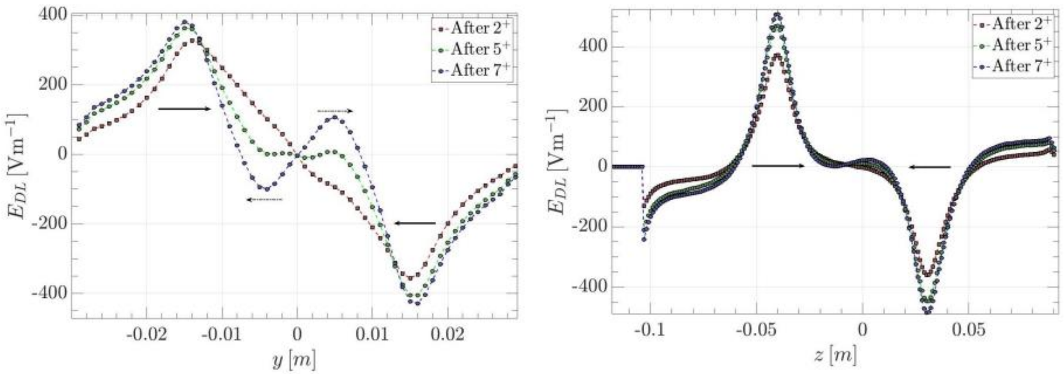

Iterative evolution of the double layer electrostatic field arising self-consistently with charge separation in the plasma, along *y*- and *z*-axes